

BOUNDARY-LAYER CONTROL OF BLUFF BODIES WITH APPLICATION
TO DRAG REDUCTION OF TRACTOR-TRAILER TRUCK CONFIGURATIONS

by

BIN YING

B.A.Sc., Nanjing Aeronautical Institute, 1982

A THESIS SUBMITTED IN PARTIAL FULFILMENT OF
THE REQUIREMENTS FOR THE DEGREE OF
MASTER OF APPLIED SCIENCE

in

THE FACULTY OF GRADUATE STUDIES

Department of Mechanical Engineering

We accept this thesis as conforming
to the required standard

THE UNIVERSITY OF BRITISH COLUMBIA

December 1991

© Bin Ying, 1991

In presenting this thesis in partial fulfilment of the requirements for an advanced degree at the University of British Columbia, I agree that the Library shall make it freely available for reference and study. I further agree that permission for extensive copying of this thesis for scholarly purposes may be granted by the head of my department or by his or her representatives. It is understood that copying or publication of this thesis for financial gain shall not be allowed without my written permission.

(Signature)

Department of Mechanical Engineering

The University of British Columbia
Vancouver, Canada

Date Dec. 27th 1991

ABSTRACT

Effectiveness of two fundamentally different concepts of boundary-layer control for the drag reduction of bluff bodies is studied experimentally. The methods are:

- (i) *Moving Surface Boundary-layer Control* (MSBC) involving momentum injection through one or more rotating elements (light hollow cylinders); and
- (ii) tripping of the boundary-layer using judiciously located fences to interrupt pressure recovery.

Wind tunnel tests with a two-dimensional wedge airfoil model suggest that injection of momentum can significantly delay separation of the boundary-layer resulting in a narrow wake and the associated reduction in the pressure drag. It also leads to a substantial increase in the lift at a given angle of attack resulting in a dramatic rise in the lift to drag ratio, from 2 to 80, under optimum conditions. Effectiveness of the momentum injection process is primarily governed by the gap-size, cylinder surface roughness and the ratio of the cylinder surface velocity (U_c) to the free stream velocity (U). A three-dimensional model of a rectangular prism and a 1/12 scale model of a typical tractor-trailer truck configuration show that both the MSBC and fence approaches are promising in reducing the aerodynamic resistance. A kit configuration is proposed for ease of implementation of the concepts on new

and existing trailers. Road tests with a full scale cube-truck are recommended to assess effectiveness of the boundary-layer control procedures in reducing the drag during highway conditions.

TABLE OF CONTENTS

ABSTRACT	ii
LIST OF TABLES	vi
LIST OF FIGURES	vii
NOMENCLATURE	xiii
ACKNOWLEDGEMENT	xv
1. INTRODUCTION	1
1.1 Background	1
1.2 A Brief Review of the Relevant Literature	2
1.3 Scope of the Present Investigation	8
2. MODELS AND TEST PROCEDURE	11
2.1 Two Dimensional Wedge Airfoil	11
2.2 Tractor-trailer Truck Model	13
2.2.1 Tractor-trailer truck model with twin rotating cylinders .	13
2.2.2 Tractor-trailer truck model with fences	15
2.2.3 Tractor-trailer truck model with a cylinder kit	17
2.3 Test Procedure for the Tractor-trailer Truck Model	20
2.3.1 Wind tunnel	20
2.3.2 Model support system	26
2.3.3 Cylinder rotation-rate measuring system	26
2.3.4 Drag measurement system	27

3. RESULTS AND DISCUSSION	29
3.1 Two Dimensional Wedge Airfoil	29
3.2 Tractor-trailer Truck Model with Twin Cylinders	53
3.3 Rectangular Prism with Fences	81
3.4 Tractor-trailer Truck Model with Fences	81
3.5 Tractor-trailer Truck Model with both Twin Cylinders and Fences	87
3.6 Tractor-trailer Truck Model with a Cylinder Kit	94
3.6.1 Cylinder kit 1	95
3.6.2 Cylinder kit 2	102
4. CONCLUDING REMARKS	109
4.1 Summary of Results	109
4.1.1 Application of the MSBC to a 2-D wedge airfoil model ..	109
4.1.2 Application of the MSBC and fences to a 3-D truck model	111
4.2 Recommendation for Future Work	112
REFERENCES	115

LIST OF TABLES

Table 1.	Wind tunnel tests conducted with different orientation of the twin helical-groove and spline cylinders: location of the front cylinder was at the top leading edge and the rear cylinder at 25.4 cm downstream from the leading edge. . . .	59
-----------------	---	----

LIST OF FIGURES

Figure	Page
1. The practical application of moving wall for boundary-layer control was demonstrated by Favre in 1938. Using an airfoil with the upper surface formed by a belt moving over two rollers, he was able to delay separation until the angle of attack reached 55° , where the maximum lift coefficient of 3.5 was realized.	4
2. Schematic diagrams explaining principles of the MSBC and the boundary-layer trip devices in reducing drag of bluff bodies.	6
3. Schematic diagrams of the bluff bodies studied during the wind tunnel test-program.	10
4. A photograph showing the cylinders with different surface roughnesses used in the test-program: (a) smooth; (b) helical grooves; (c) roughness squares; (d) spline-1; (e) spline-2.	12
5. Photographs showing the wind tunnel test arrangement for the 2-D wedge airfoil. The model was supported by the lift-drag strain gage balance with an oil damper to minimize vibration. . .	14
6. Schematic diagrams showing arrangement of rotating cylinders and fences for the boundary-layer control:	
(a) MSBC using twin cylinders;	18
(b) fences for tripping of the boundary-layer.	19
7. Kit configurations developed for application to existing trucks as an add-on device:	
(a) schematic diagrams of kit 1 with the rotating element projecting 12.7 mm in the fluid stream;	21
(b) schematic diagrams of kit 2 with the cylinder projecting 31.8 mm in the flow;	22
(c) close-up showing a splined cylinder serving as the momentum injection unit and two vertical fences for	

tripping the boundary-layer with kit 2. 23

8. The boundary-layer wind tunnel, with a test cross-section of 2.44x1.6 m, was used to study 1/12 scale models of the trailer and truck configurations:

(a) schematic diagram showing details of the tunnel with the model near the entrance to the test-section (first-bay); 24

(b) photographs showing a tractor-trailer truck model (1/12 scale), with boundary-layer control devices, being prepared for wind-tunnel tests. 25

9. 3-D tractor-trailer truck model test arrangement in the U.B.C. boundary-layer wind tunnel. 28

10. Aerodynamic coefficients for a two-dimensional wedge airfoil as affected by the rotation of the smooth cylinder:

(a) lift coefficient; 31

(b) drag coefficient; 32

(c) C_L/C_D 33

11. Variation of the aerodynamic coefficients with the angle of attack and helical groove cylinder rotation:

(a) lift; 35

(b) drag; 36

(c) C_L/C_D 37

12. Plots showing effect of the cylinder surface roughness condition on the lift and drag coefficient:

(a) C_L ; 39

(b) C_D ; 40

(c) C_L/C_D 41

13. Influence of axial surface grooves on the momentum injection (spline-1) as reflected through the variation of lift and drag coefficients:

(a) C_L ; 42

(b) C_D ; 43

(c) C_L/C_D 44

14.	Effect of the surface roughness designated as spline-2 on the aerodynamic coefficients:	
(a)	C_L ;	45
(b)	C_D ;	46
(c)	C_L/C_D .	47
15.	Comparison charts showing relative merit of the surface condition on the boundary-layer control:	
(a)	C_{Lmax} ;	49
(b)	C_{Dmin} ;	50
(c)	$(C_L/C_D)_{max}$.	51
16.	A schematic diagram of the closed circuit water channel facility used in the flow visualization study. Slit lighting was used to minimize distortion due to three dimensional character of the flow. Long exposure provided path-lines with polyvinyl chloride particles serving as tracers. The dimensions are in mm.	52
17.	Typical flow visualization photographs for a wedge shaped airfoil, with a smooth surface cylinder, showing remarkable effectiveness of the MSBC concept for $\alpha = 30^\circ$, $R_n = 3 \times 10^4$. Note the progressive downstream shift of the separation point as the U_c/U increase. Eventually the flow appears to approach the potential character.	54
18.	The concept of moving surface boundary-layer control continues to be effective event at a high angle of attack of 55° as shown dramatically by these flow visualization pictures ($R_n = 3 \times 10^4$) . . .	55
19.	Effect of the moving surface boundary-layer control on the drag coefficient of a tractor-trailer truck configuration. Note, an increase in the sandpaper roughness contributes to the drag reduction through efficient momentum injection.	57
20.	Effect of the twin helical cylinder configuration on the momentum injection and boundary-layer control:	
(a)	Case 1: both cylinders flush;	60
(b)	Case 2: front cylinder flush, rear cylinder raised 6.35 mm;	61

(c)	Case 3: front cylinder flush, rear cylinder raised 12.7 mm;	62
(d)	Case 4: front cylinder raised 6.35 mm, rear cylinder raised 12.7 mm;	63
(e)	Case 5: front cylinder raised 6.35 mm, rear cylinder flush;	64
(f)	Case 6: front cylinder raised 12.7 mm, rear cylinder flush;	65
(g)	Case 7: front cylinder raised 12.7 mm, rear cylinder raised 6.35 mm;	66
(h)	Case 8: front cylinder raised 12.7 mm, rear cylinder raised 12.7 mm;	67
(i)	Case 9: front cylinder raised 6.35 mm, rear cylinder raised 6.35 mm.	68
21.	Variation of the drag coefficient C_D with the speed ratio for the twin spline cylinder configurations:	
(a)	Case 1: both cylinders flush;	70
(b)	Case 2: front cylinder flush, rear cylinder raised 6.35 mm;	71
(c)	Case 3: front cylinder flush, rear cylinder raised 12.7 mm;	72
(d)	Case 4: front cylinder raised 6.35 mm, rear cylinder raised 12.7 mm;	73
(e)	Case 5: front cylinder raised 6.35 mm, rear cylinder flush;	74
(f)	Case 6: front cylinder raised 12.7 mm, rear cylinder flush;	75
(g)	Case 7: front cylinder raised 12.7 mm, rear cylinder raised 6.35 mm;	76
(h)	Case 8: front cylinder raised 12.7 mm, rear cylinder raised 12.7 mm;	77
(i)	Case 9: front cylinder raised 6.35 mm, rear cylinder raised 6.35 mm.	78
22.	Effect of cylinder rotation on the flow past a tractor-trailer truck configuration.	79
23.	Effect of cylinder rotation on the flow past a tractor-trailer truck configuration. Note, the tractor geometry and spacing between the tractor and trailer are different here.	80
24.	Effect of the fence width and height on the drag of a three-dimensional prism.	83
25.	A schematic diagram showing application of the fences on the	

	front, exposed face of the trailer of a truck.	84
26.	Variation of the drag coefficient with the position of horizontal fence 1.	85
27.	Variation of the drag coefficient with the position of horizontal fence 2 when fence 1 is fixed at its critical orientation.	86
28.	Variation of the drag coefficient with the position of twin vertical fences 3 and 4 when fences 1 and 2 are fixed at their critical orientations.	88
29.	Stages in fine tuning of the fence dimensions and associated drag coefficient:	
	(a) The fences were extended to the edges of the trailer front face in both horizontal and vertical directions.	89
	(b) The twin vertical fences were truncated to horizontal 2 fence position from the bottom edge of the trailer front face.	90
	(c) The twin vertical fences were truncated further to horizontal 1 fence position from the top edge of the trailer front face.	91
	(d) The twin horizontal fences had offset from both side edges of the trailer front face.	92
30.	Variation in the drag coefficient with the cylinder speed ratio for a hybrid configuration involving two vertical fences and twin rotating cylinders in their optimum geometry.	93
31.	Variation in the drag coefficient with the cylinder speed ratio as affected by kit 1 vertical orientation:	
	(a) absence of the front cover;	97
	(b) with the front cover.	98
32.	Variation in the drag coefficient with the cylinder speed ratio and kit 1 position with two vertical fences mounted optimally on the front face of the kit.	99

- 33.** Variation in the drag coefficient with the cylinder speed ratio for kit 1 at the optimum vertical orientation. Note the influence of cover and fence geometry. 100
- 34.** Variation in the drag coefficient with the cylinder speed ratio for kit 2 at different vertical position. Note the effect of gap. 104
- 35.** The drag coefficient as affected by position of the two vertical fences on the front face of kit 2, set at the optimum position, with the gap covered and stationary cylinder. 105
- 36.** Variation in the drag coefficient as affected by the position of a horizontal fence with two critically-oriented vertical fences on the front face of kit 2. The gap was covered and the cylinder was held stationary. 106
- 37.** Variation in the drag coefficient with the cylinder speed ratio for kit 2 at its optimum vertical orientation, gap covered and fences in critical geometry. 108

NOMENCLATURE

U	free stream velocity
U_c	cylinder surface speed
α	angle of attack
c	wedge airfoil chord
ρ	air density
l	wedge airfoil span
A	projected area normal to the free stream
C_L	mean lift coefficient, lift / $(1/2)\rho U^2 cl$
C_D	mean airfoil drag coefficient, drag / $(1/2)\rho U^2 cl$ or drag / $(1/2)\rho U^2 A$
U_{cf}	front cylinder surface speed
U_{cr}	rear cylinder surface speed
d	hydraulic diameter, $(4A/\pi)^{1/2}$
H	trailer height
B	trailer width
L	trailer length
h_f	fence height
b_f	fence width
b_{fh}	horizontal fence width
b_{fv}	vertical fence width
y_f	vertical coordinate of the horizontal fence

- x_f horizontal coordinate of the vertical fence
- $()_{cr}$ critical value
- $()_{min}$ minimum value
- $()_{max}$ maximum value
- H_k cylinder kit coordinate representing distance from the top surface of the trailer to the horizontal center line of the cylinder
- B_c kit front cover width, same as that of the trailer
- H_c kit front cover height
- G_p gap between the cylinder kit and the cab
- μ standard air viscosity, 17.8×10^{-6} kg/ms
- R_n Reynolds number, $\rho U d / \mu$

ACKNOWLEDGEMENT

A special thank is extended to my supervisor, Dr. V. J. Modi for his time and guidance throughout the project. His insight and amiable nature has made this project a thoroughly enjoyable experience. I would not have got the key points without his novel ideas and hints during the study.

Assistance of Professor T. Yokomizo in the flow visualization study is gratefully acknowledged. It was carried out in his laboratory at Kanto Gakuin University, Yokohama, Japan.

The assistance of Mr. E. Abell, Senior Technician, in construction of the model is gratefully acknowledged.

The investigation reported here was supported by the Science Council of British Columbia, Grant Nos. AGAR 5-53628, 5-53698 and Natural Sciences and Engineering Research Council of Canada, Grant No. A-2181.

1. INTRODUCTION

1.1 Background

Identification and exploitation of energy sources such as fossil fuels, solar, wind, geothermal, tidal, biomass, etc. have received attention for quite some time. The oil embargo emphasized a need for self-sufficiency in energy. At the same time, energy conservation measures as reflected in the improved design of engine, aircraft with high lift/drag ratio, aerodynamically shaped cars, better insulated houses, heat recovery in industrial processes, etc. have also gained importance. The proposed project focuses on one such energy conservation area, which promises to have a significant economic consequence. It addresses the sector of energy consumption, the commercial road transportation industry, which is :

- (i) already significant in size;
- (ii) presently growing and promising to maintain that trend.

The present investigation is directed at energy conservation through an effective reduction in aerodynamic resistance of a typical truck configuration.

It should be recognized that:

- (a) two-thirds of all the goods in North America are transported by trucks;
- (b) on an average a truck covers around 130,000 - 150,000 km/year;

- (c) 50 - 70% of the truck's power (at 80 - 100 km/hr speed) is consumed in overcoming aerodynamic resistance, compared to around 20 - 30% for rolling friction and 10 - 15% lost in the transmission system.

A simple analysis of this set of data suggests that even 1% reduction in the aerodynamic drag can amount to a significant saving in the fuel cost [1]. Aerodynamic resistance is a result of the complex three dimensional flow field associated with the truck geometry, and is governed by the boundary layer separation as well as reattachment regions. It is sensitive to speed and the relative wind direction (yaw incident angle). In general, the drag coefficient for a conventional truck may vary significantly depending on its geometry, speed and yaw [2].

1.2 A Brief Review of the Relevant Literature

Ever since the introduction of the boundary-layer concept by Prandtl, there has been a constant challenge faced by scientists and engineers to minimize its adverse effects and control it to advantage. Methods such as suction, blowing, vortex generators, turbulence promoters, etc., have been investigated at length and employed in practice with a varying degree of success. The vast body of literature accumulated over years has been reviewed rather effectively by several authors including Goldstein [3], Lachmann [4],

Rosenhead [5], Schlichting [6], Chang [7], and others. However, the use of moving surface for boundary-layer control has received relatively less attention.

Irrespective of the method used, the main objective of a control procedure is to prevent, or at least delay, separation of the boundary-layer. A moving surface attempts to accomplish this in two ways:

- (i) it retards growth of the boundary-layer by minimizing relative motion between the surface and the free stream;
- (ii) it injects momentum into the existing boundary-layer.

A practical application of moving wall for boundary-layer control was demonstrated by Favre [8]. Using an airfoil with upper surface formed by a belt moving over two rollers (Figure 1), he was able to delay separation until the angle of attack reached 55° where the maximum lift coefficient $C_{Lmax} = 3.5$ was realized. Alvarez-Calderon and Arnold [9] carried out tests on a rotating cylinder flap to develop a high lift airfoil for STOL type aircraft. The system was tested in flight on a single engine high-wing research aircraft.

Of some interest is the North American Rockwell designed OV-10A aircraft which was flight tested by NASA's Ames Research Center [10-12]. Cylinders located at the leading edges of the flaps were rotated at high speed with the flaps in lowered position. The main objective of that test program was to assess handling qualities of the propeller powered STOL type aircraft at higher lift coefficients. The aircraft was flown at speeds of 29-31 m/s, along

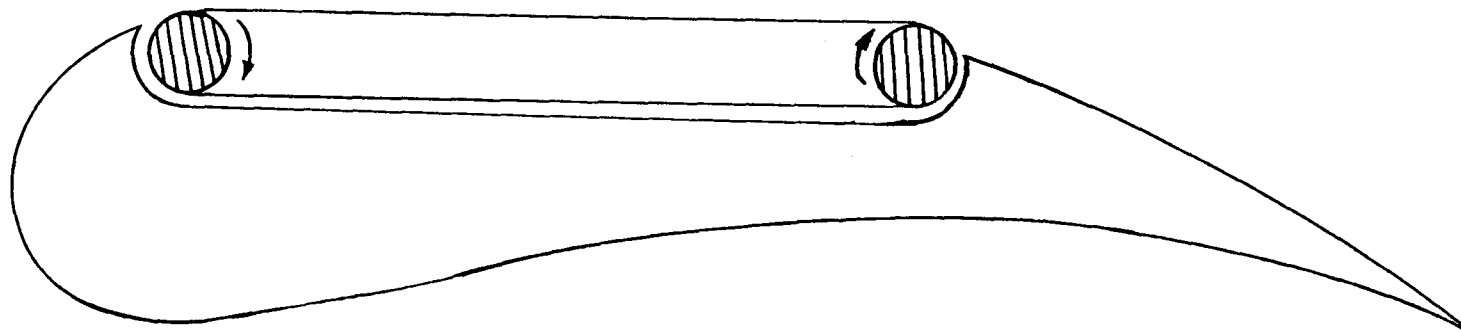


Figure 1. The practical application of moving wall for boundary-layer control was demonstrated by Favre in 1938. Using an airfoil with the upper surface formed by a belt moving over two rollers, he was able to delay separation until the angle of attack reached 55° , where the maximum lift coefficient of 3.5 was realized.

approaches up to -8° , which corresponded to a lift coefficient $C_D \approx 4.3$. In the pilot's opinion any further reductions in approach speed were limited by the lateral-directional stability and control characteristics.

In terms of trying to understand the phenomenon at the fundamental level Tennant's contribution to the field is significant. Tennant et al. [13] have conducted tests with a wedge shaped flap having a rotating cylinder as the leading edge. Flap deflection was limited to 15° and the critical cylinder velocity necessary to suppress separation was determined. Effect of increasing the gap-size (between the cylinder and the flap surface) was also assessed. No effort was made to observe the influence of an increase in the ratio of cylinder surface speed (U_c) to the free stream velocity (U) beyond 1.2.

Through a comprehensive wind tunnel test program involving a family of airfoils with one or more cylinders forming moving surfaces, complemented by the surface singularity numerical approach and flow visualization, earlier studies by Modi et al. [14 - 17] have shown spectacular effectiveness of the concept, which increased the maximum lift coefficient by more than 200% and delayed the stall angle to 48° .

Yet another approach to boundary-layer control can be through its tripping by judiciously located fences on the front face of a bluff body. This interferes with the pressure recovery thus promising to reduce drag.

The basic concepts involved in the boundary-layer control through the above two methods are illustrated in Figure 2. It shows a bluff body, a two-



It is apparent that by increasing P_b or reducing P_f we can reduce the pressure drag.

- (i) MSBC tends to increase P_b by keeping the flow attached;
- (ii) Fences tend to reduce P_f by tripping the boundary-layer and preventing the pressure recovery.

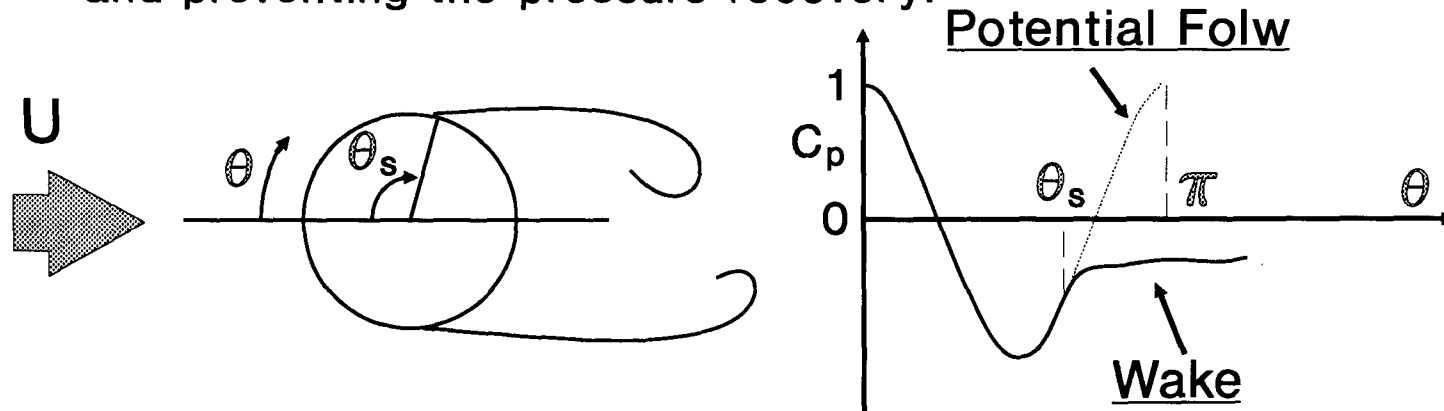


Figure 2. Schematic diagrams explaining principles of the MSBC and the boundary-layer trip devices in reducing drag of bluff bodies.

dimensional prism, located in a fluid stream at zero angle of attack. P_f and P_b are pressures on the front and rear faces, respectively. They are assumed to be uniform over the faces, in this illustrative example, for simplicity. Obviously, by increasing P_b and/or decreasing P_f we can reduce the pressure drag. MSBC tries to increase P_b by keeping the flow attached. On the other hand, fences reduce P_f by tripping the boundary-layer. These principles are explained through diagrams of the flow past a circular cylinder in the same figure. At the stagnation point the pressure is the largest and pressure coefficient is 1. The boundary-layer separates at θ_s forming the wake. In the wake the pressure is essentially uniform at a lower value. This is what fences try to achieve. If the separation is prevented, ideally the pressure will reach the stagnation value. This is what the MSBC tries to accomplish.

A comprehensive literature review of the road vehicle aerodynamics suggests that although aerodynamically contoured car design has become a standard practice lately, the trucks and buses have changed little during the past 30 years [18 - 21]. Most of the modifications have been limited to rounded edges with provision for vanes, skirts and flow deflectors. The benefit due to some of the “add-on” devices is still a matter of controversy and, at best, marginal under conditions other than the specific ones used in their designs. Bearman [22] has presented an excellent review on the subject (with 54 references cited). The thesis by Wacker [23] also discusses limited influence of “add - on” devices with a possibility of increasing the drag under non-optimal

conditions. On the other hand, it was found that judicious choice of ground clearance, gap-size between the tractor and the trailer, and back inclination can reduce the drag coefficient by a significant amount.

A word concerning numerical analysis of the complex aerodynamics associated with road vehicles would be appropriate. A reliable and cost-effective methodology, if available, can assist in design with reduced dependence on time consuming and expensive wind tunnel tests. With the advent of supercomputers, parallel processing and neural network concepts, considerable progress has been made in that direction. However, modelling of three dimensional boundary layers around a complex geometry at supercritical Reynolds numbers, with separation, reattachment and reattachment of unsteady turbulent flows, still represents a challenging problem [24,25].

1.3 Scope of the Present Investigation

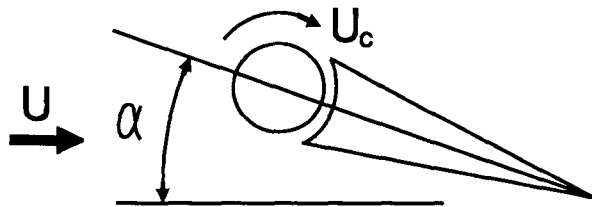
The present study builds on this background and explores application of the two concepts: (a) Moving Surface Boundary-layer Control (MSBC); and (b) trip fences; to a two-dimensional wedge airfoil and tractor-trailer truck configurations. The extensive wind tunnel test program, complemented by a flow visualization study, investigates effectiveness of:

- (i) the MSBC for 2-D wedge airfoil;
- (ii) the MSBC for 3-D tractor-trailer truck;

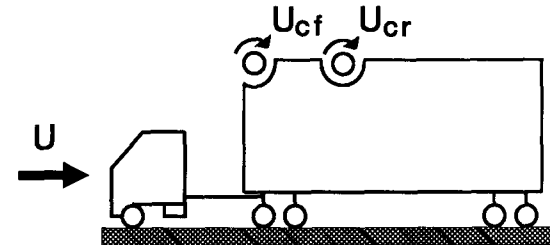
- (iii) the trip fences when applied to the upstream face of a rectangular prism and the trailer; and
- (iv) combinations of the MSBC and fences as applied to a tractor-trailer truck configuration.

A schematic diagram of the configurations studied is presented in Figure 3. An important parameter during the MSBC is the ratio of the cylinder surface velocity (U_c) to the free stream velocity (U), which was systematically varied during the test-program conducted in the smooth flow condition. In the fence study, the variables of interest are the fence width and height (b_f and h_f , respectively) and their locations that would lead to a maximum reduction in drag.

MSBC for 2-D Wedge Airfoil



MSBC for 3-D Tractor-trailer Truck



Fences for Rectangular Prism and Truck



Combination of MSBC and Fences for Truck

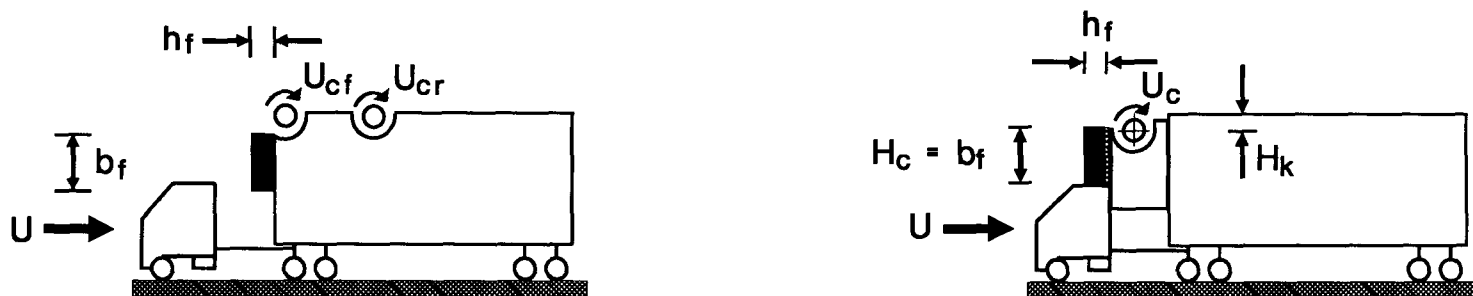


Figure 3. Schematic diagrams of the bluff bodies studied during the wind tunnel test-program.

2. MODELS AND TEST PROCEDURE

2.1 Two Dimensional Wedge Airfoil

The two dimensional wedge-airfoil model was tested in a 45 x 45 cm cross-section wind tunnel with a maximum speed of 50 m/s. The large converging nozzle at the entrance of the tunnel (contraction ratio = 10 : 1) makes the flow in the test-section uniform with a level of turbulence less than 0.5%. The tunnel speed can be adjusted by a variac transformer and measured using a pitot static tube connected to an inclined alcohol manometer.

The wedge model with a chord length of 11.5 cm and the tail angle of $\approx 14^\circ$ was constructed from aluminum with the nose replaced by a cylinder of 2.54 cm diameter and of desired surface roughness. Five different surface conditions were used in the test-program (Figure 4) designated as:

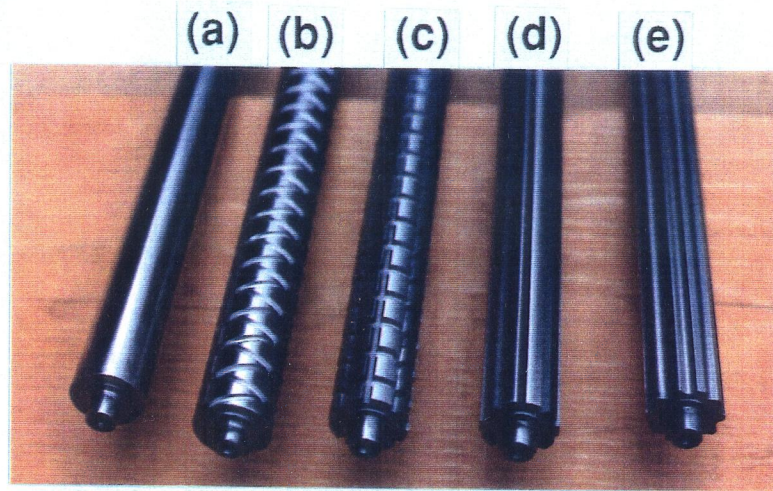
- (i) smooth;
- (ii) helical grooves;
- (iii) roughness squares;
- (iv) spline-1;
- (v) spline-2.

The difference between (iv) and (v) is essentially characterized by the shape of splines. The (iv) is with sharp teeth whereas the (v) with round ones.

The cylinder was driven by a variac controlled 1/8 H.P. a.c. motor



Figure 4. A photograph showing the cylinders with different surface roughnesses used in the test-program: (a) smooth; (b) helical grooves; (c) roughness squares; (d) spline-1; (e) spline-2.



through a flexible belt system. The motor speed was monitored using a digital stroboscope. In the present test-program the ratio U_c/U was varied from 0 - 4. This corresponds to a maximum cylinder speed of around 12,000 rpm at a free stream speed of 3.85 m/s ($R_n = 3 \times 10^4$). To ensure two dimensionality of the flow the model was fitted with end plates. The lift and drag forces were recorded over a range of the angle of attack of $0^\circ - 55^\circ$ with 5° increment. The force can be measured with an accuracy of 0.5 gm/mV.

The models were susceptible to vibration, particularly at high angles of attack, due to the turbulent wake created by the shedding vorticity. This was minimized by an externally located viscous oil damper. The test arrangement is shown in Figure 5.

2.2. Tractor-trailer Truck Model

A 1/12 scale tractor-trailer truck model was constructed out of Plexiglas. The model has a trailer with width $B = 22.7$ cm, height $H = 26.2$ cm, and length $L = 128.4$ cm, with a hydraulic diameter of . It can be used to assess effectiveness of the MSBC, tripping of the boundary-layer using fences, or a combination of the two.

2.2.1 Tractor-trailer truck model with twin rotating cylinders

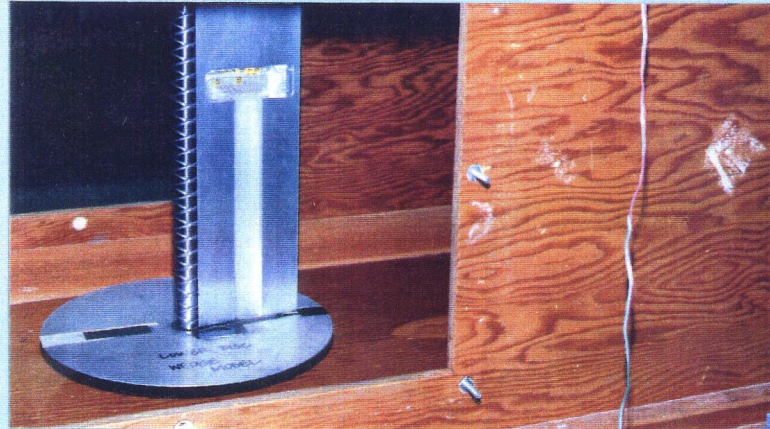


Figure 5. Photographs showing the wind tunnel test arrangement for the 2-D wedge airfoil. The model was supported by the lift-drag strain gage balance with an oil damper to minimize vibration.

The two identical cylinders of diameter 6.35 cm were mounted on the top face of the truck-trailer model with the front one forming the trailer's leading edge while the rear one was positioned 25.4 cm downstream. The vertical orientation of each cylinder can be adjusted to three different heights as: 0 (the cylinder flush with the trailer top face), 0.635 cm and 1.27 cm. Different combinations of the cylinder arrangement resulted in nine cases. The tests were conducted with helical grooves and spline surface conditions which appeared more promising. As before, each cylinder was driven by a 1/8 H.P. motor, with an optical sensor in conjunction with a slotted disk to monitor its speed. A feedback control system was used to maintain the speed at a desired level.

2.2.2 Tractor-trailer truck model with fences

A typical fence is a thin flat plate of width b_f , height h_f and negligible thickness. In the test-program, fences made of aluminum were used. To assess the effectiveness of fences as a drag reducing "add on" device, a three-dimensional rectangular prism ($B = 22$ cm, $H = 23$ cm, $L = 101.5$ cm, $d = 25.4$ cm) with four fences forming a square about the geometric center served as the model. The coordinate system to position fences has its origin at the geometric center of the front face. The two fence variables b_f and h_f determine the height and size of square frame. In the test-program, size of the square geometry and

height of the fence were varied systematically to arrive at an optimum configuration ($b_f = 0, 12.7, 15.24, 17.78, 19.05$ cm; $h_f = 0, 0.85, 1.45, 2.2, 2.7, 3.35, 3.9$ cm).

As the fence results with the three-dimensional prism showed encouraging trends, the next logical step was to assess their effectiveness in reducing drag of a tractor-trailer configuration. To this end, a 1/12 scale model of the truck with $H = 26$ cm, $B = 22.7$ cm and $L = 128.4$ cm was constructed from Plexiglas, with hydraulic diameter, d , equal to 31.14 cm. The coordinate system to identify position of the fences had its origin at the geometric center of the front face of the trailer. The fence positions were varied systematically to arrive at an optimum (critical) configuration as indicated below:

- (a) Position of the horizontal fence 1 varied along the y direction to arrive at the critical orientation $(y_{f1})_{cr}$.
- (b) With the fence 1 fixed at $(y_{f1})_{cr}$, the critical position of the horizontal fence 2, $(y_{f2})_{cr}$, was established.
- (c) With fences 1 and 2 held fixed at their critical locations, the twin vertical fences were symmetrically located about the y_f axis to arrive at the critical position $(x_f)_{cr}$ leading to a minimum drag coefficient.
- (d) The fences were extended both vertically and horizontally to the front face edges to assess the influence of their extension.
- (e) The effect of increase and decrease of the fence lengths was

assessed systematically to arrive at a configuration leading to a maximum reduction in the drag coefficient.

Figure 6 shows typical test arrangement for boundary-layer control through momentum injection and tripping devices.

2.2.3 Tractor-trailer truck model with a cylinder kit

Ideally, introduction of MSBC through rotating cylinders should proceed with design of the new generation of trailers. The boundary-layer control system in this way can become an integral part of the trailer configuration. However, until the concept has demonstrated its economic potential convincingly through exhaustive road tests, such far-reaching design change cannot be expected. This is understandable as the investment commitment involved is indeed significant.

An alternative would be to implement the concept on existing trucks in service, however, this would entail modification of the trucks to accommodate the cylinder(s), drive and control systems, cylinder speed monitoring arrangement and feedback device, etc. Obviously, this may not be always attractive. To alleviate the situation, it was decided to design a self-contained MSBC-kit, which can be attached to the trailer's front face judiciously to capture most of the desirable influence of the boundary-layer control without modifying the trailer.

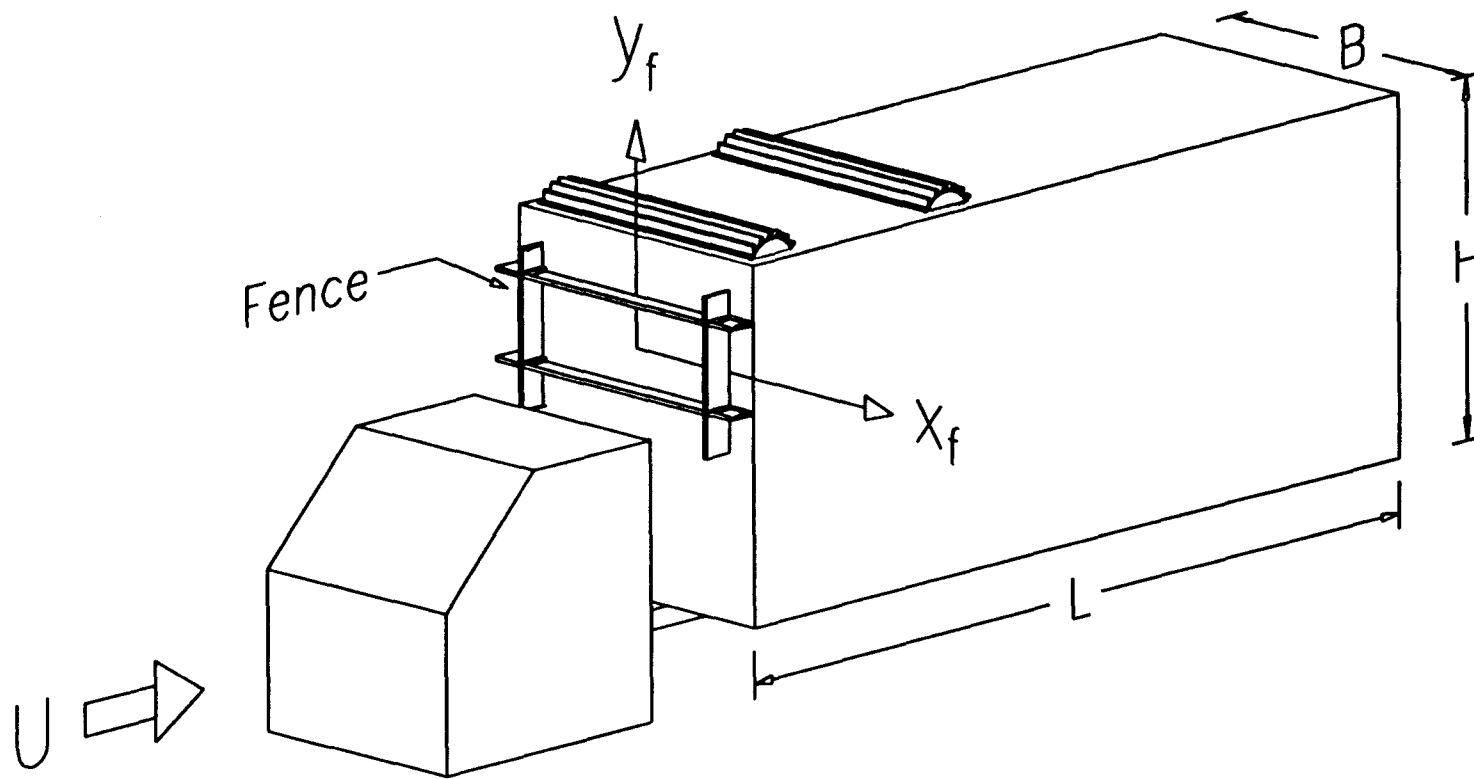


Figure 6. Schematic showing arrangement of rotating cylinders and fences for the boundary-layer control:
(a) MSBC using twin cylinders;

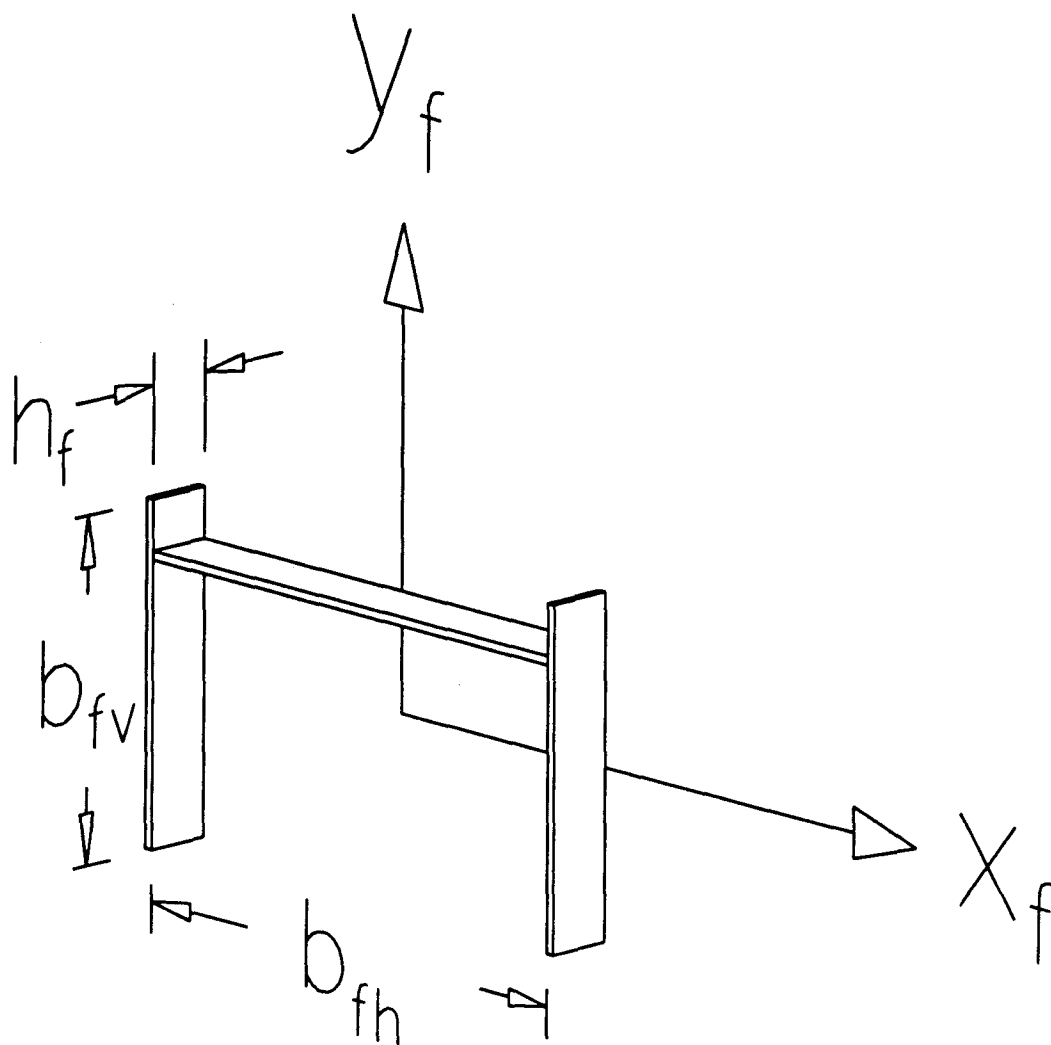


Figure 6. Schematic showing arrangement of rotating cylinders and fences for the boundary-layer control: (b) fences for tripping of the boundary-layer.

Two different self-contained kits, each containing a cylinder with a 1/8 H.P. motor and the speed control system, were designed for model tests. The kits have the same width as the trailer and occupy the space near the gap between the tractor and the trailer. Position of the kit with reference to the trailer is adjustable in the vertical direction.

The difference between the two kits is primarily characterized by the extent of the cylinder exposed above the top face of the kit. This also reflects on the surface exposed to the fluid stream. In the case of kit 1, the cylinder is initially raised 12.7 mm above the kit's top surface. For kit 2, half the cylinder is exposed to the fluid stream. Details of the two kits are shown in Figure 7.

2.3 Test Procedure for the Tractor-trailer Truck Model

2.3.1 Wind tunnel

The trailer and truck models were tested in the boundary-layer wind tunnel at the University of British Columbia (Figure 8). The tunnel is an open-circuit type powered by an 80 kW three phase motor which drives an axial flow fan at a constant 700 rpm. The tunnel wind speed is varied using a pneumatic controller to alter either the rotating frequency of the fan or the blade pitch. The settling section contains a honeycomb and four screens to smooth the flow as it enters a 4.7 to 1 contraction section which accelerates the flow and improves its uniformity. The tunnel has a test-section 2.44 m wide, 1.6 m high

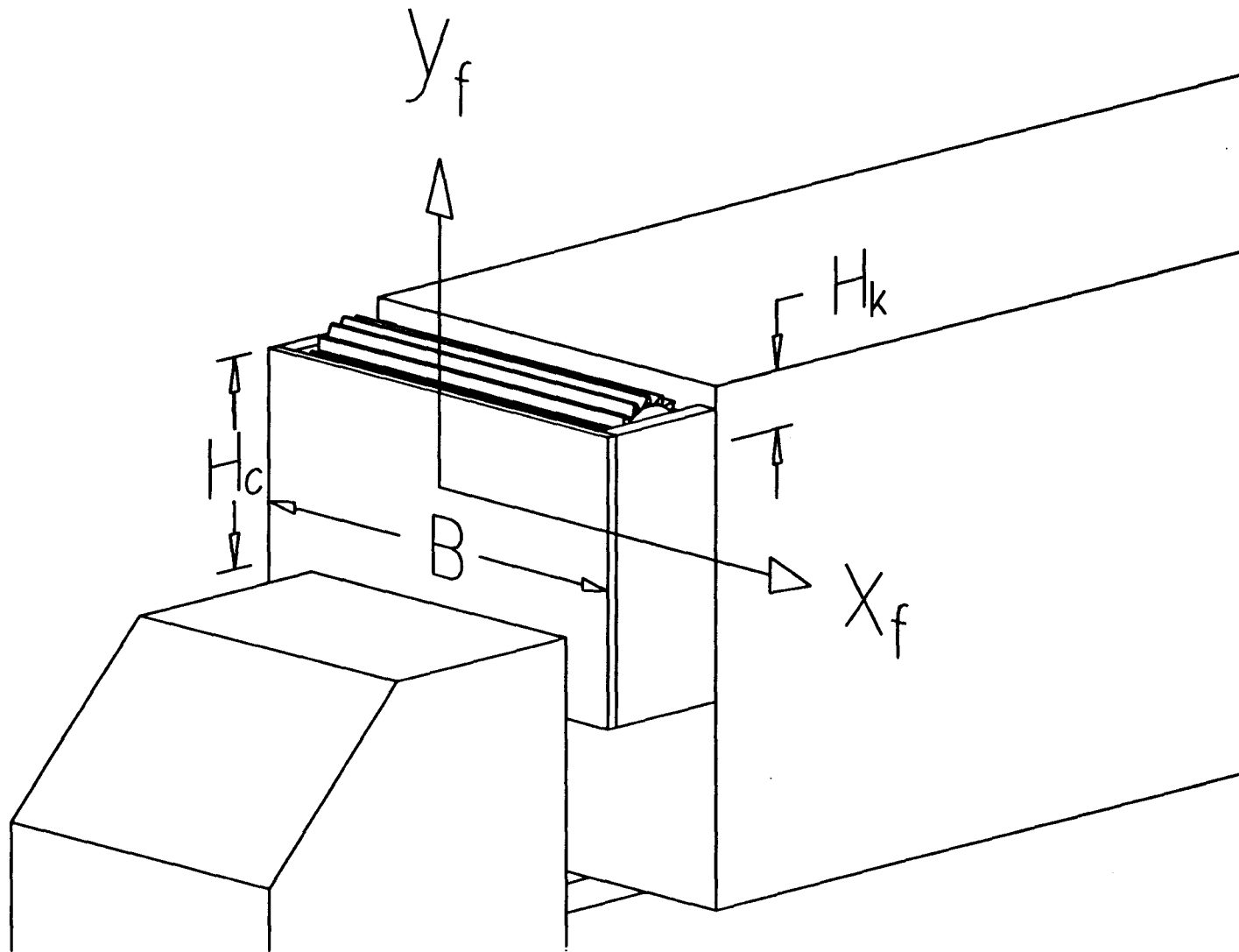


Figure 7. Kit configuration developed for application to existing trucks as an add-on device: (a) schematic diagrams of kit 1 with the rotating element projecting 12.7 mm in the fluid stream;

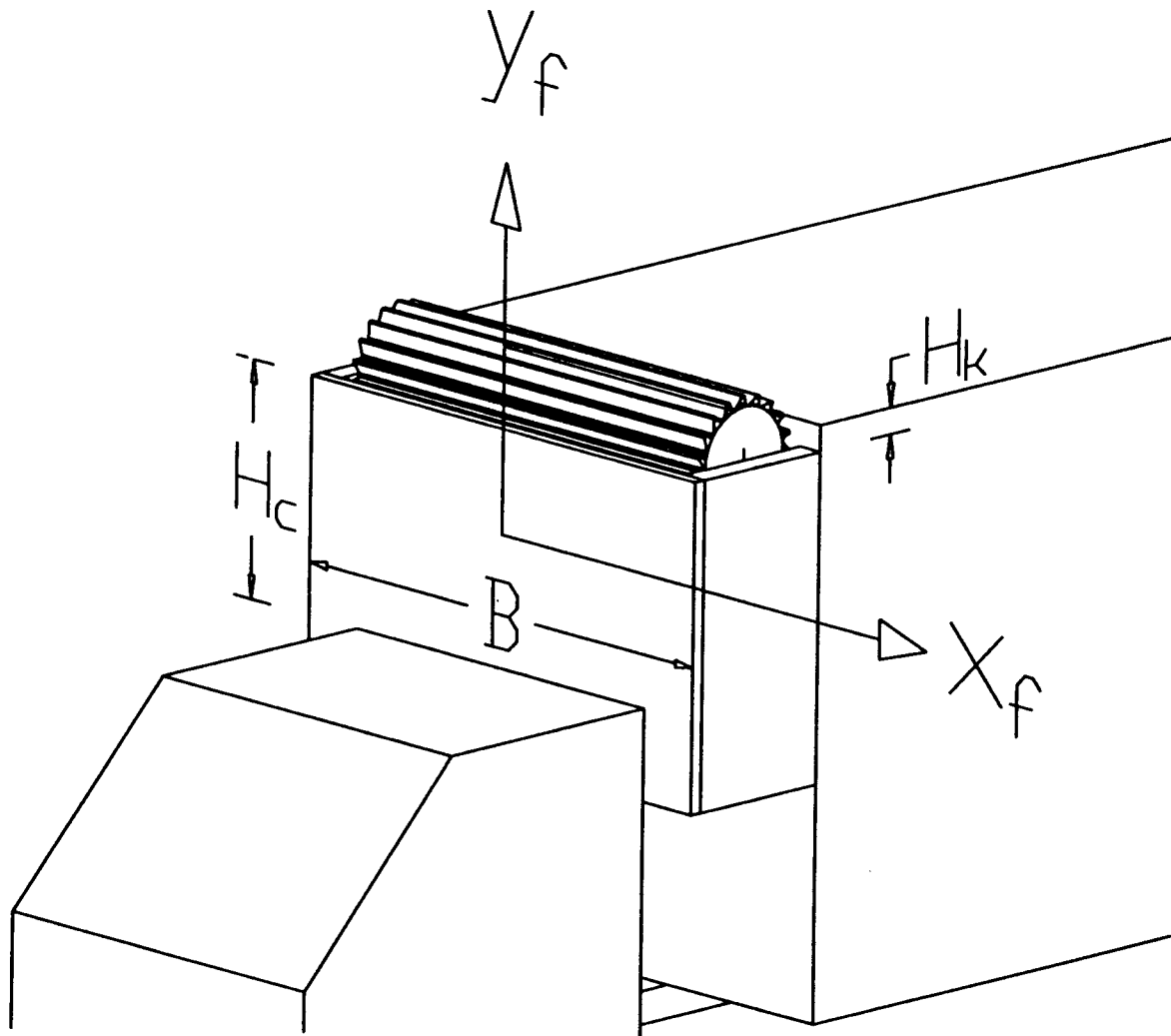


Figure 7. Kit configuration developed for application to existing trucks as an add-on device: **(b)** schematic diagrams of kit 2 with the cylinder projecting 31.8 mm in the fluid stream;

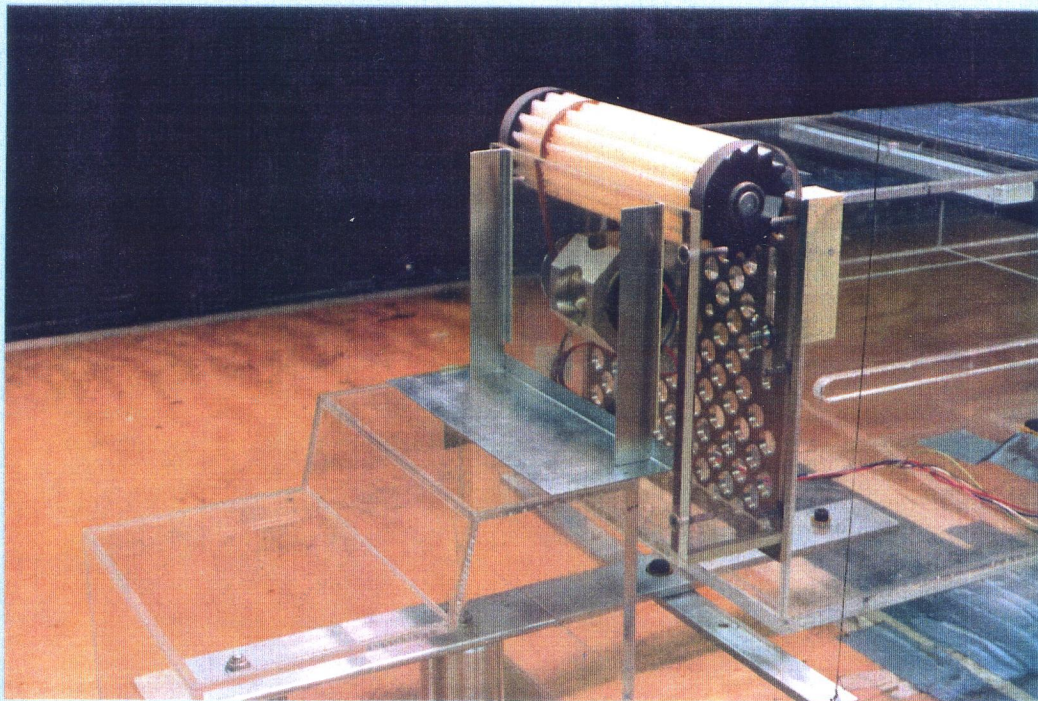
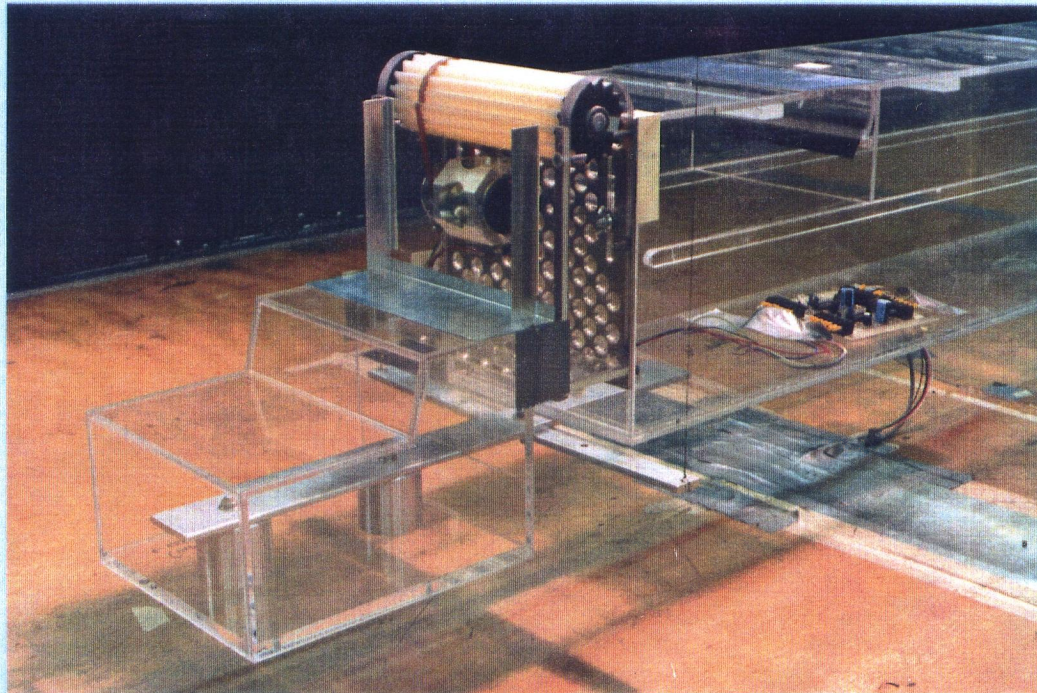


Figure 7. Kit configuration developed for application to existing trucks as an add-on device: (c) close-up showing a splined cylinder serving as the momentum injection unit and two vertical fences for tripping the boundary-layer with kit 2.

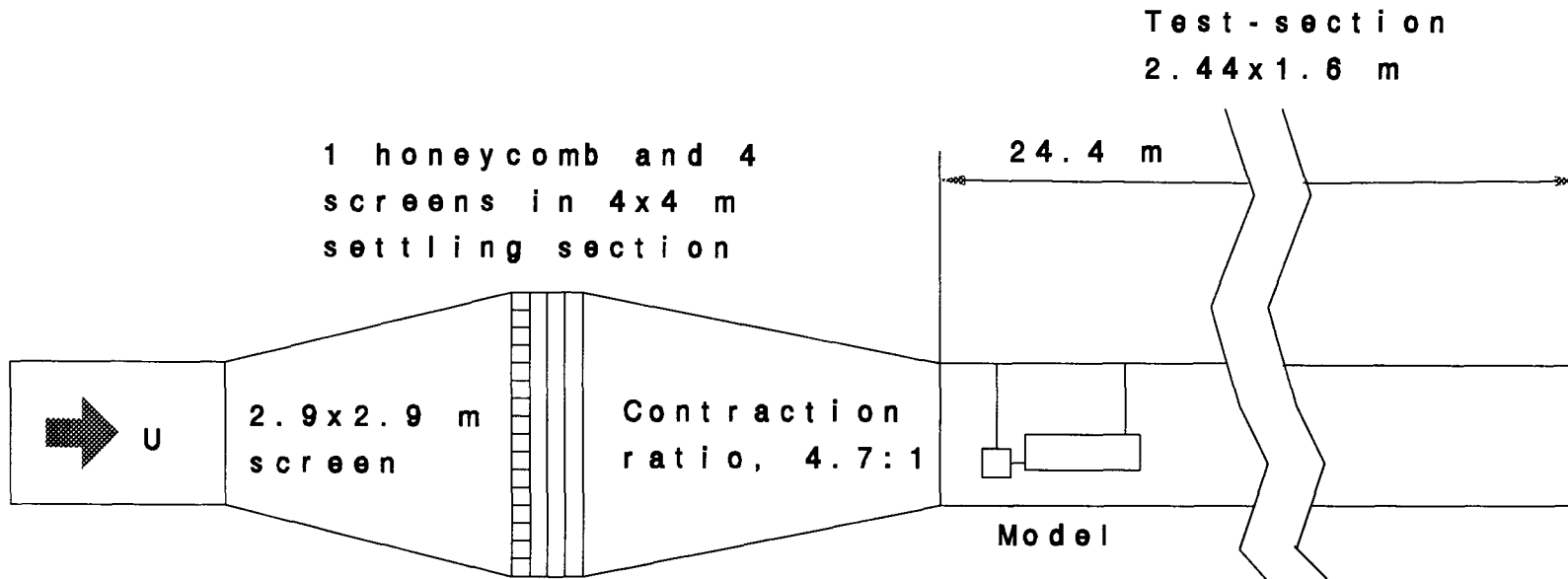


Figure 8. The boundary-layer wind tunnel, with a test cross-section of 2.44x1.6 m, was used to study 1/12 scale models of the trailer and truck configurations: (a) schematic diagram showing details of the tunnel with the model near the entrance to the test-section (first-bay);

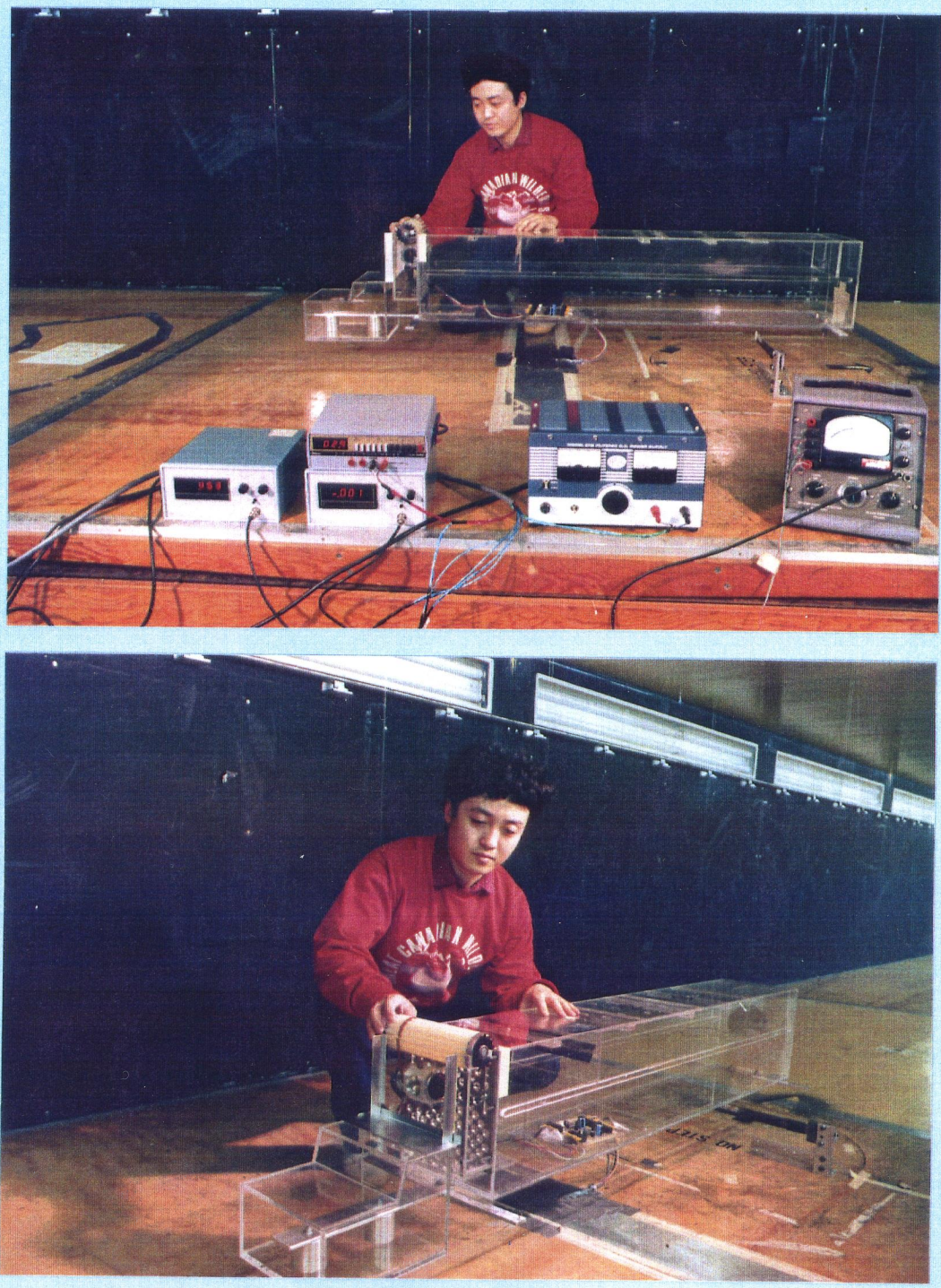


Figure 8. The boundary-layer wind tunnel, with a test cross-section of 2.44x1.6 m, was used to study 1/12 scale models of the trailer and truck configurations: **(b)** photographs showing a tractor-trailer truck model (1/12), with boundary-layer control devices, being prepared for wind-tunnel tests.

and 24.4 m long consisting of eight 3.05 m long bays, and a variable height roof to allow for the boundary-layer correction. The stable wind speed of the tunnel is in the range of 2.5 - 25 m/s. The adjustable test-section roof was set for a zero pressure gradient. The present set of experiments were carried out in the second bay which provided smooth flow with a turbulence level less than 0.4%. The typical test Reynolds number based on the hydraulic diameter was 10^5 .

2.3.2 Model support system

A typical truck model was supported by four steel guy wires which were suspended from the ceiling and carried turnbuckles to help level the model. As the length of the wire (≈ 145 cm) is much larger than the maximum horizontal displacement of the truck model (≤ 5 cm), the drag induced displacement was essentially linear in the downstream direction.

2.3.3 Cylinder rotation-rate measuring system

As pointed before, the moving surface element used for the momentum injection is a circular cylinder driven by a 1/8 H.P. variable speed D.C. motor. A system of pulleys with a belt connection transmits the motion from the motor to the cylinder. A slotted disk in conjunction with an optical sensor (photomultiplier) and an amplifier are used to measure the cylinder speed. The

amplifier signal was filtered and displayed on a *DISA* voltameter. The least square fit of the results when calibrated using a digital stroboscope resulted in a linear plot of mV against the rpm.

2.3.4 Drag measurement system

Variation in the drag due to the boundary-layer control devices being relatively small, required development of a sensitive transducer for its measurements. The model was suspended from the ceiling by four wires as described before to minimize frictional effects. The drag induced downstream motion of the model was transmitted by an inelastic string to a cantilever beam with a pair of strain gages near its root. The gages formed a part of the Wheatstone Bridge (of the *Bridge Amplifier Meter*, BAM) and the amplified filtered output was recorded using a *DISA* voltameter. The sensitivity of the drag measurements was around 0.4 gm/mV. The Calibration of the cantilever using static loads was performed, with the model suspended as described, twice during a test-session, before and after the tests; and the average calibration value was adopted to account for any drift. Figure 9 shows schematically the model support and drag measurement system.

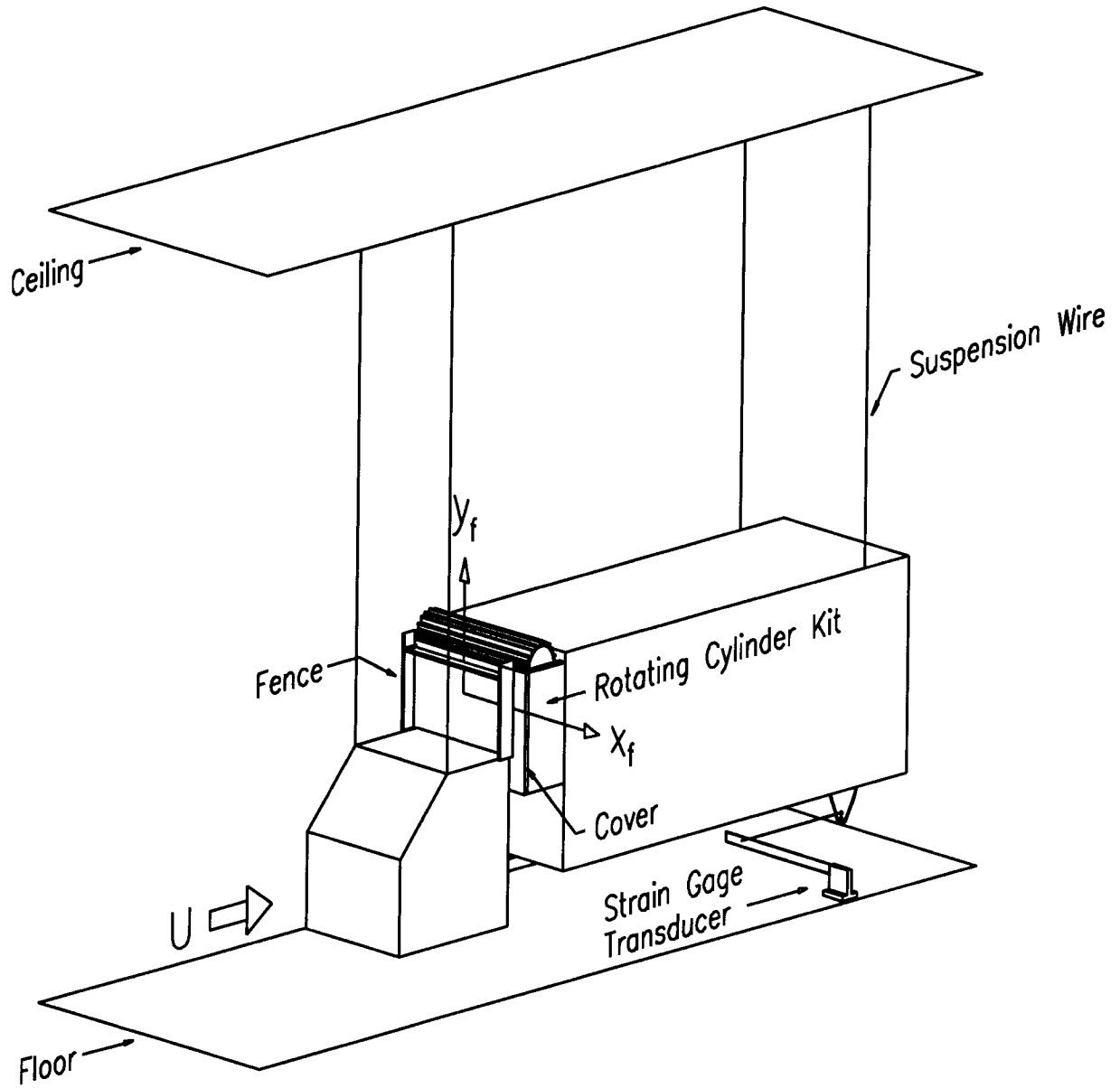


Figure 5. 3-D tractor-trailer truck model test arrangement in the U.B.C. boundary-layer wind tunnel.

3. RESULTS AND DISCUSSION

3.1 Two Dimensional Wedge Airfoil

The lift and drag characteristics of an airfoil is significantly affected by its geometry, i.e., thickness and camber distribution. In order to focus on the effect of momentum injection, the model selected for study was purposely taken to be simple: a wedge shaped airfoil. The airfoil model is free of camber (symmetrical about the chord-line) and two dimensional. The amount of information obtained through a systematic variation of the angle of attack, cylinder's surface condition and speed of rotation is really enormous. Influence of the Reynolds number in the subcritical range $10^4 - 5 \times 10^5$ was found to be negligible. The results presented here for the wind tunnel tests conducted at a fixed Reynolds number of $R_n \approx 3 \times 10^4$.

The relatively large angles of attack used in the experiments result in a considerable blockage of the wind tunnel ($\approx 20\%$ at $\alpha = 55^\circ$). The wall confinement leads to an increase in the local wind speed at the location of the model, thus resulting in higher aerodynamic forces. Several approximate correction procedures have been reported in literature to account for this effect. However, these approaches are mostly applicable to streamlined bodies with attached flow. A satisfactory procedure applicable to a "bluff body" offering a large blockage and with separating shear layers is still not available.

With rotation of the cylinder(s), the problem is further complicated. As shown by the pressure data and confirmed by the flow visualization [26], the unsteady flow can be separating and reattaching over a large portion of the top surface. In absence of any reliable procedure to account for wall confinement effects in the present situation, the results are purposely presented in the uncorrected form.

To establish a reference which can be used to assess the influence of cylinder rotation and surface condition, the first step was to obtain lift and drag characteristics of the wedge-airfoil with the smooth stationary cylinder ($U_c / U = 0$) forming its nose and the gap between the cylinder and rest of the wedge sealed. The results are presented in Figure 10 which also shows effect of the cylinder rotation. The reference configuration gave a maximum lift coefficient $C_{Lmax} \approx 1.47$ at $\alpha = 55^\circ$. However, with the cylinder rotation, slope of the lift curve dramatically increase and the stall is delayed significantly. At $U_c / U \approx 4$ and $\alpha = 55^\circ$ the peak lift coefficient reaches 3.95, an increase of around 168% ! The corresponding results for drag are presented in Figure 10b. It is of interest to recognize that, in general, the drag coefficient also shows a favourable trend. With an increase in speed of the cylinder, there is a distinct drop in the drag coefficient at a given angle of attack. For example, at $\alpha = 55^\circ$, the decrease in C_D from ≈ 1.85 for $U_c / U = 4$ to the reference value of 1.18 corresponds to a reduction of 36% ! Of course, one way to assess effectiveness of the momentum injection in controlling the boundary-layer separation would

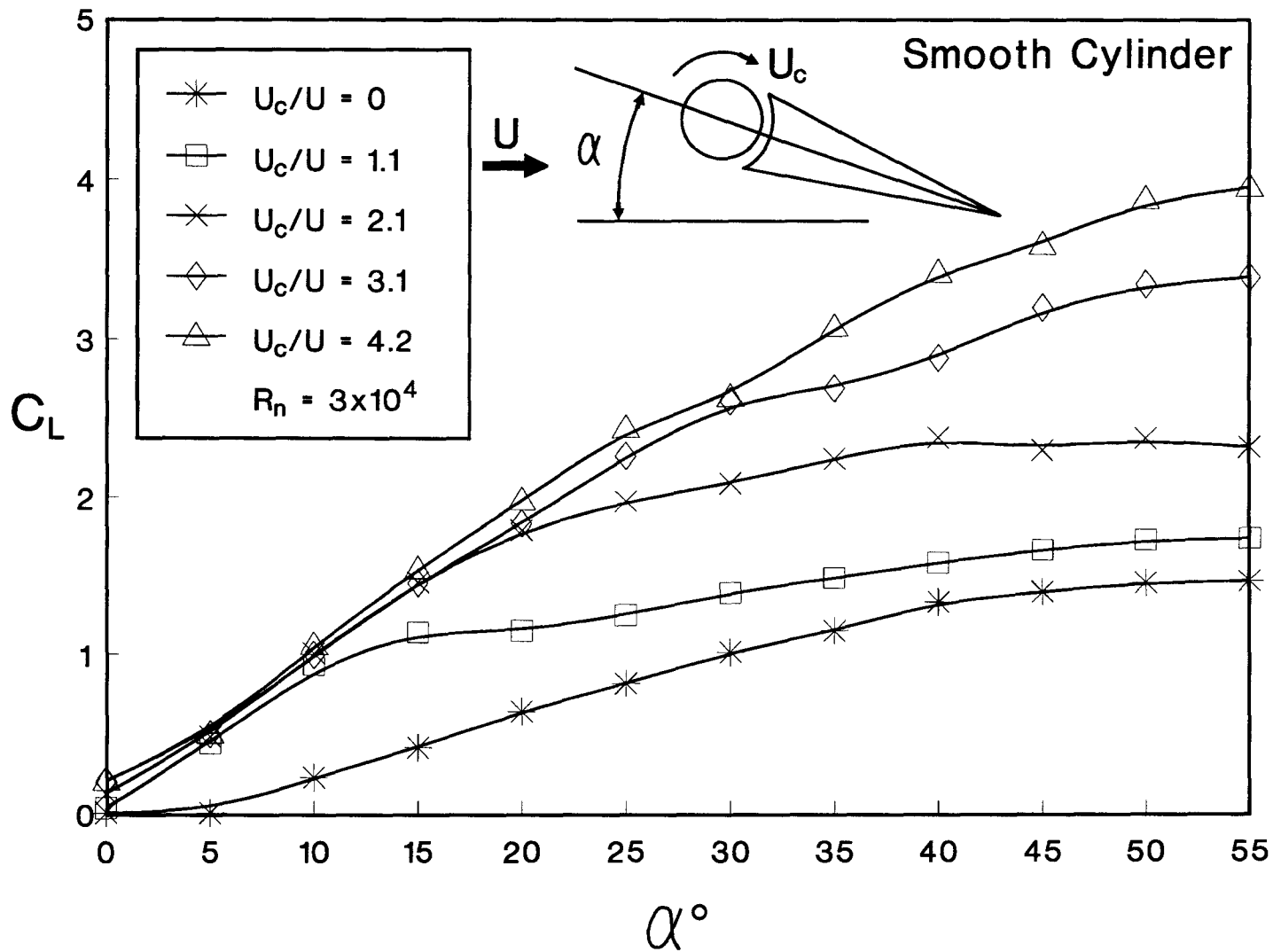


Figure 10. Aerodynamic coefficients for a two-dimensional wedge airfoil as affected by the rotation of the smooth cylinder: (a) lift coefficient;

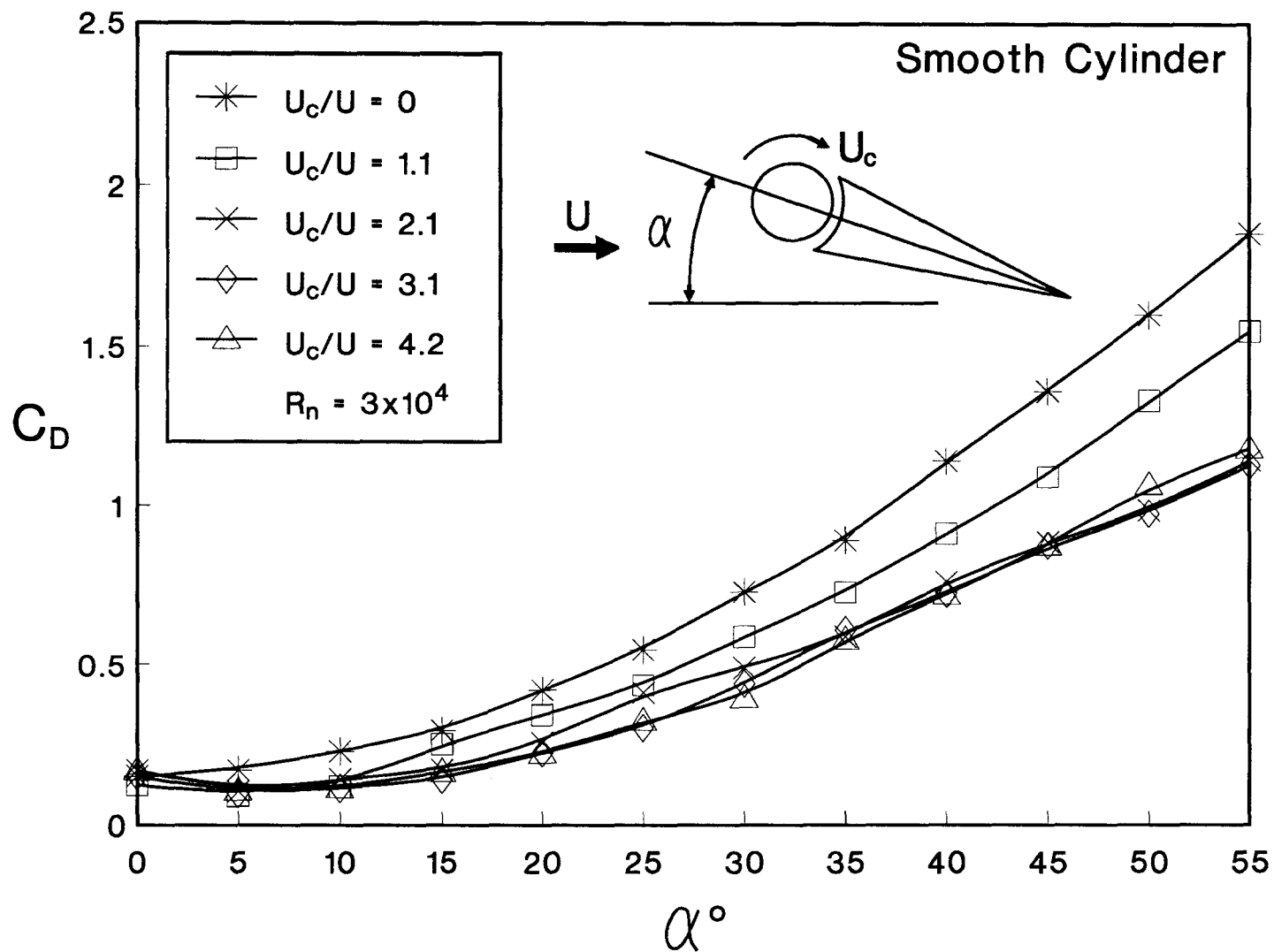


Figure 10. Aerodynamic coefficients for a two-dimensional wedge airfoil as affected by the rotation of the smooth cylinder: (b) drag coefficient;

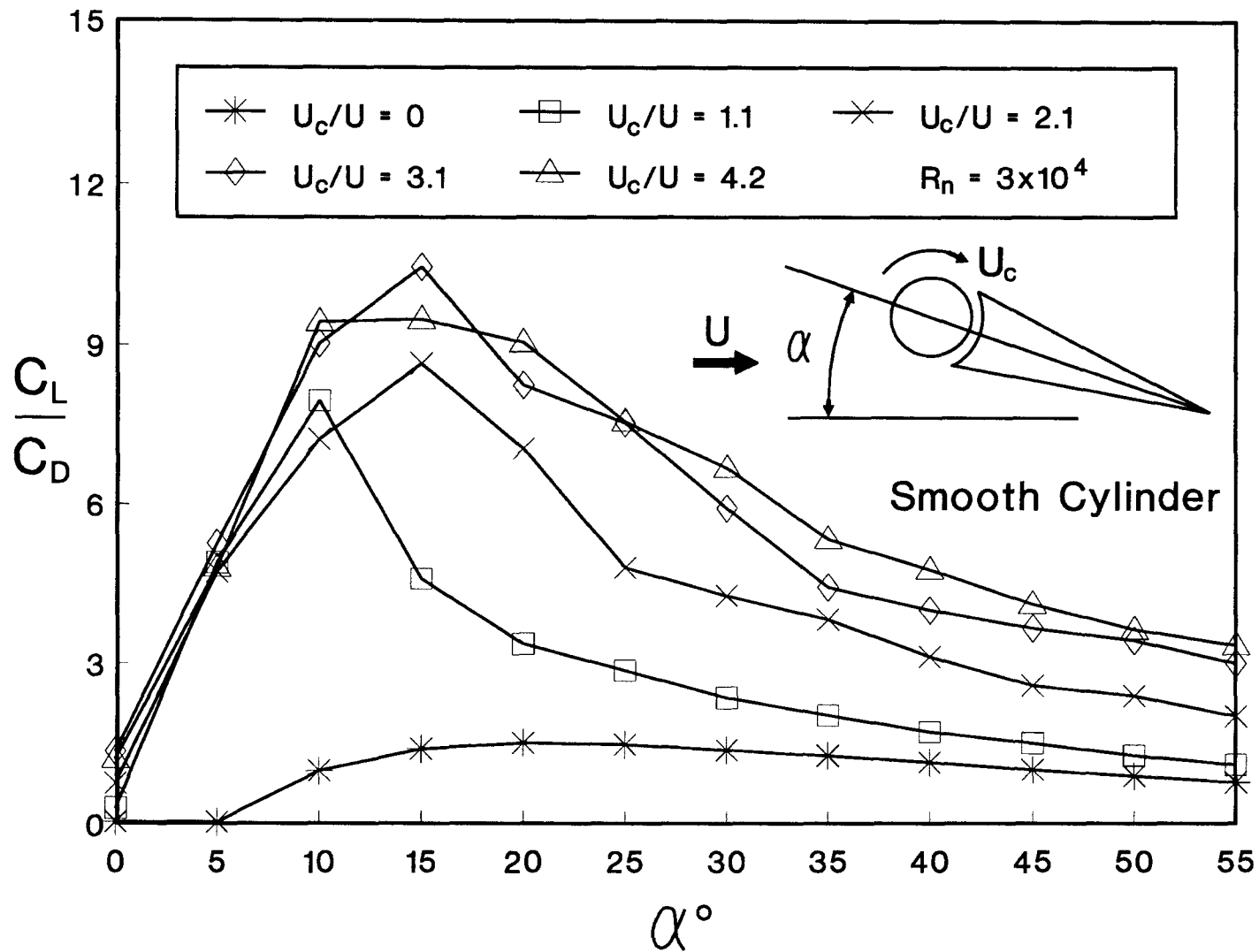


Figure 10. Aerodynamic coefficients for a two-dimensional wedge airfoil as affected by the rotation of the smooth cylinder: (c) C_L/C_D .

be to study the variation of C_L/C_D with α as affected by the cylinder rotation. This is shown in Figure 10c. Note, in absence of the cylinder rotation (reference case, U_c/U), the peak value of lift to drag ratio, $(C_L/C_D)_{\max}$, is around 1.58 (at $\alpha = 20^\circ$). It attains a value of $(C_L/C_D)_{\max} \approx 10.5$ at $\alpha = 15^\circ$ and $U_c/U \approx 3$, an increase of around 580% !

It seems logical that character of the cylinder surface roughness should improve the efficiency of the process of momentum injection. Hence, as mentioned before, the experiments were carried out with five distinctly different rough surfaces (Figure 4).

For the helical-groove cylinder (Figure 11) at $\alpha = 55^\circ$ the maximum lift changes from $C_{L_{\max}} \approx 1.98$ to 4.58 with the speed of the cylinder increasing from $U_c/U = 0$ to 4, an increase of around 130% (Fig. 11a). The corresponding drag deduction is around 21% from the $C_{D_{\max}} \approx 1.8$ down to 1.4 at the same angle of attack (Figure 11b). It is interesting to note that now the $(C_L/C_D)_{\max} \approx 16$ at $\alpha = 15^\circ$ and $U_c/U \approx 2$ (Fig. 11c), an increase by a factor ≈ 10.5 (compared to the reference value of 1.58). This suggests that an optimum choice of cylinder surface can improve the momentum injection and hence delay the boundary-layer separation.

To that end, the cylinder surface characterized by slotted squares (roughness squares) and splines running parallel to the cylinder axis appeared promising. Figure 12-14 show some typical results for the three surface characteristics: roughness squares, spline-1 and spline-2). The mechanism of

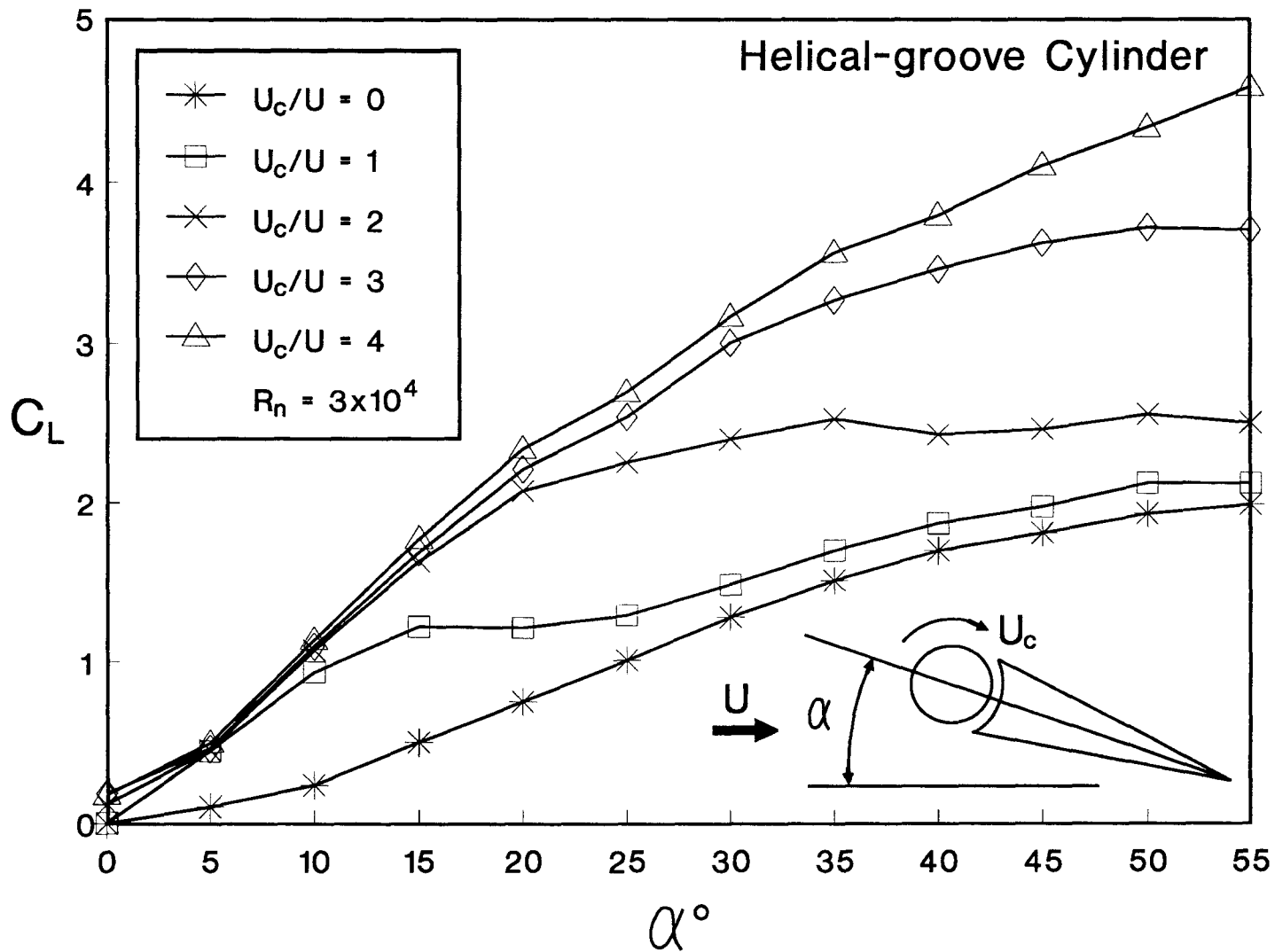


Figure 11. Variation of the aerodynamic coefficients with the angle of attack and helical groove cylinder rotation: (a) lift;

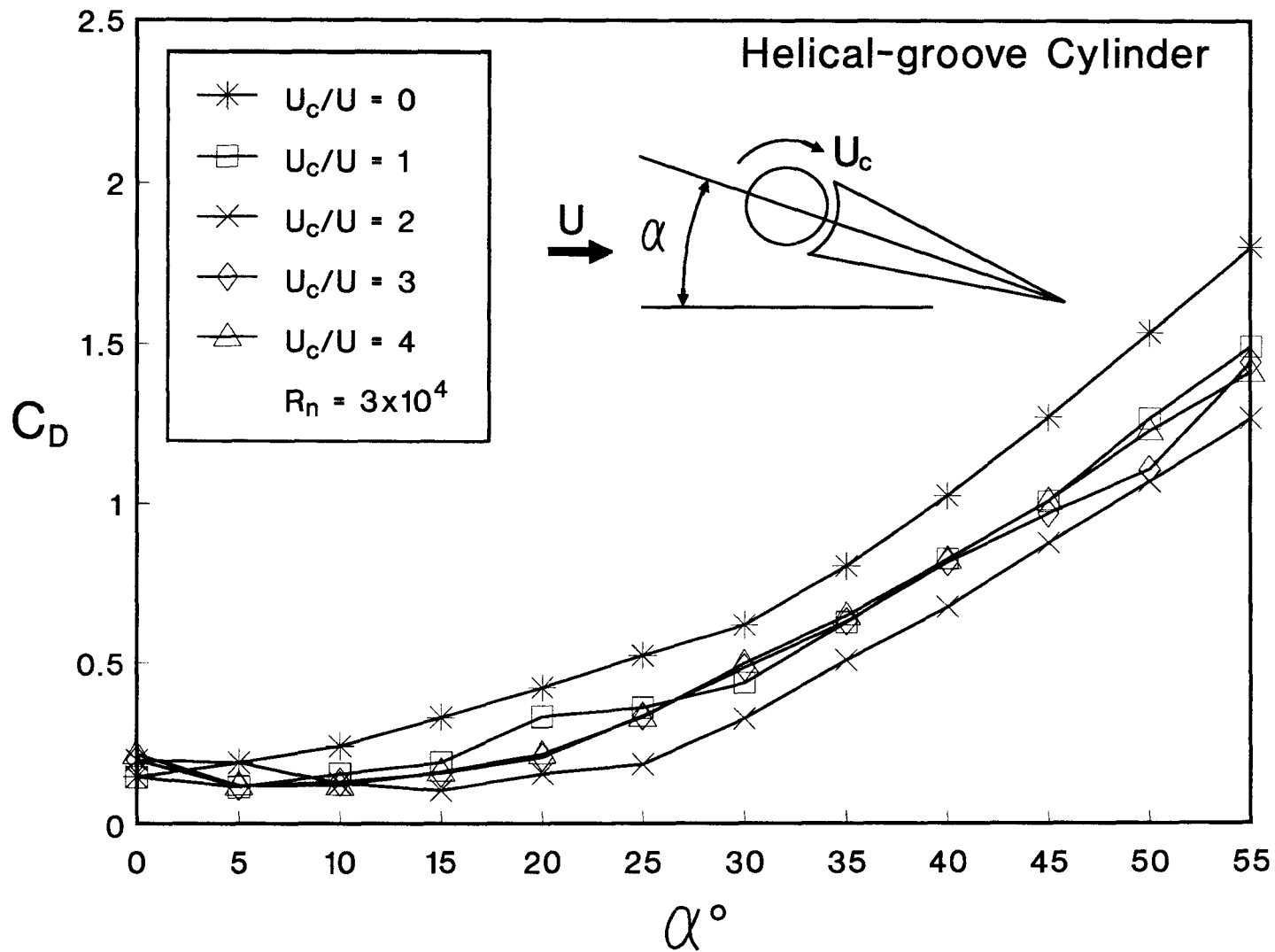


Figure 11. Variation of the aerodynamic coefficients with the angle of attack and helical groove cylinder rotation: **(b)** drag;

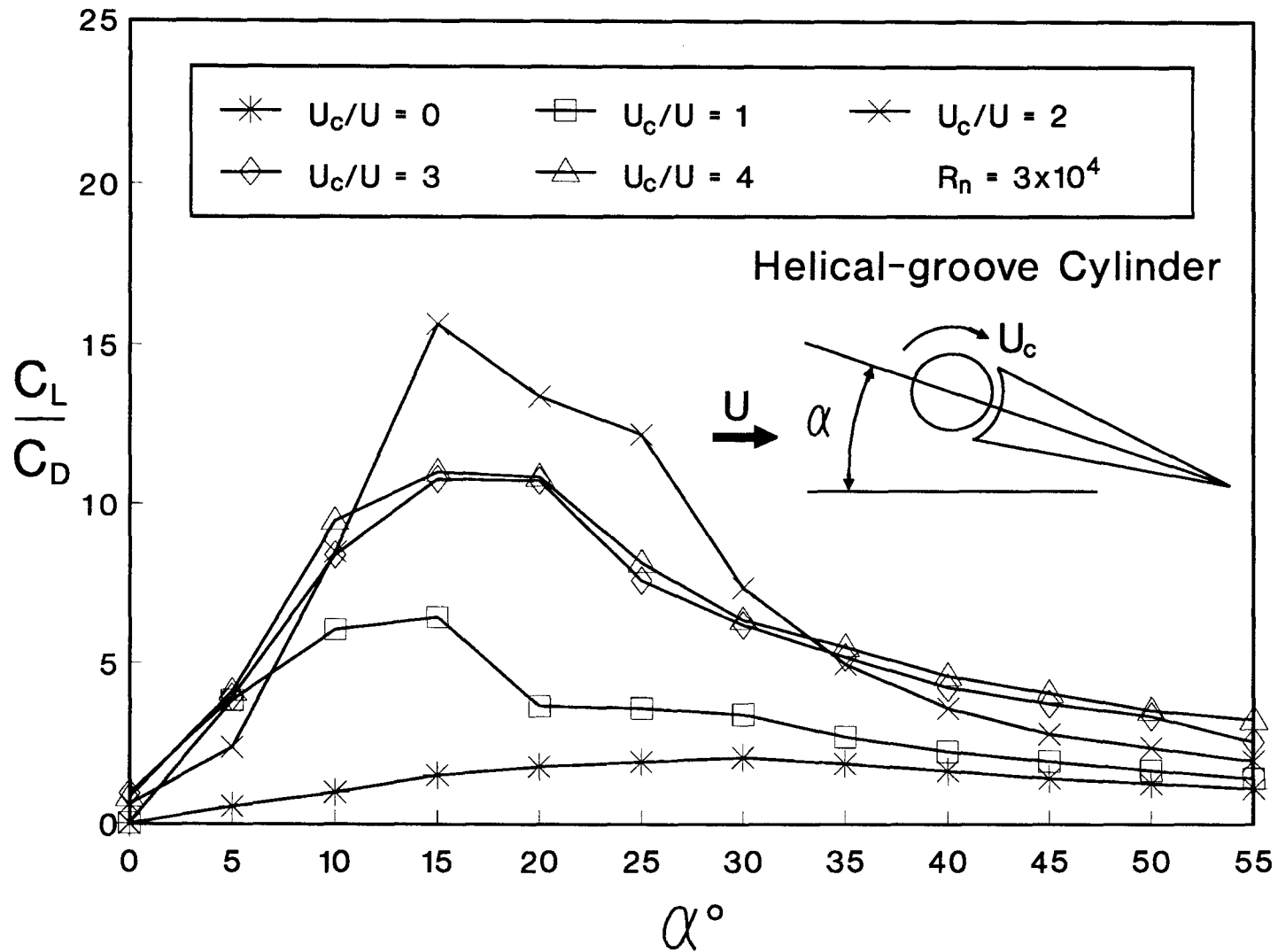


Figure 11. Variation of the aerodynamic coefficients with the angle of attack and helical groove cylinder rotation: (c) C_L/C_D .

momentum injection in the two cases, roughness squares and splines, appears to be fundamentally different. Square projections serve as large scale roughness elements rendering the flow turbulent. Splines, on the other hand, act like turbine blades thus injecting momentum in a more direct way. With the roughness square case, the peak lift coefficient attained a value of 4.15 at $\alpha = 50^\circ$ and $U_c/U = 4$ (compared to C_{Lmax} of 1.5 for the reference case) as shown in Figure 12a. In general, the drag coefficient also reduced as expected (Figure 12b). As before, the optimum performance appears to occur at a lower angle of attack of $\alpha = 15^\circ$ where C_L/C_D of around 22 is realized (Figure 12c), an increase by a factor of 13 !

Effectiveness of the spline geometry as a momentum injection device is illustrated rather dramatically by the performance plots in Figure 13. Simultaneous increase in C_L and decrease in C_D leads to an optimum value of $\alpha = 15^\circ$ where C_L/C_D reaches a spectacular value of around 75 !

Of course, this suggests that spline geometry itself should be studied thoroughly through a systematic variation of the spline parameters: width, height, taper, number, etc. Obviously, this represents a project in itself and beyond the scope and focus of the present study. However, to gain some appreciation, a cylinder with rounded splines was constructed as explained before (spline-2). Although the further improvement in performance is only marginal with $(C_L/C_D)_{max}$ rising to $\approx 80^\circ$ at $\alpha = 15$, it is indeed distinct and definite (Figure 14c). Such an increase in $(C_L/C_D)_{max}$ by a factor of around 52

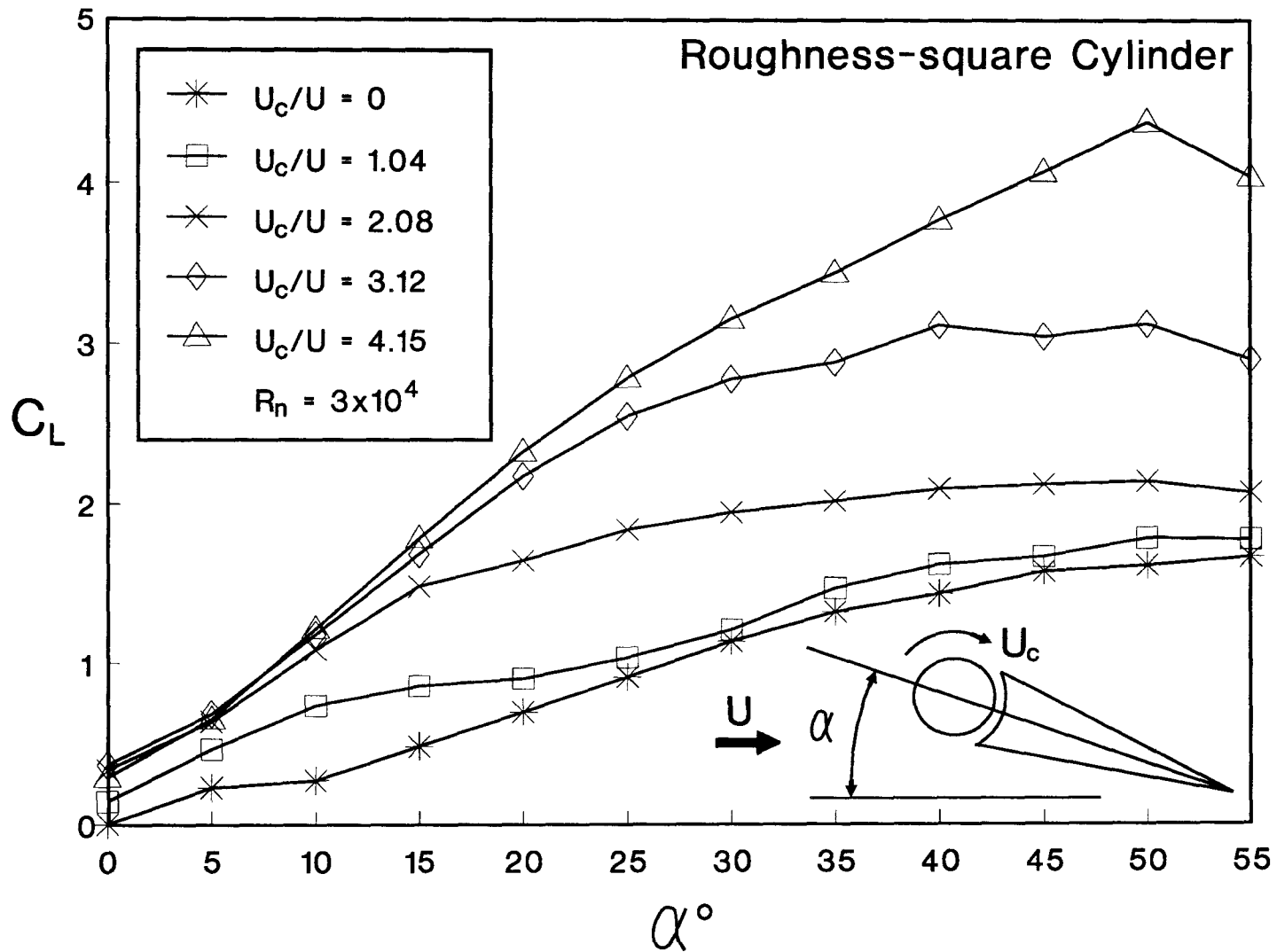


Figure 12. Plots showing effect of the cylinder surface roughness condition on the lift and drag coefficient: (a) C_L ;

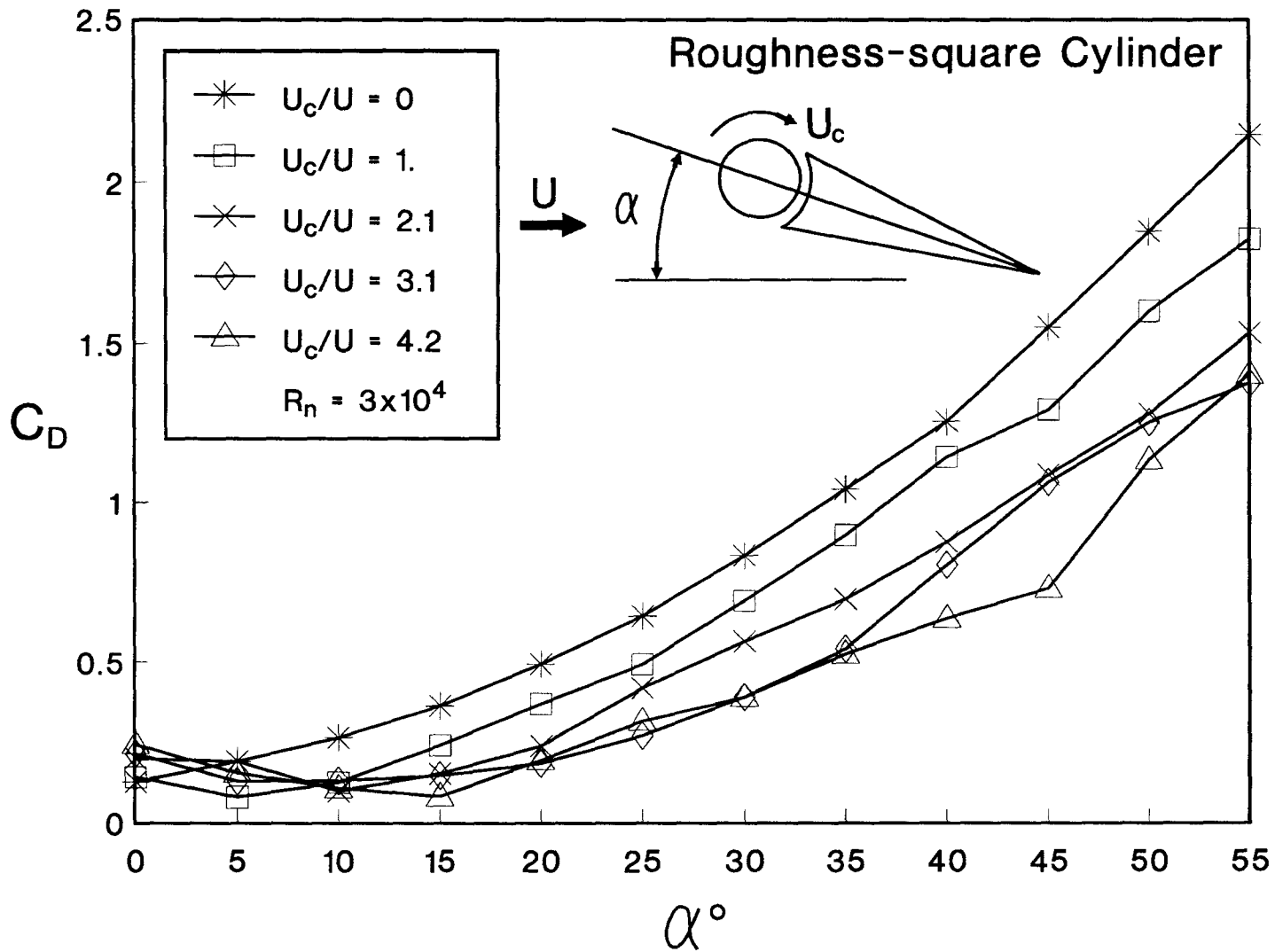


Figure 12. Plots showing effect of the cylinder surface roughness condition on the lift and drag coefficient: **(b)** C_D ;

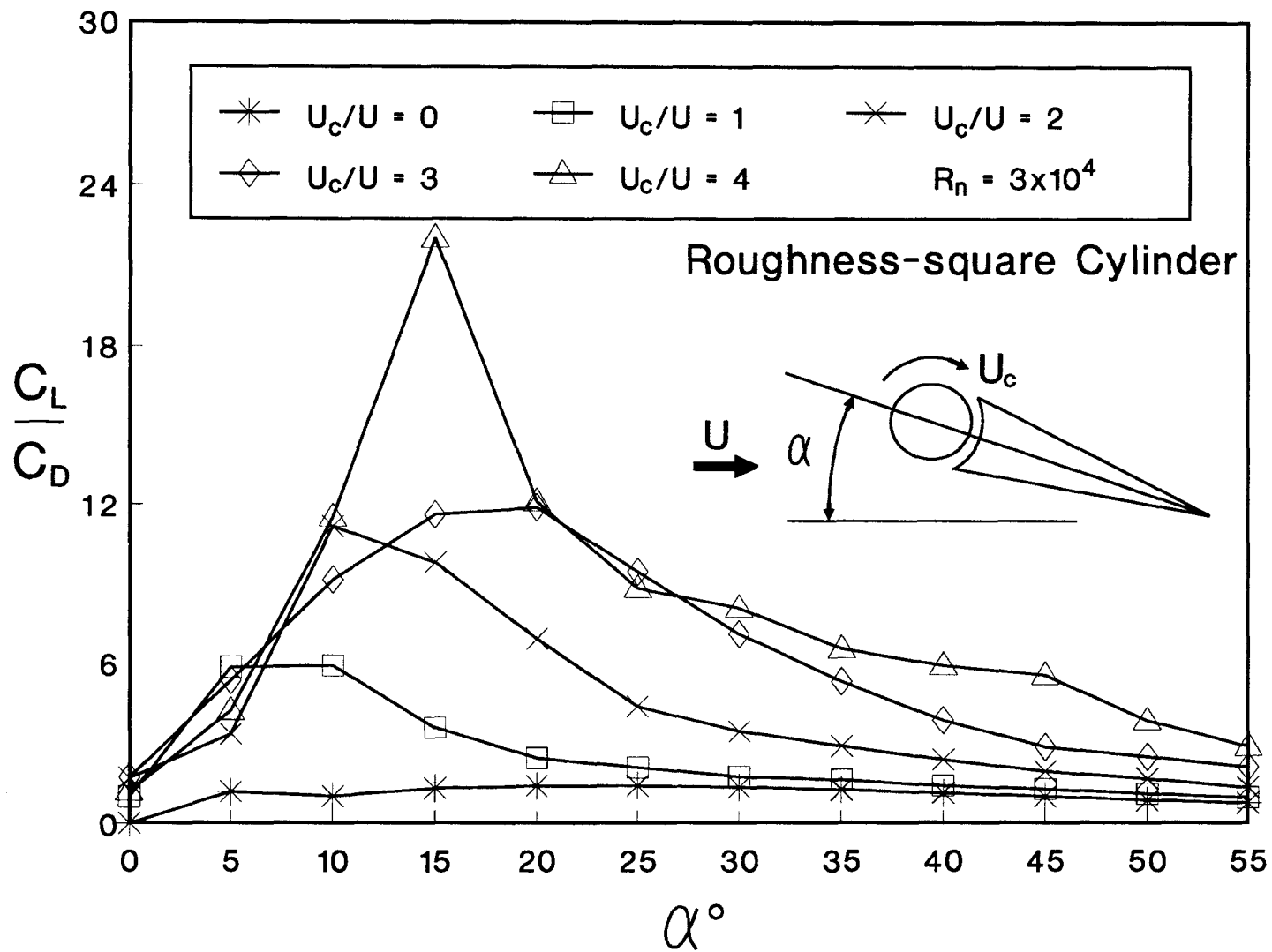


Figure 12. Plots showing effect of the cylinder surface roughness condition on the lift and drag coefficient: (c) C_L/C_D .

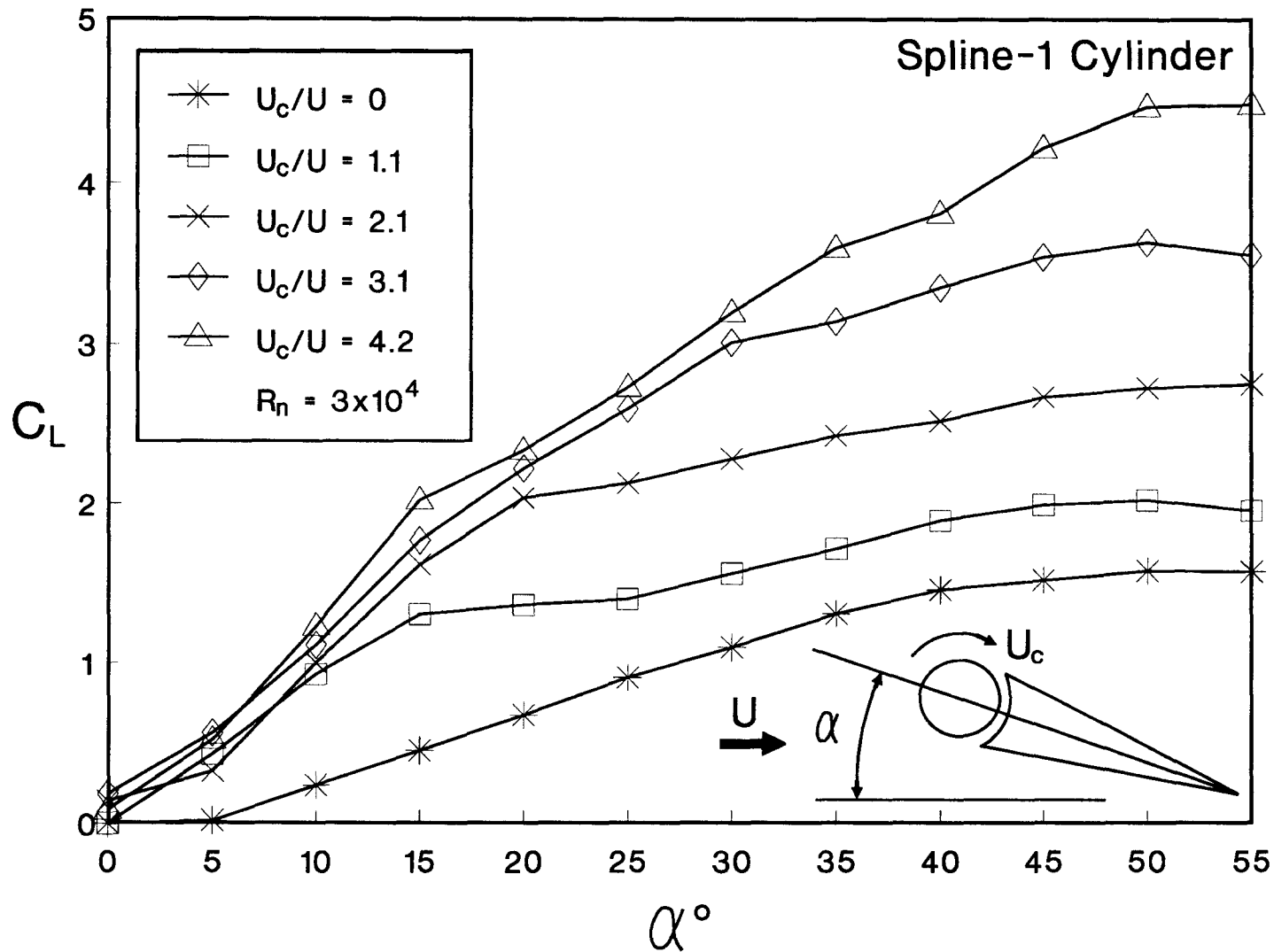


Figure 13. Influence of axial surface grooves on the momentum injection (spline-1) as reflected through the variation of lift and drag coefficients: (a) C_L ;

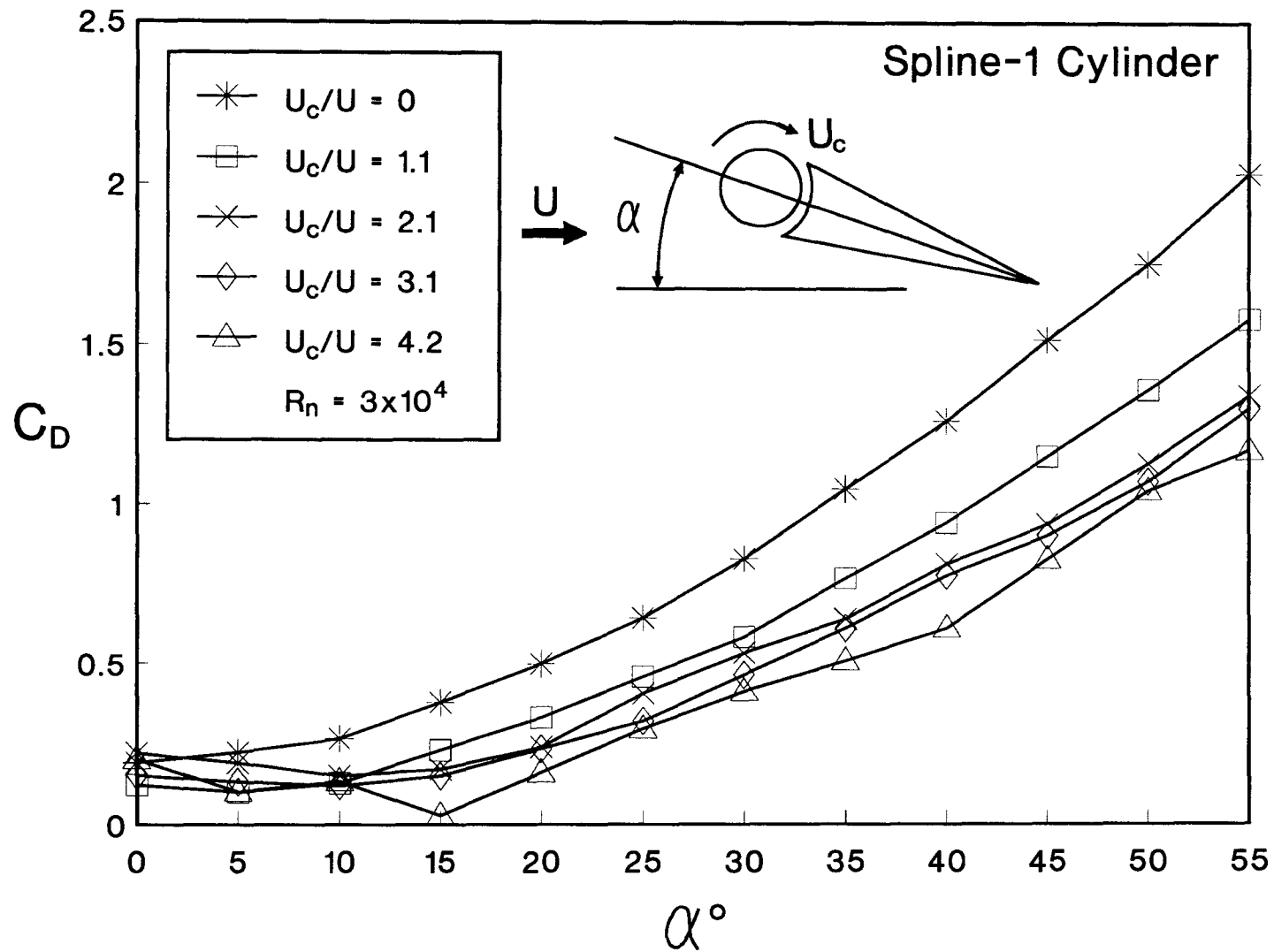


Figure 13. Influence of axial surface grooves on the momentum injection (spline-1) as reflected through the variation of lift and drag coefficients: (b) C_D ;

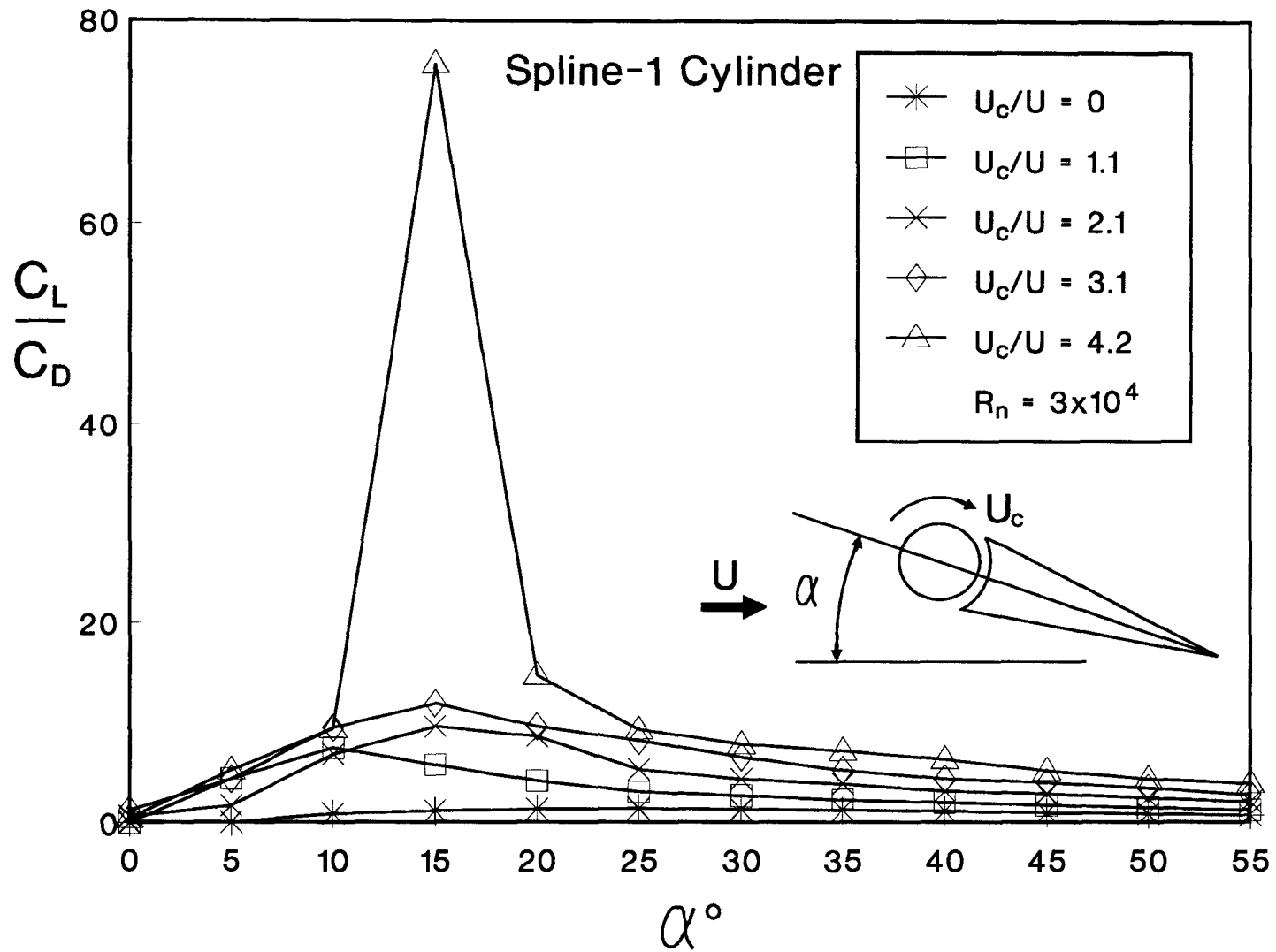


Figure 13. Influence of axial surface grooves on the momentum injection (spline-1) as reflected through the variation of lift and drag coefficients: (c) C_L/C_D .

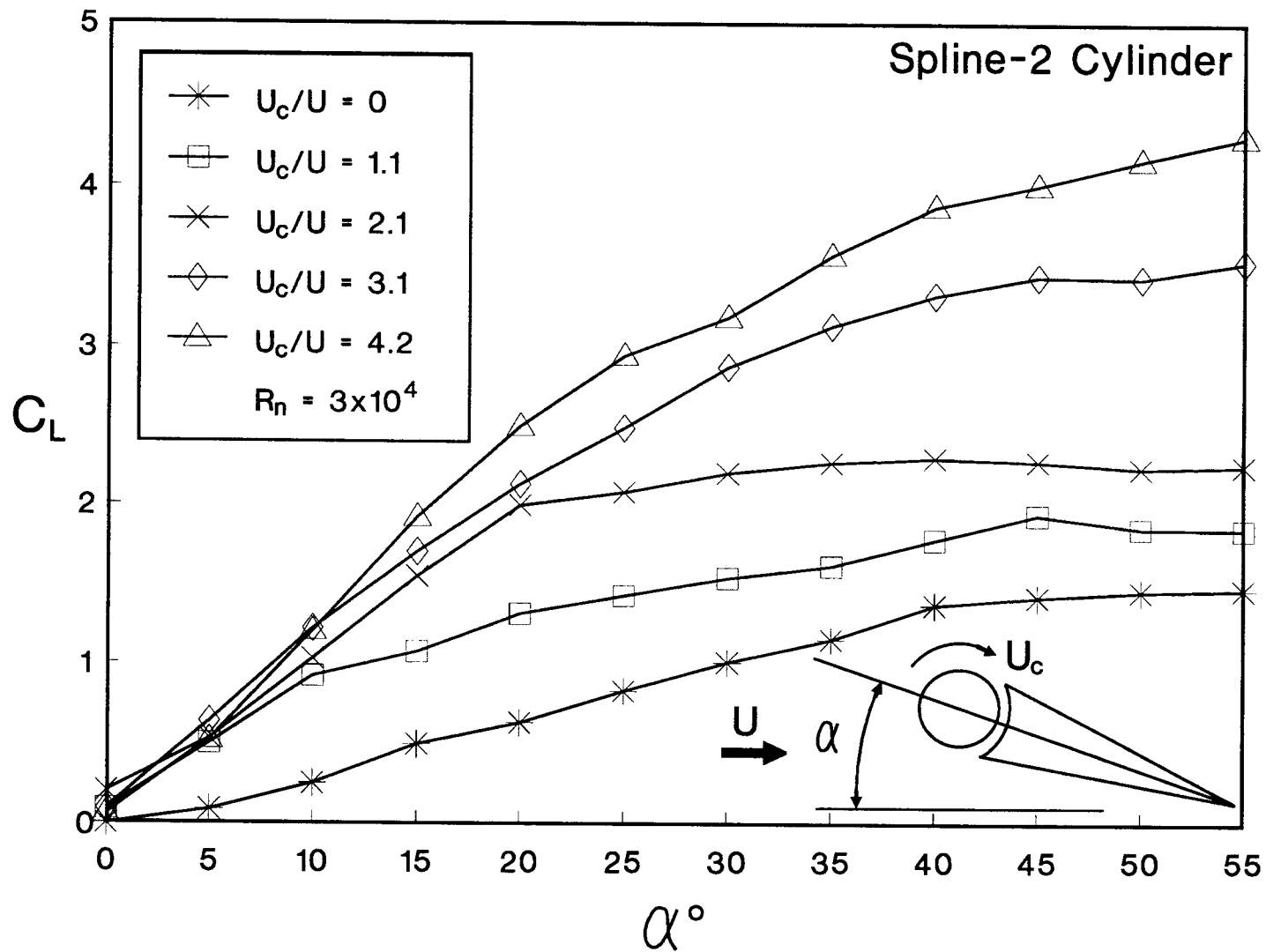


Figure 14. Effect of the surface roughness designated as spline-2 on the aerodynamic coefficients: (a) C_L ;

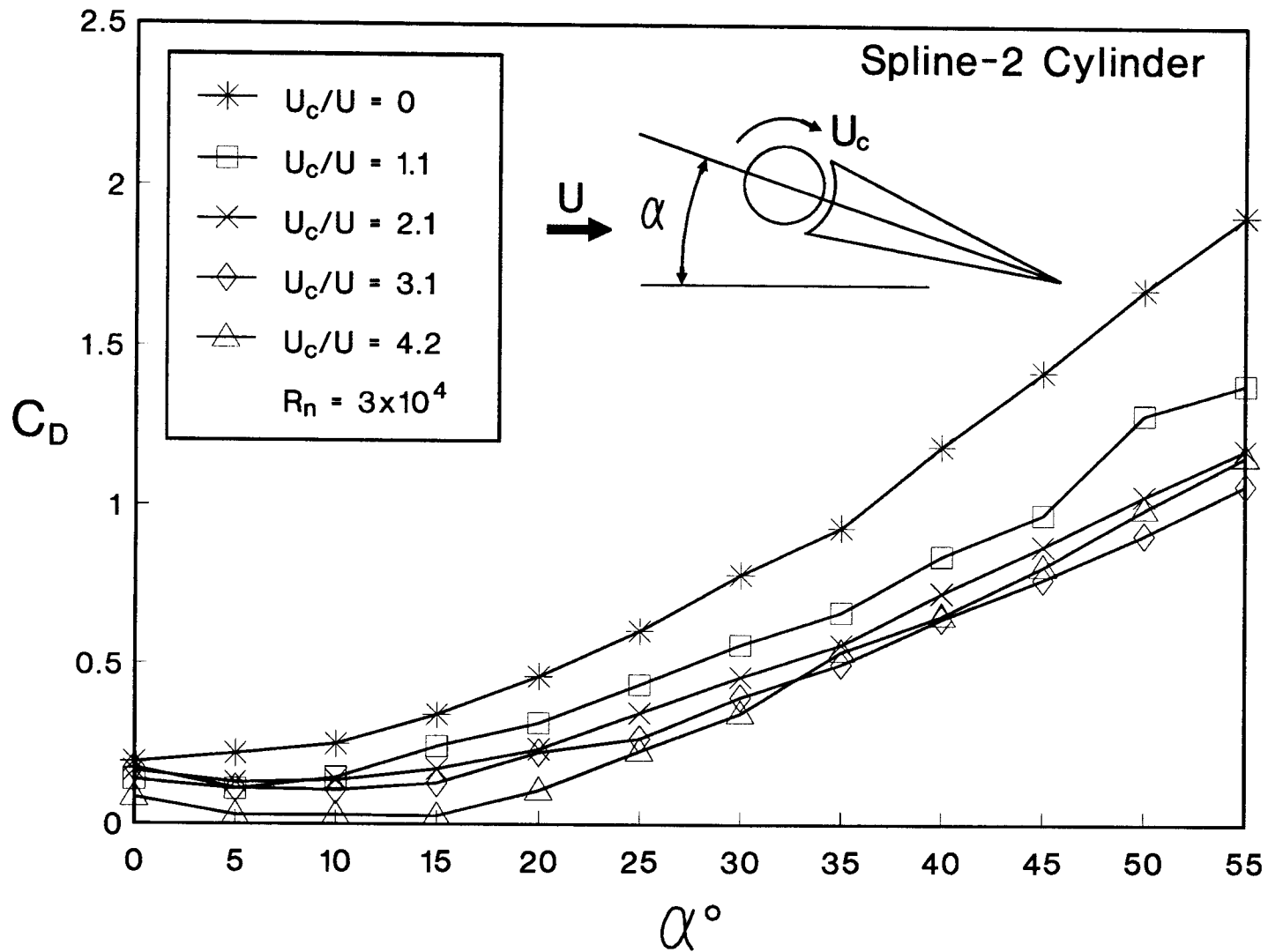


Figure 14. Effect of the surface roughness designated as spline-2 on the aerodynamic coefficients: **(b)** C_D ;

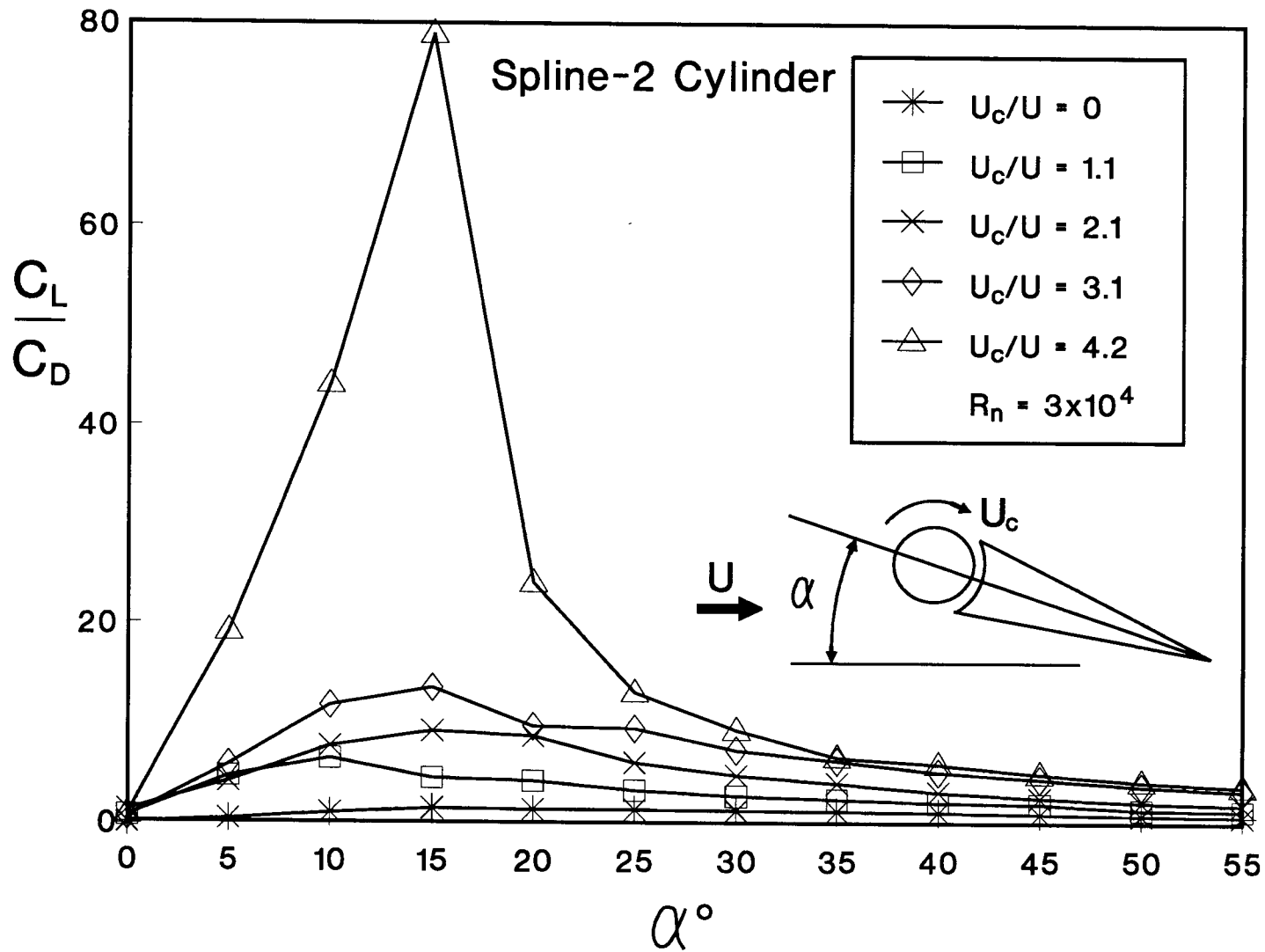


Figure 14. Effect of the surface roughness designated as spline-2 on the aerodynamic coefficients: (c) C_L/C_D .

(compared to the reference case) can be used to advantage by the next generation of highly manoeuvrable airplanes.

Figure 15 summarizes the results concerning C_{Lmax} , C_{Dmin} and $(C_L/C_D)_{max}$ as affected by the cylinder surface roughness. It is interesting to note that although the maximum lift coefficient is associated with higher α ($\alpha = 50^\circ$ or 55° , Figure 15a) the $(C_L/C_D)_{max}$ corresponds to α in the range of 15° to 20° (Figure 15c). Of course, this is because of the drag characteristics as shown in Fig. 15b. It is useful to recognize that before differences in shape of the splines, as with the spline-1 and spline-2 cases, have relatively little effect on C_{Lmax} , C_{Dmin} and $(C_L/C_D)_{max}$.

To have better appreciation as to the character of the flow in presence of the MSBC, a flow visualization study was undertaken with the help and test facility of Professor T. Yokomizo*. The tests were carried out in a water channel (Figure 16) using slit lighting with polyvinyl chloride particles serving as tracers. The flow visualization pictures were taken over a range of model orientation, cylinder surface condition and speed. A video was also taken. The test Reynolds number, based on the free stream speed and chord length was around 3×10^4 . Although this is close to the wind tunnel test condition, it is

* Dr. T. Yokomizo, Professor, Department of Mechanical Engineering, Kanto Gakuin University, Mitsuura, Kanazawa, Yokohama, Japan 239.

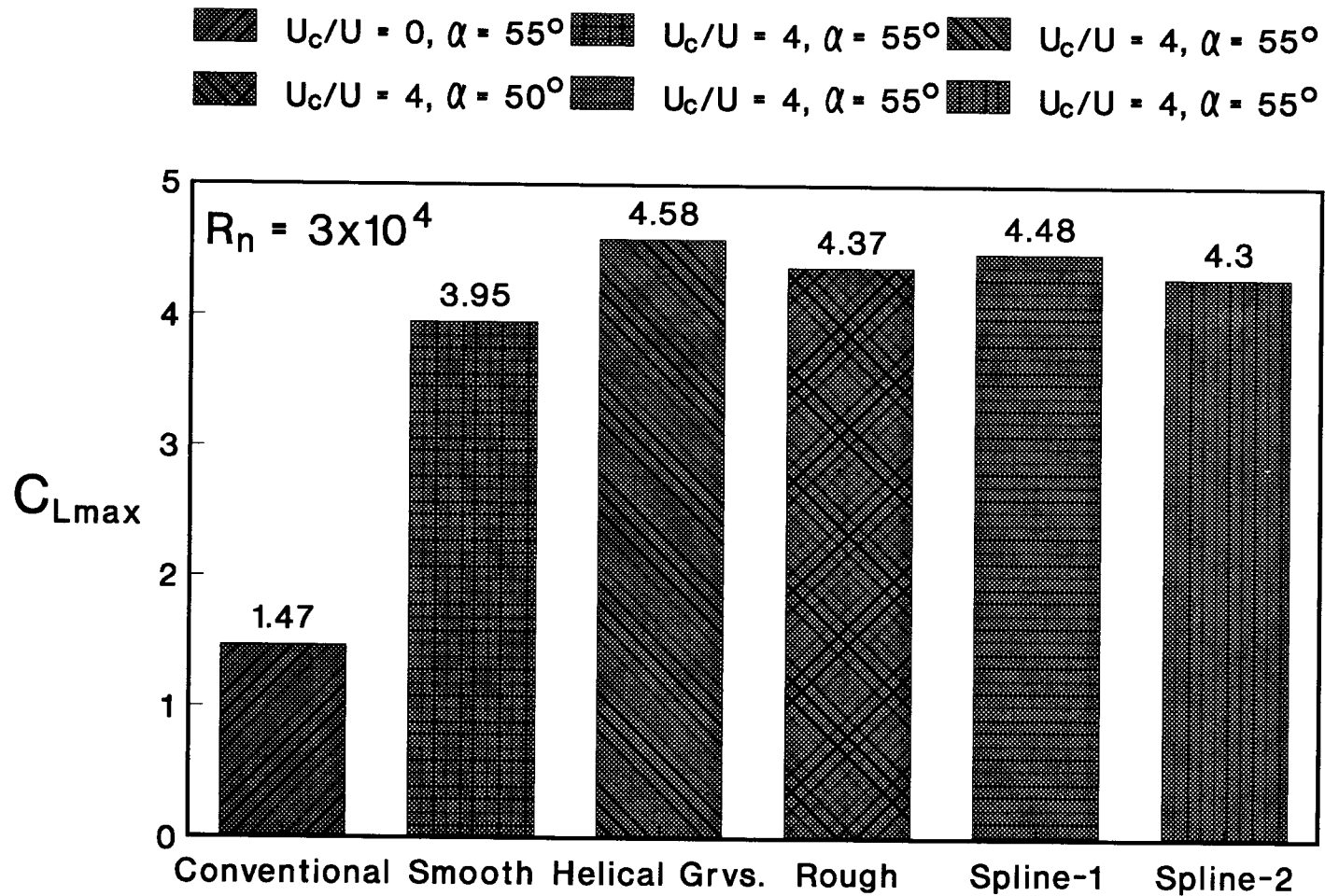


Figure 15. Comparison charts showing relative merit of the surface condition on the boundary-layer control: (a) C_{Lmax} ;

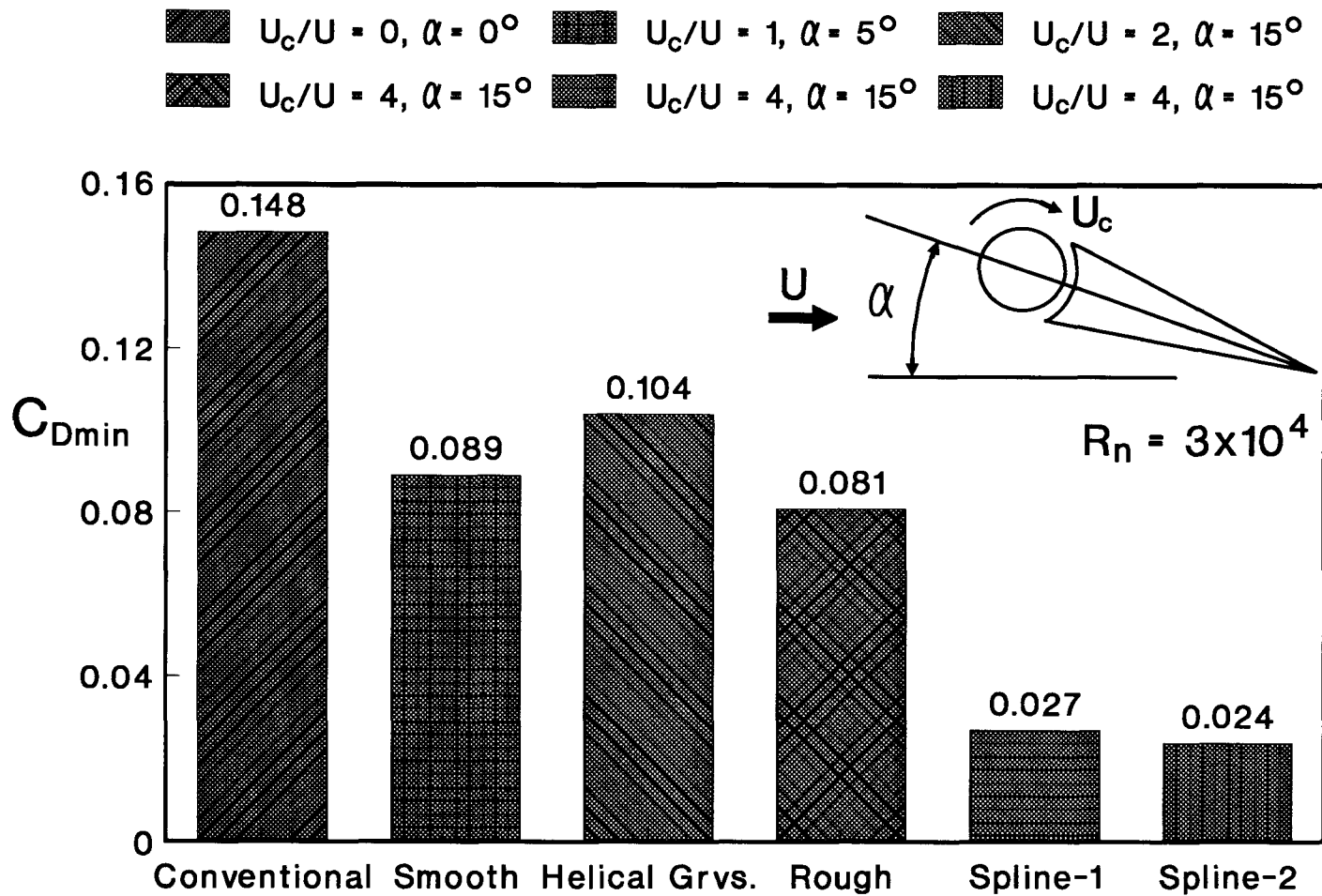


Figure 15. Comparison charts showing relative merit of the surface condition on the boundary-layer control: (b) C_{Dmin} ;

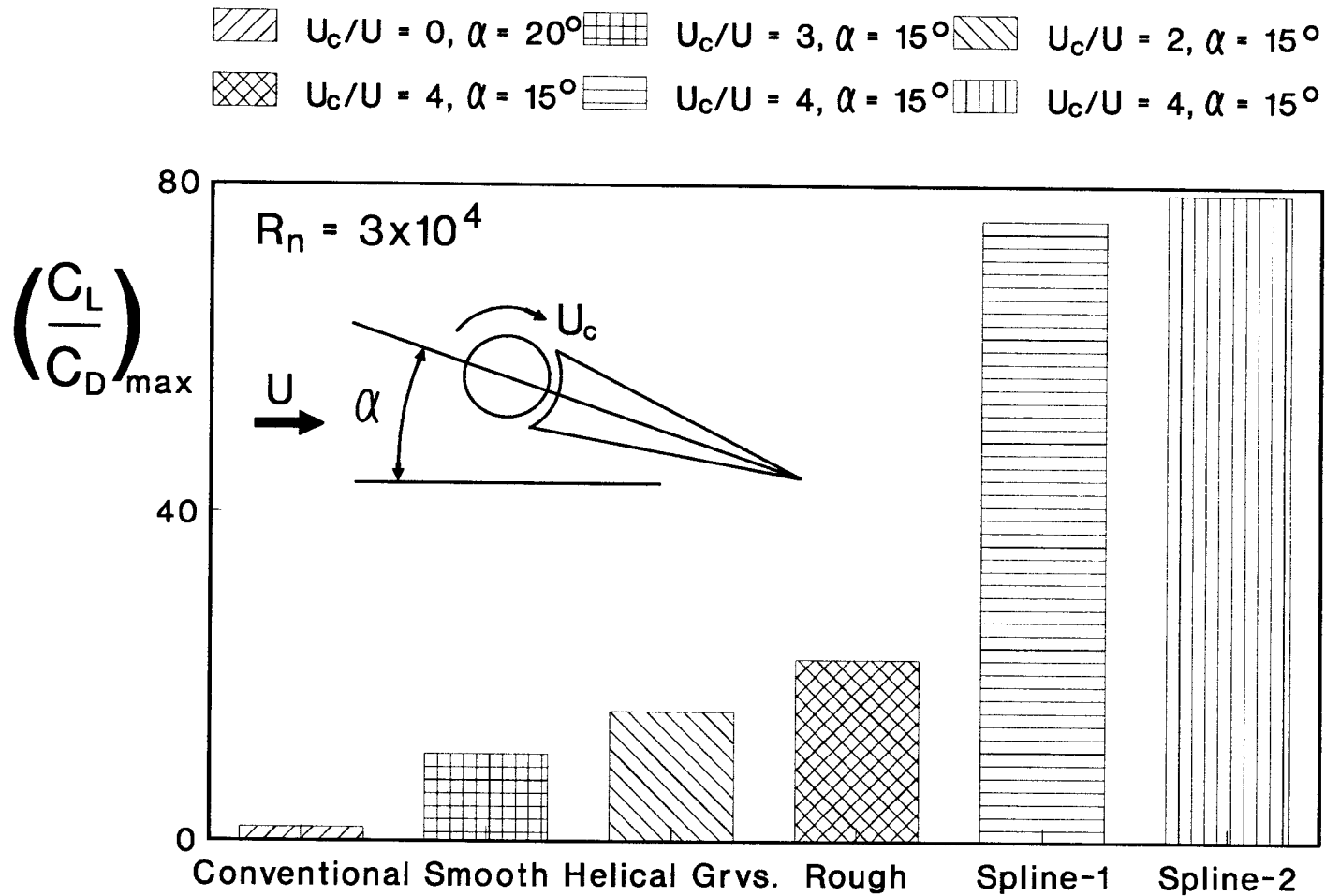


Figure 15. Comparison charts showing relative merit of the surface condition on the boundary-layer control: (c) $(C_L/C_D)_{\max}$.

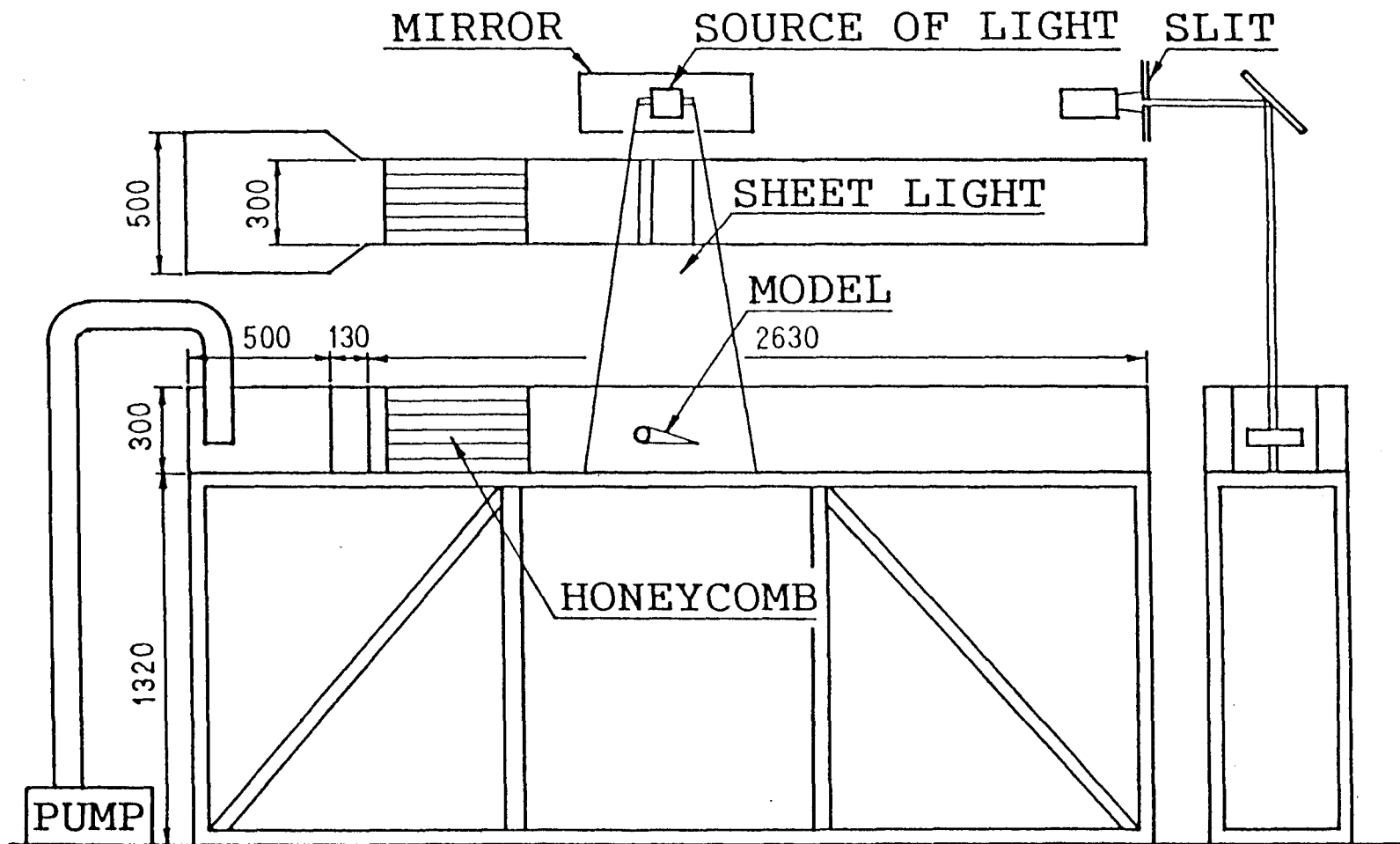


Figure 16. A schematic diagram of the closed circuit water channel facility used in the flow visualization study. Slit lighting was used to minimize distortion due to three dimensional character of the flow. Long exposure provided path-lines with polyvinyl chloride particles serving as tracers. The dimensions are in mm.

quite different from the real life situation. Hence the results should be considered only qualitative in character, however, they do show effectiveness of the moving surface boundary-layer control procedure.

Figure 17 shows typical pictures of flow past the wedge airfoil at $\alpha = 30^\circ$ as affected by the momentum injection. Effectiveness of MSBC is strikingly apparent even at such a high angle of attack. In fact the concept continues to be effective even for α as high as 55° (Figure 18) !

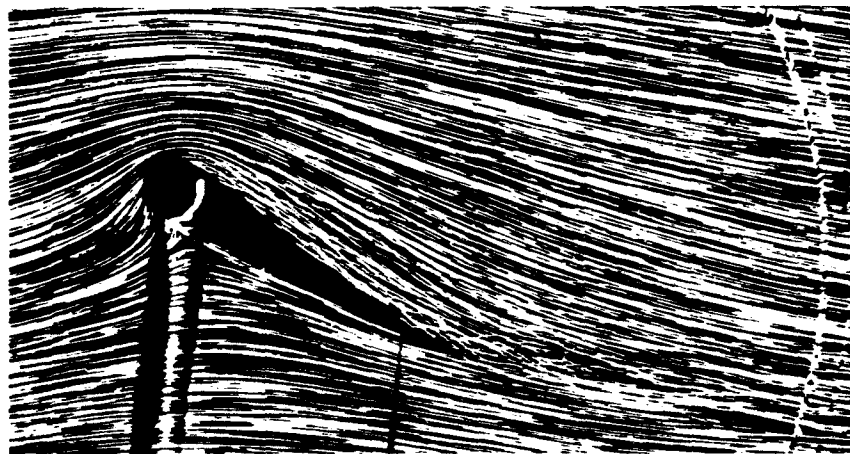
3.2 Tractor-trailer Truck Model with Twin Cylinders

Based on the 2-D wedge airfoil results the concept of the MSBC has been established and it was decided to apply this idea to a typical bluff body, a tractor-trailer truck, in a real life. The 2-D wedge airfoil data showed the importance of cylinder roughness in improving efficiency of the momentum injection process and associated reduction in the drag. Therefore, it seemed reasonable to introduce the momentum more directly to the tractor-trailer truck model. This was achieved in several ways:

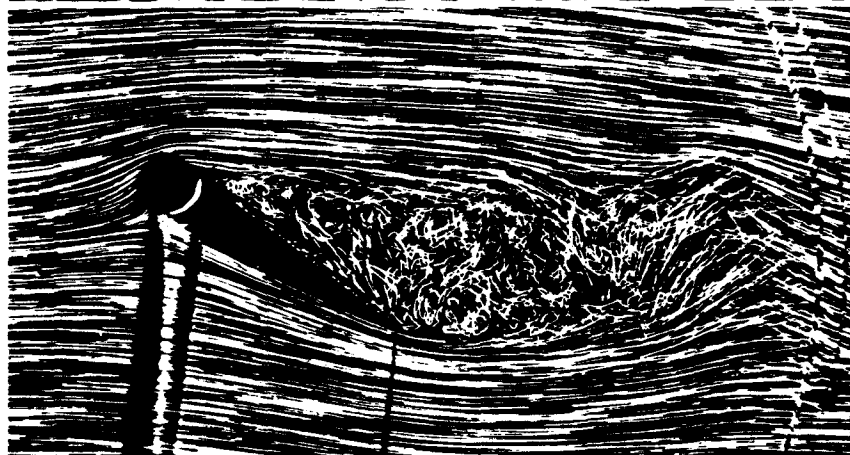
- (i) Modify the cylinder surface by coating it with sand particles (sandpaper of grades 80 and 40).
- (ii) Provide increased cylinder surface roughness through helical grooves or splines running parallel to the cylinder axis.
- (iii) Keep one cylinder at the top leading edge of the trailer (referred

$$\alpha = 30^\circ, \quad R_n = 3 \times 10^4$$

$$U_c/U = 4$$



$$U_c/U = 2$$



$$U_c/U = 0$$



Figure 17. Typical flow visualization photographs for a wedge shaped airfoil, with a smooth surface cylinder, showing remarkable effectiveness of the MSBC concept for $\alpha = 30^\circ$, $R_n = 3 \times 10^4$. Note the progressive downstream shift of the separation point as the U_c/U increase. Eventually the flow appears to approach the potential character.

$$\alpha = 55^\circ, \quad R_n = 3 \times 10^4$$

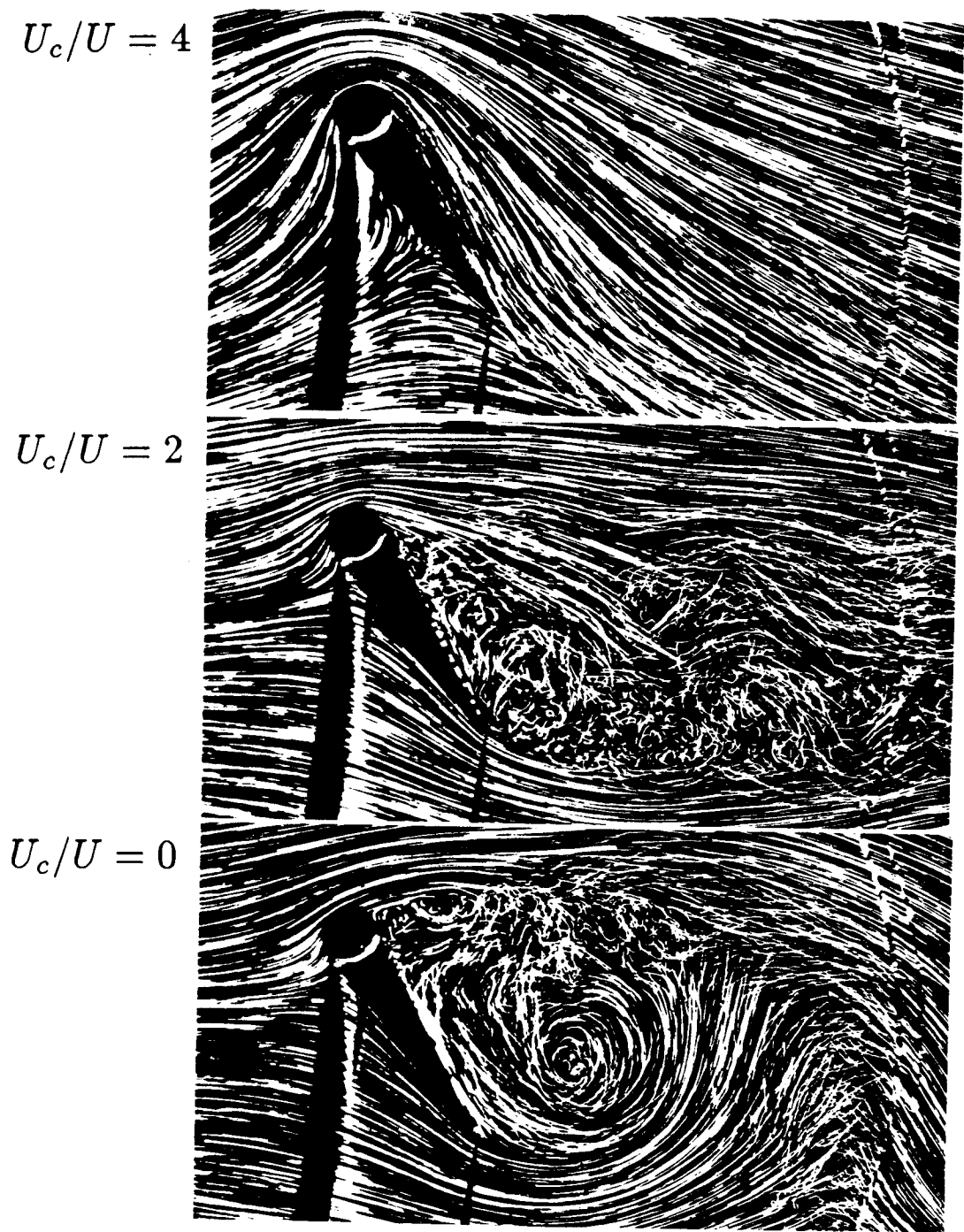


Figure 18. The concept of moving surface boundary-layer control continues to be effective even at a high angle of attack of 55° as shown dramatically by these flow visualization pictures ($R_n = 3 \times 10^4$)

to as the front cylinder) and locate the second cylinder (rear cylinder) at an optimum distance downstream. Objective is to inject additional momentum in the boundary-layer to compensate for dissipation of the momentum introduced by the front cylinder and thus counter the emergence of adverse pressure gradient.

- (iv) Raise the cylinders so as to immerse them in the boundary-layer and assess the effect of cylinder orientation.

Tests with a 1/12 scale model of the truck were carried out in the boundary-layer tunnel with negligible blockage effect (blockage ratio = 1.2%). The trailer was provided with rotating cylinders at its top leading edge and downstream locations. The L/H ratio for the trailer was approximately 3.75 which suggested that rotation of the trailing edge cylinder will have virtually no effect on the drag reduction. The wind tunnel tests substantiated this observation. Figure 19 shows variation of C_D with the cylinder speed ratio U_c/U for three cases: cylinder with smooth surface; cylinder surface roughness of grade 80; and cylinder surface roughness of grade 40. In absence of the momentum injection ($U_c/U = 0$), the truck drag coefficient is around 0.81 and reduces to 0.765 at $U_c/U = 2$ for the smooth cylinder case. The surface roughness of the cylinder improves the performance further reducing C_D to around 0.73 at $U_c/U = 2.1$ for the roughness grade of 80. Increasing the surface roughness to 40 drops the minimum C_D to 0.7, a reduction of around 13%.

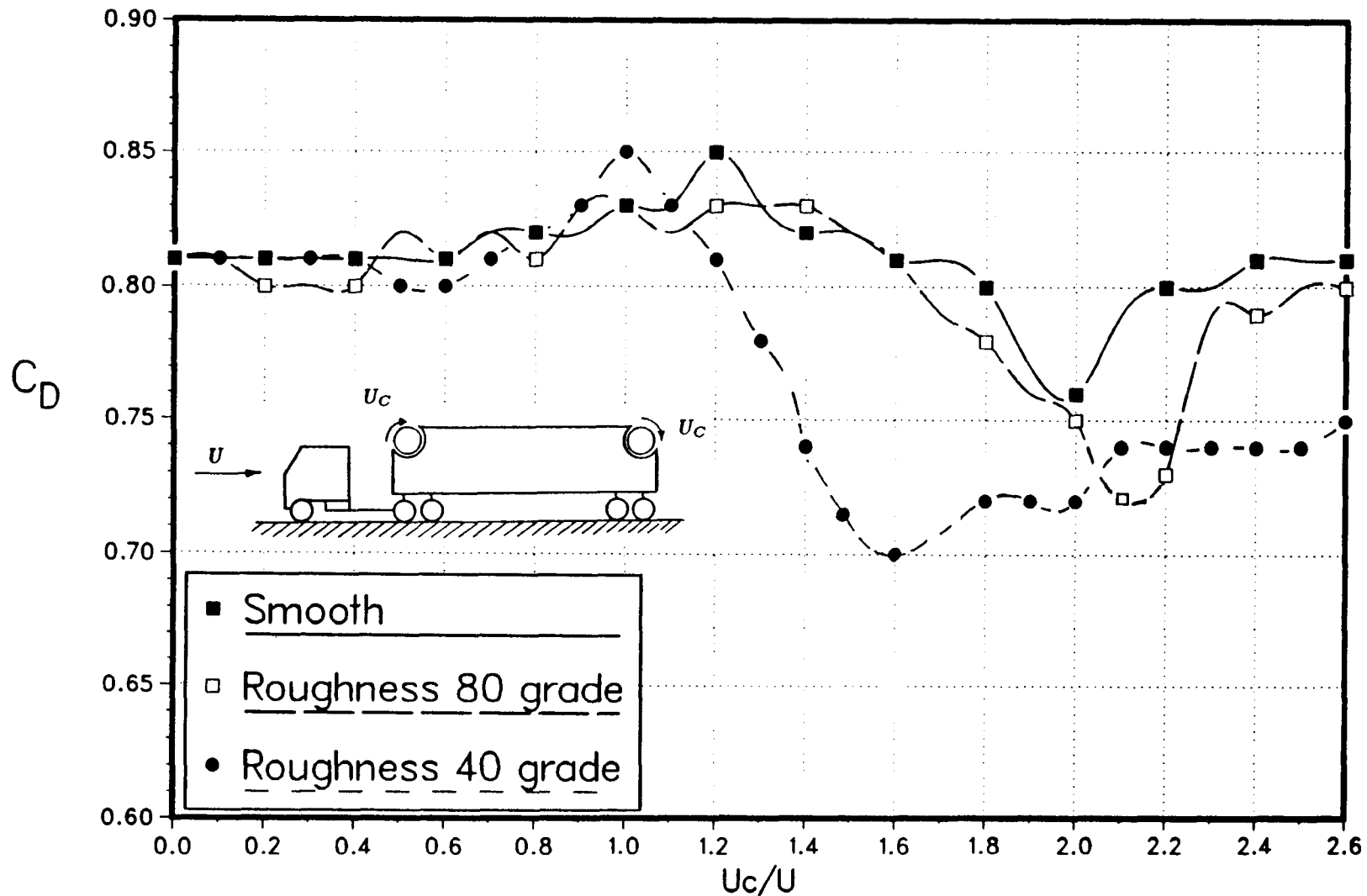


Figure 19. Effect of the moving surface boundary-layer control on the drag coefficient of a tractor-trailer truck configuration. Note, an increase in the sandpaper roughness contributes to the drag reduction through efficient momentum injection.

For the subsequent studied in (ii), (iii) and (iv) a different model of the tractor trailer configuration was used (also 1/12 scale). It had corresponded to the configuration selected for future road-tests. The cylinder orientations studied with helical and spline set of cylinders are indicated in Table 1.

Figure 20 shows effect of the twin cylinders with helical grooves. At the outset it is apparent that the front cylinder rotation reduces the drag as before, however, character of the plot is rather different. There is a monotonic reduction in the drag coefficient with U_{cf}/U ($U_{cr}/U = 0$). Although the rear cylinder rotation further diminishes C_D , the reduction is relatively small. Raising the cylinders does improve efficiency of the momentum injection, however, the maximum drag reduction attained was around 14.3% (Case 2, Figure 20b), not much different than that given by the grade 40 sandpaper (Figure 19).

On the other hand, the spline cylinder reduces the drag coefficient dramatically. To begin with, it should be recognized that the base drag coefficient of the truck with flush mounted spline cylinders in a absence of rotation is higher than before (1.12 against 1.015 for the helical groove cylinders, Case 1). Note, with the spline cylinder raised and with only the front cylinder rotating ($U_{cf}/U = 6.1$), the drag coefficient reduces by about 37% (Figure 21f). With the rear cylinder rotation, the drag reduction jumps to 52% (Case 6, $U_{cf}/U = 6.1$, $U_{cr}/U = 5.7$). Even with the speed ratio of 4, the C_D reduced by around 26%. Thus the spline geometry with raised position of the

Table 1. Wind tunnel tests conducted with different orientation of the twin helical-groove and spline cylinders: location of the front cylinder was at the top leading edge and the rear cylinder at 25.4 cm downstream from the leading edge.

Case	CYLINDER ORIENTATION	
	Front Raised, mm	Rear Raised,mm
1	—	—
2	—	6.35
3	—	12.7
4	6.35	12.7
5	6.35	—
6	12.7	—
7	12.7	6.35
8	12.7	12.7
9	6.35	6.35

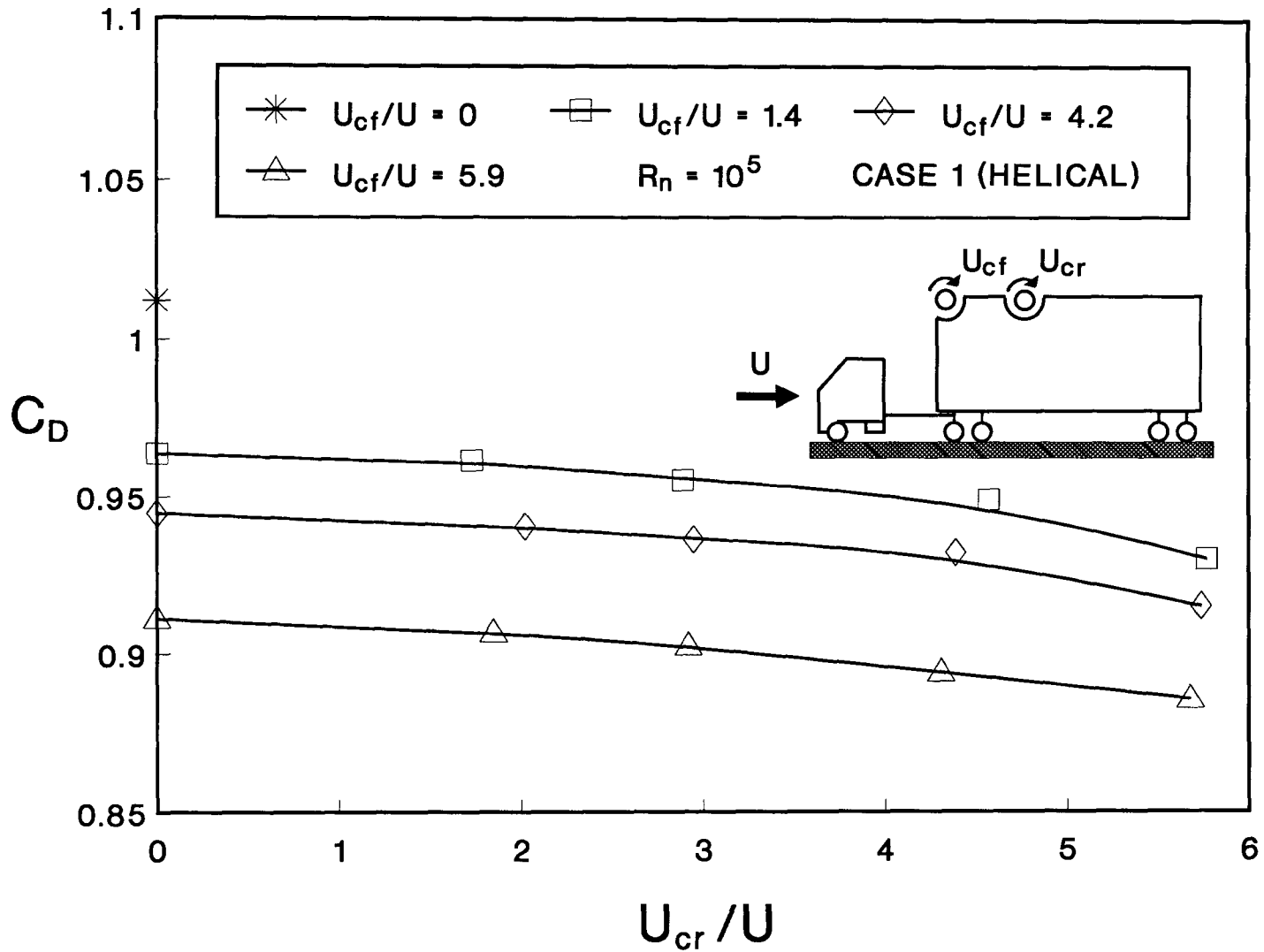


Figure 20. Effect of the twin helical cylinder configuration on the momentum injection and boundary-layer control: (a) Case 1: both cylinders flush;

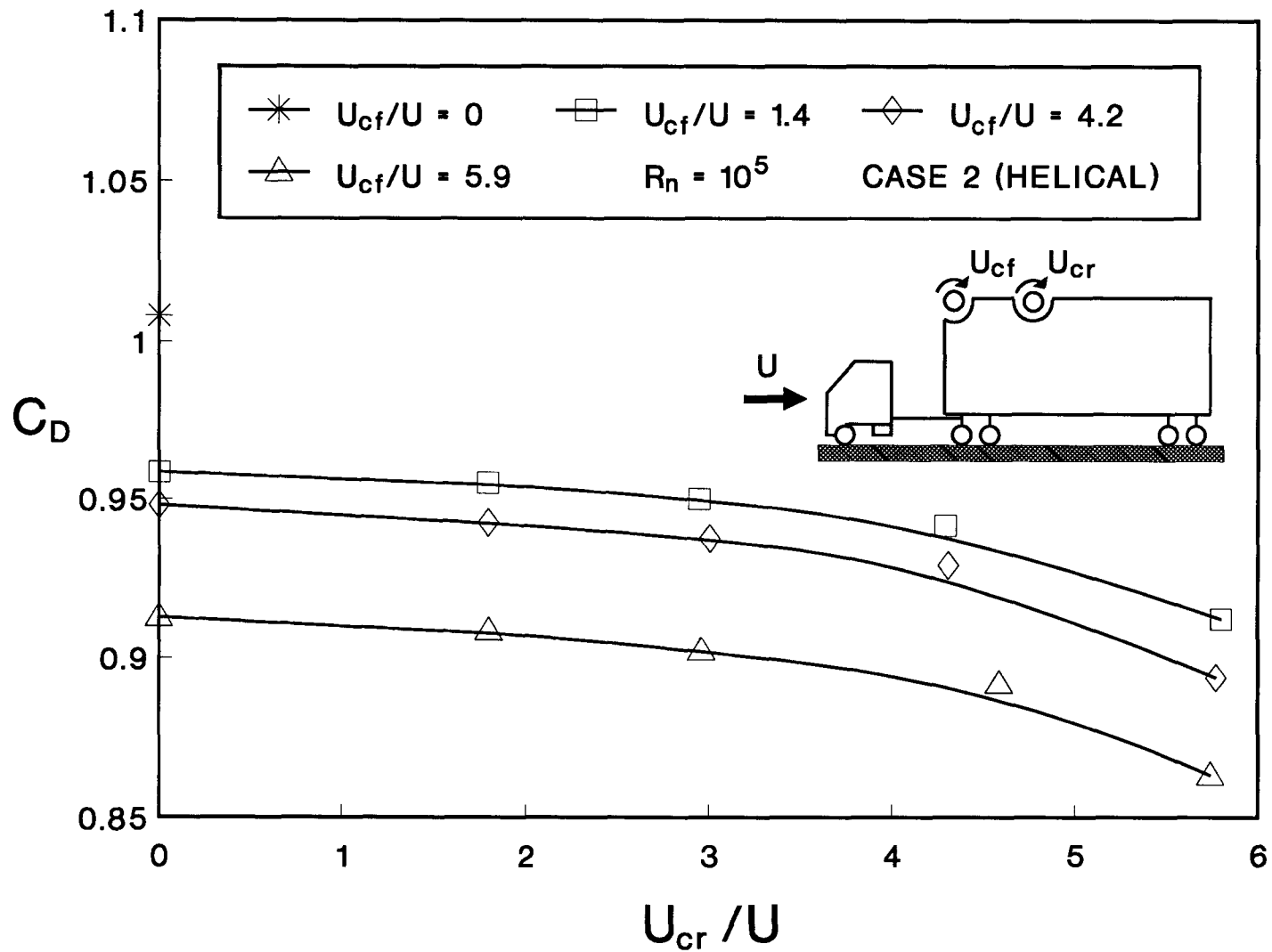


Figure 20. Effect of the twin helical cylinder configuration on the momentum injection and boundary-layer control: **(b)** Case 2: front cylinder flush, rear cylinder raised 6.35 mm;

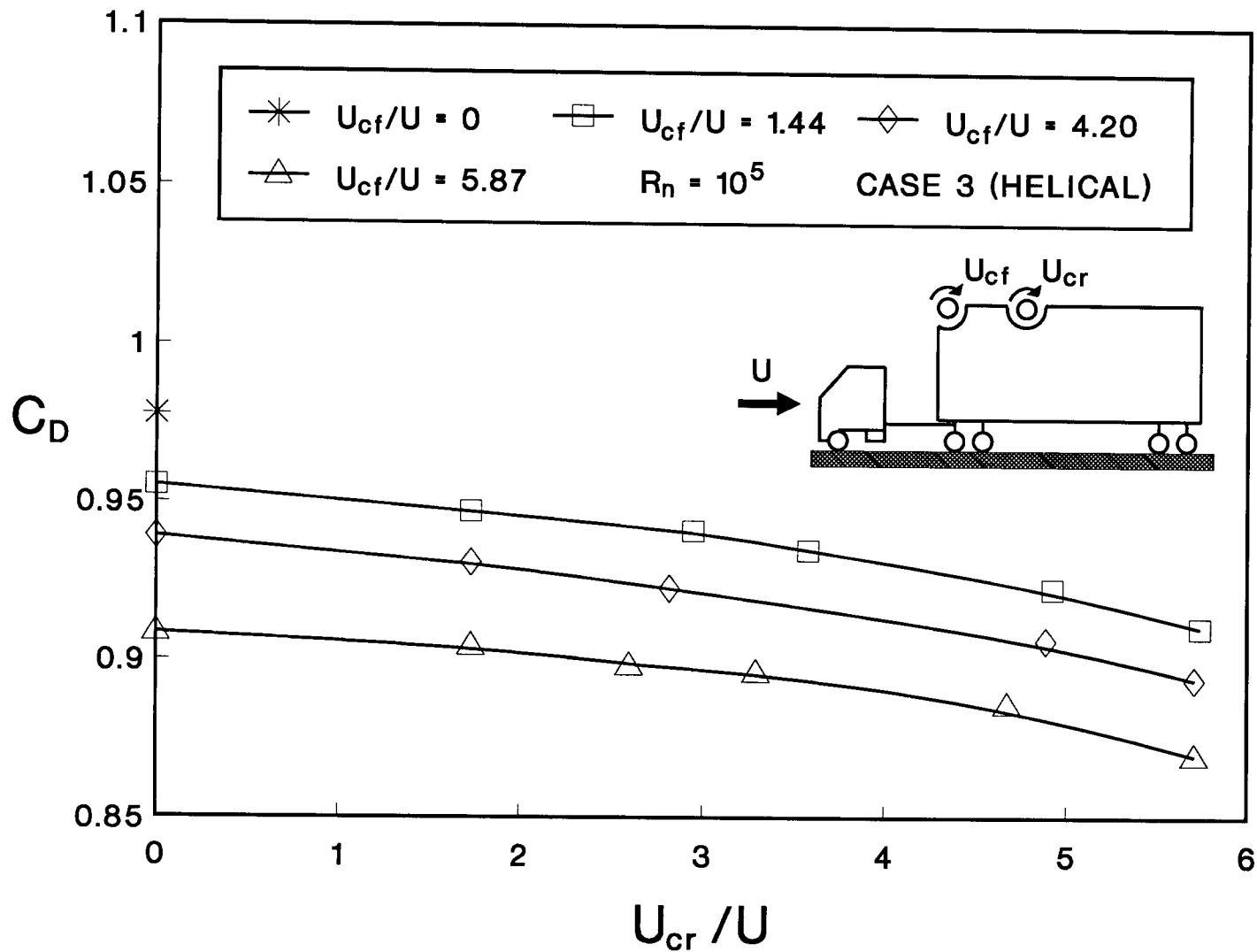


Figure 20. Effect of the twin helical cylinder configuration on the momentum injection and boundary-layer control: (c) Case 3: front cylinder flush, rear cylinder raised 12.7 mm;

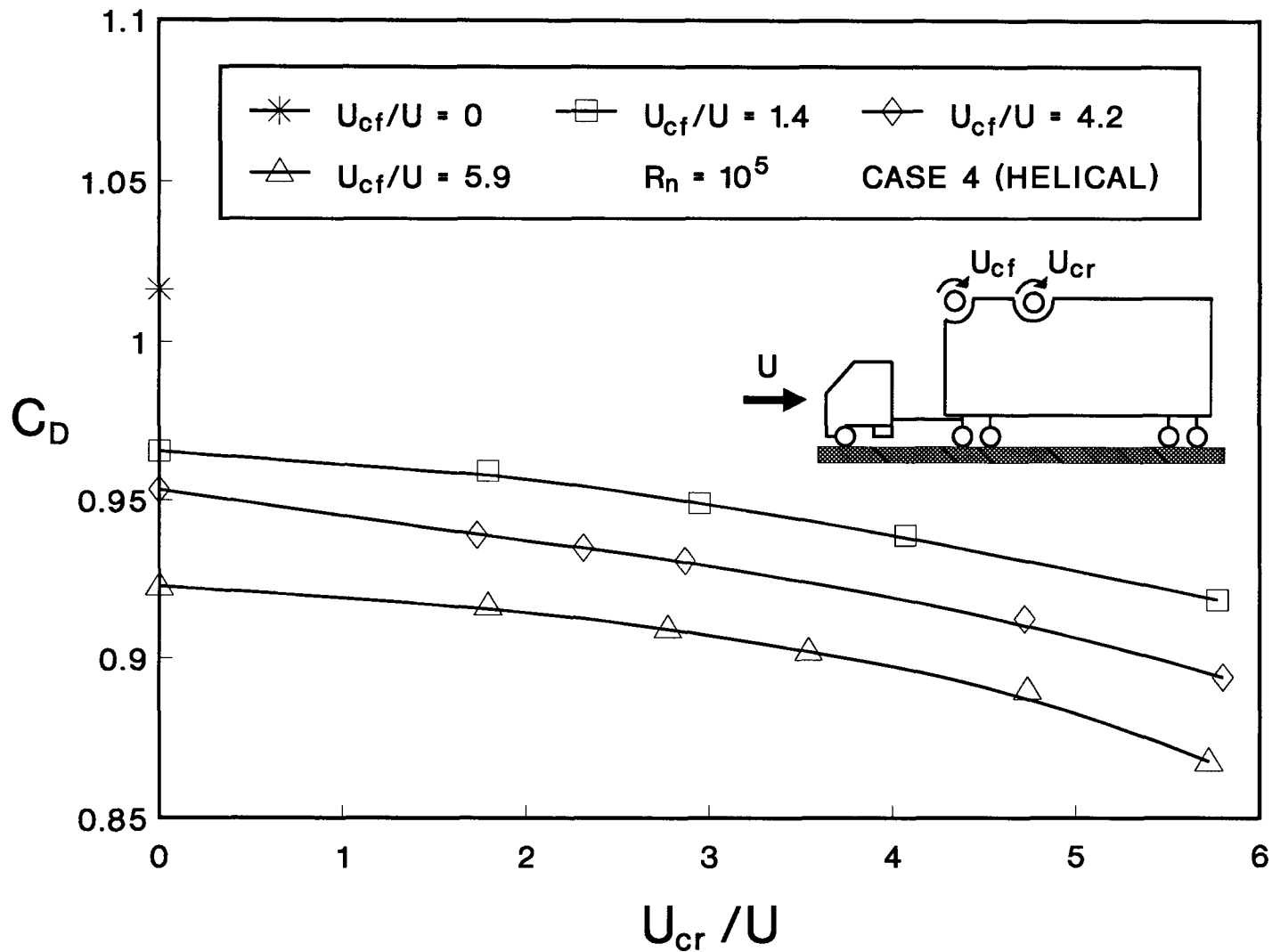


Figure 20. Effect of the twin helical cylinder configuration on the momentum injection and boundary-layer control: (d) Case 4: front cylinder raised 6.35 mm, rear cylinder raised 12.7 mm;

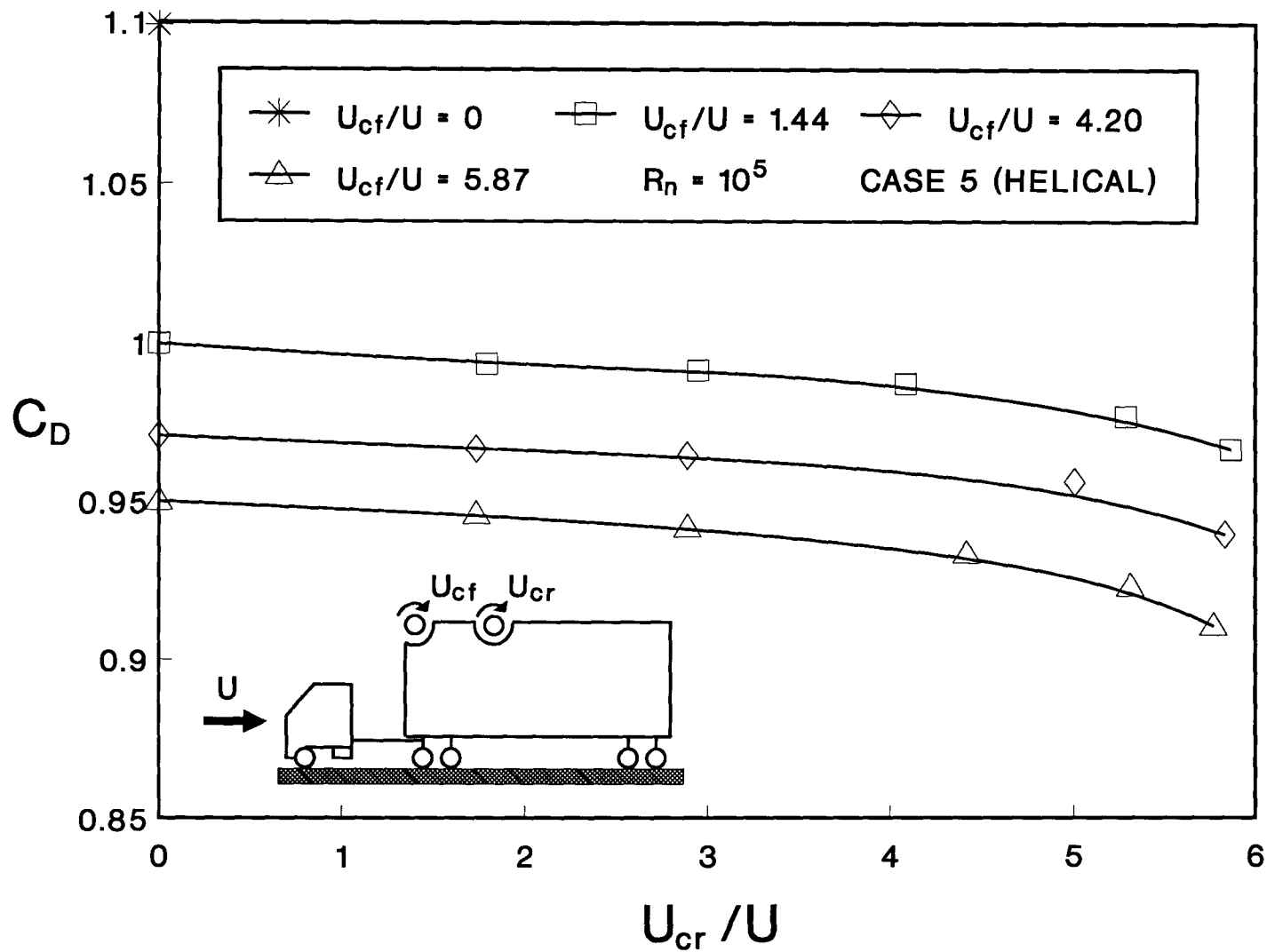


Figure 20. Effect of the twin helical cylinder configuration on the momentum injection and boundary-layer control: (e) Case 5: front cylinder raised 6.35 mm, rear cylinder flush;

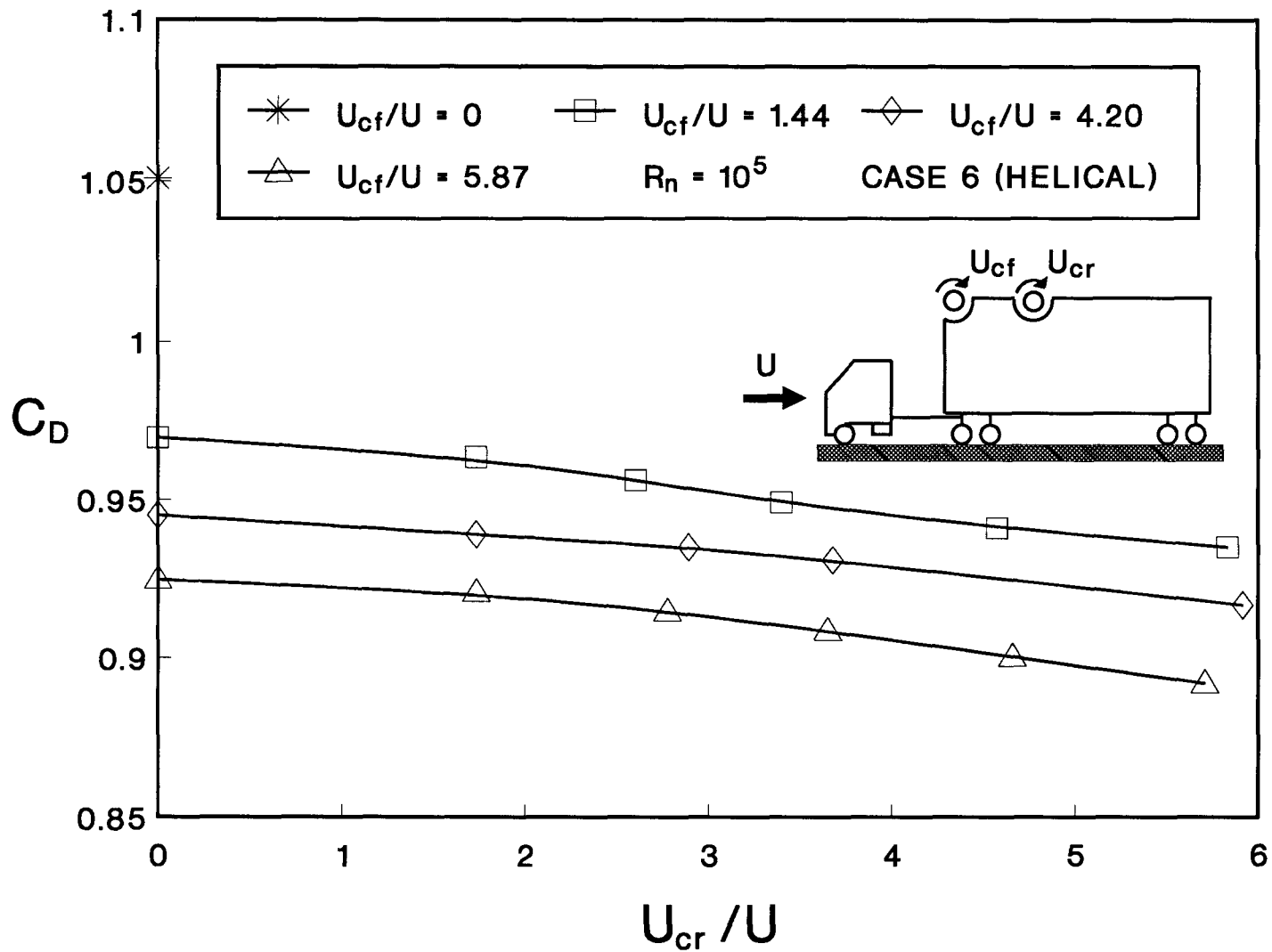


Figure 20. Effect of the twin helical cylinder configuration on the momentum injection and boundary-layer control: (f) Case 6: front cylinder raised 12.7 mm, rear cylinder flush;

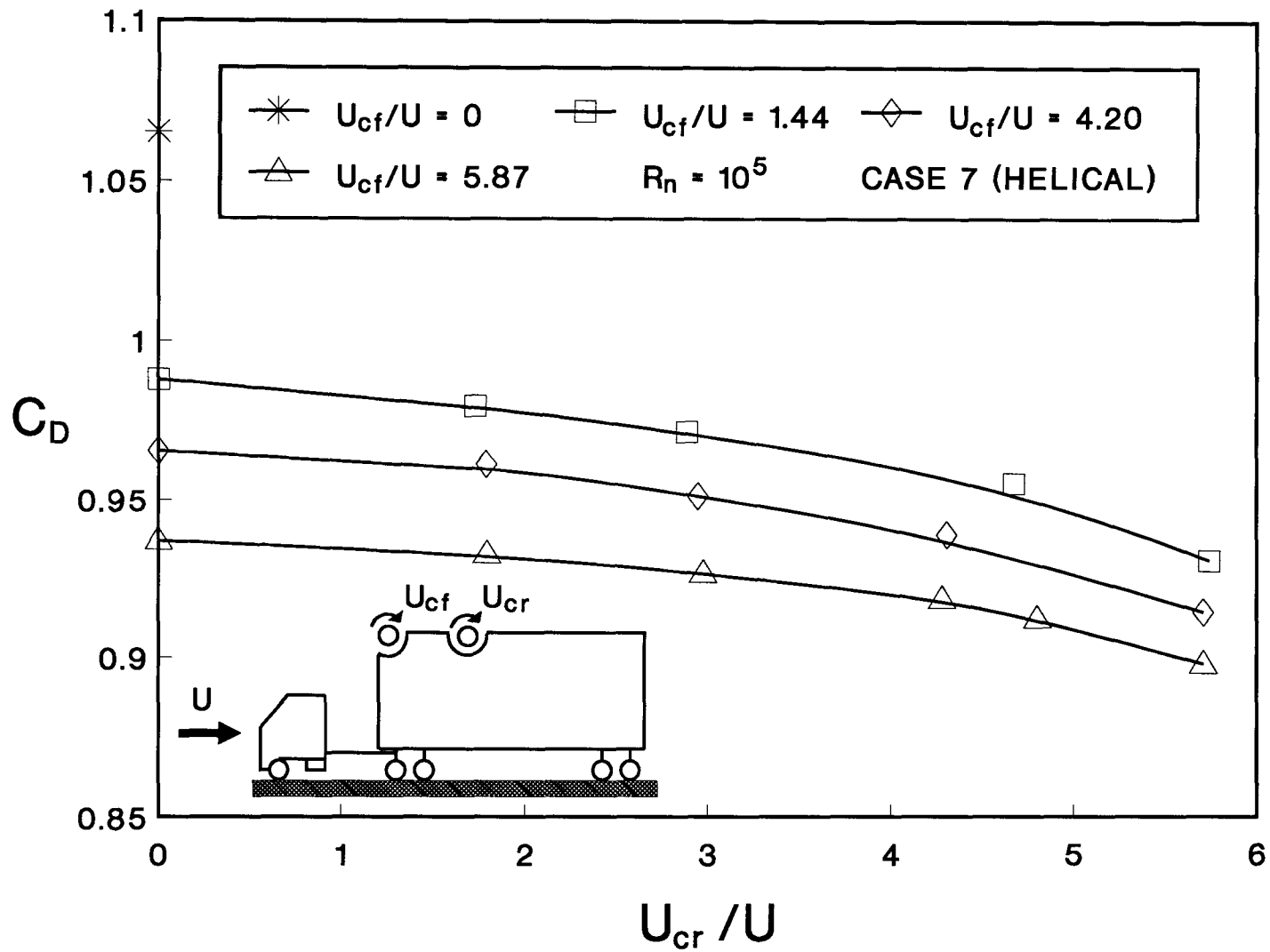


Figure 20. Effect of the twin helical cylinder configuration on the momentum injection and boundary-layer control: (g) Case 7: front cylinder raised 12.7 mm, rear cylinder raised 6.35 mm;

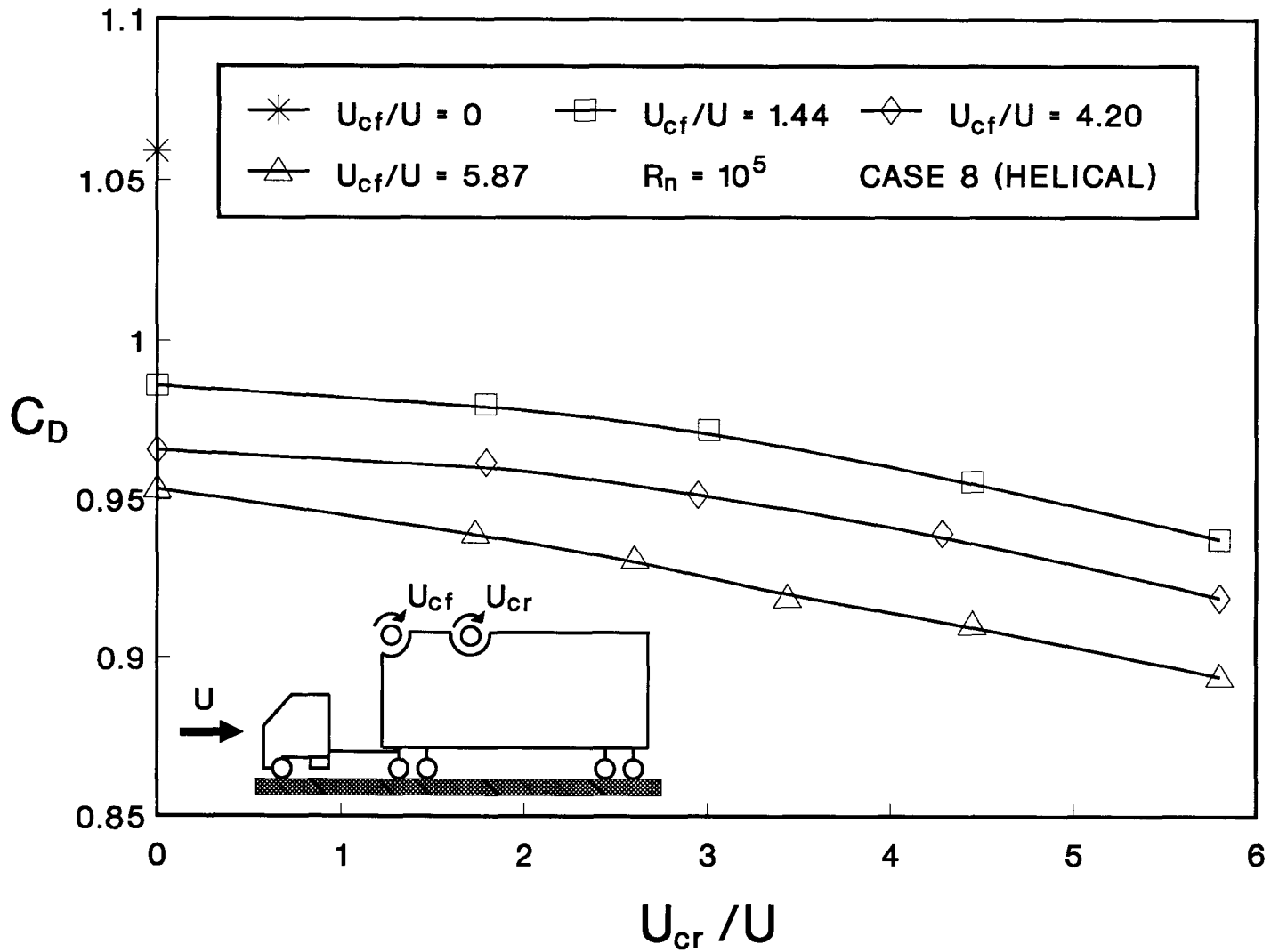


Figure 20. Effect of the twin helical cylinder configuration on the momentum injection and boundary-layer control: (h) Case 8: front cylinder raised 12.7 mm, rear cylinder raised 12.7 mm;

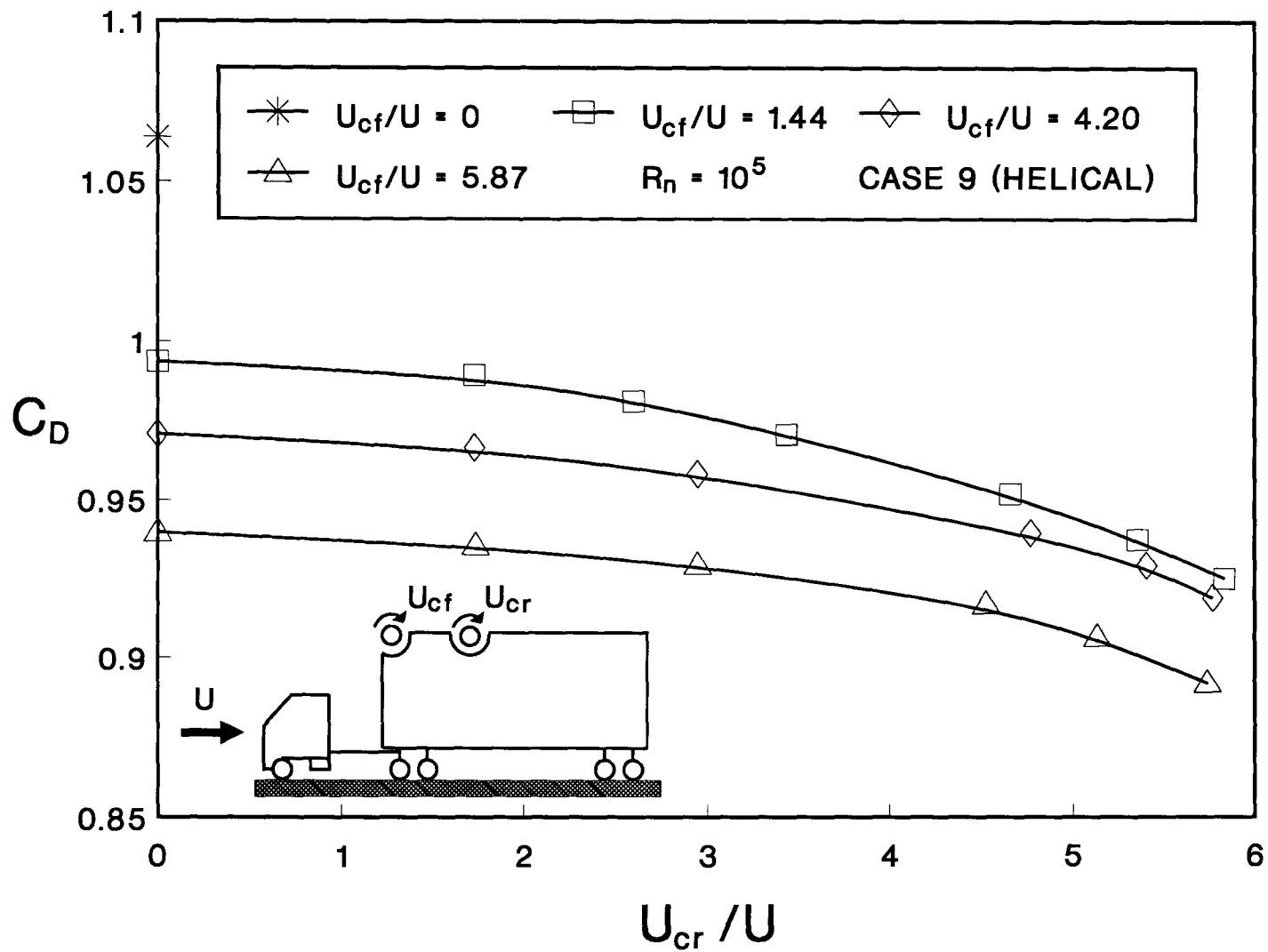


Figure 20. Effect of the twin helical cylinder configuration on the momentum injection and boundary-layer control: (i) Case 9: front cylinder raised 6.35 mm, rear cylinder raised 6.35 mm.

cylinder(s) appears quite promising in reducing pressure drag of the tractor-trailer truck configuration through MSBC (Figure 21).

Both the truck configurations were subjected to extensive flow visualization study to get better appreciation of the flow particularly with reference to stagnation, separation reattachment and wake condition. The tests were carried out in a water channel using slit lighting with polyvinyl chloride particles serving as tracers as mentioned before. The test Reynolds number based on freestream speed and trailer height (H) was around 4×10^4 .

The flow visualization pictures were obtained over a wide range of cylinder orientations and speeds. For brevity, only a typical set of results for two cylinders at front face of the trailer are presented here for two different cab geometries (Figures 22, 23).

Figure 22 considers a truck configuration where the trailer projects significantly higher than that in Figure 23. The gap between the cab and the trailer is also relatively large. In absence of the cylinders, the flow separated at the top leading edge of the trailer and a large bubble covers the top face. A long wake was also observed which is partially visible. Rounding of the corners by the cylinders, even in absence of their rotation, reduces the size of the separation bubble. Note, even with $U_c/U = 1$, the flow on the top face is essentially attached. With $U_c/U = 3$, the flow on both top and bottom faces of the trailer is rather smooth and there is a significant reduction in the size of the turbulent wake.

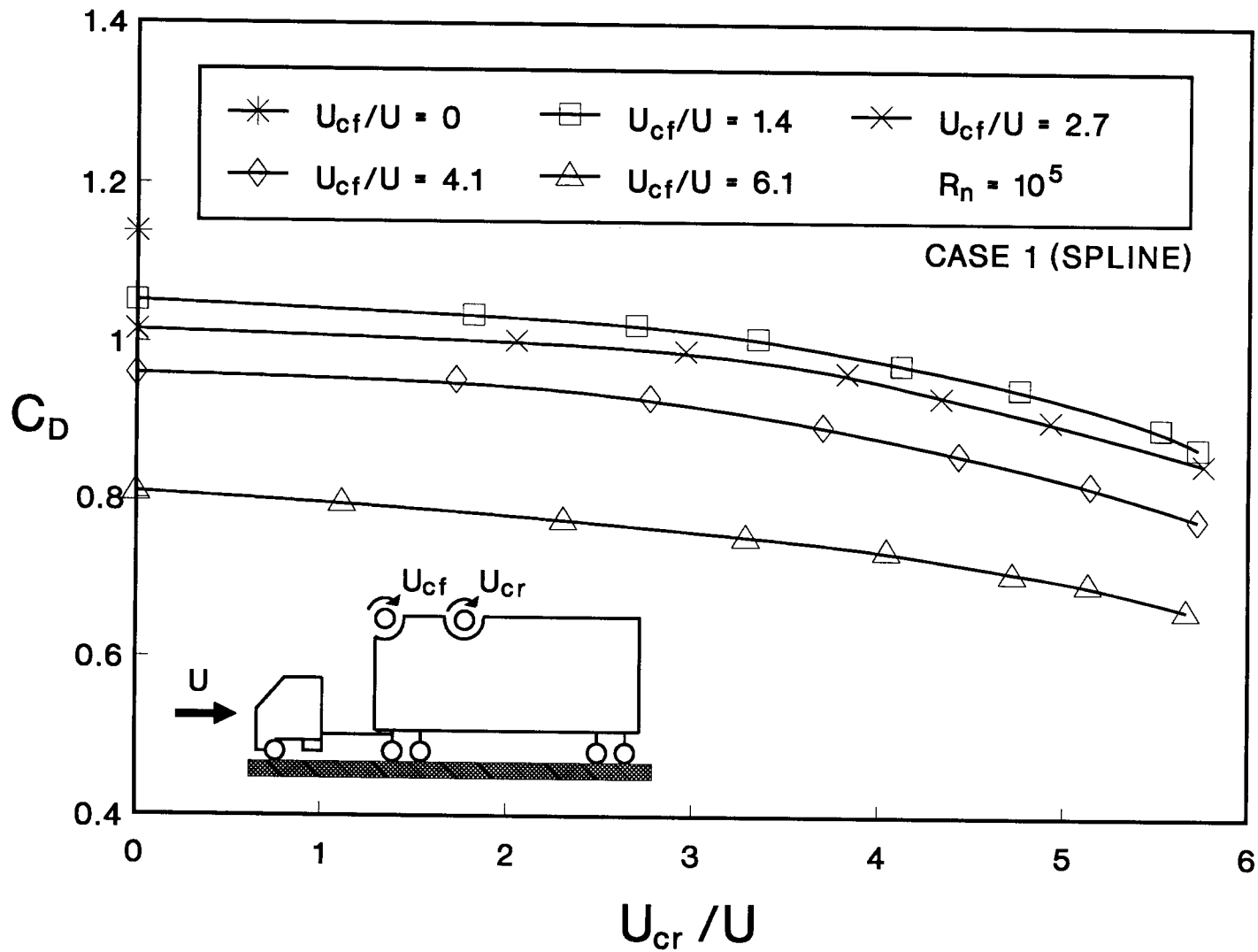


Figure 21. Variation of the drag coefficient C_D with the speed ratio for the twin spline cylinder configurations: (a) Case 1: both cylinders flush;

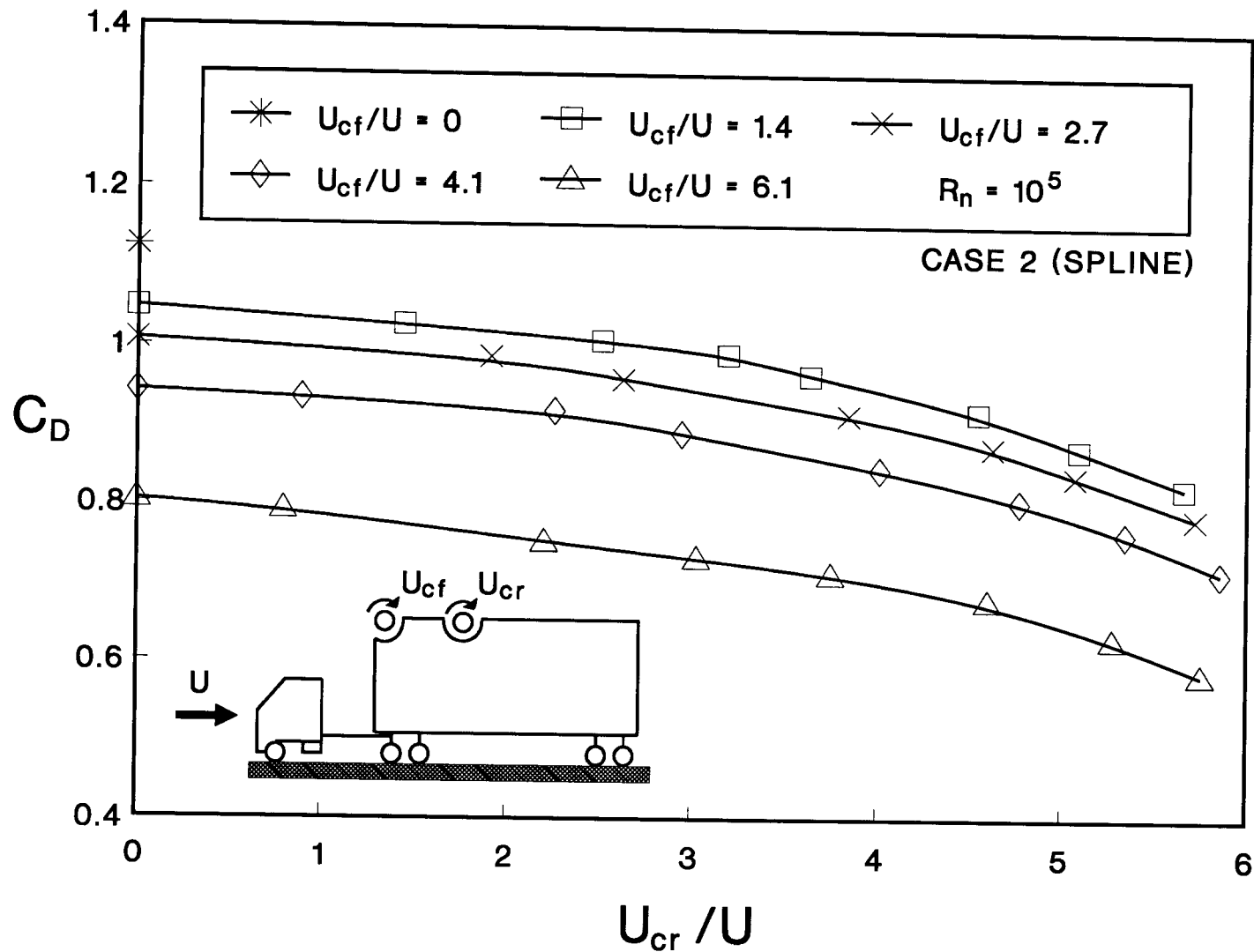


Figure 21. Variation of the drag coefficient C_D with the speed ratio for the twin spline cylinder configurations: (b) Case 2: front cylinder flush, rear cylinder raised 6.35 mm;

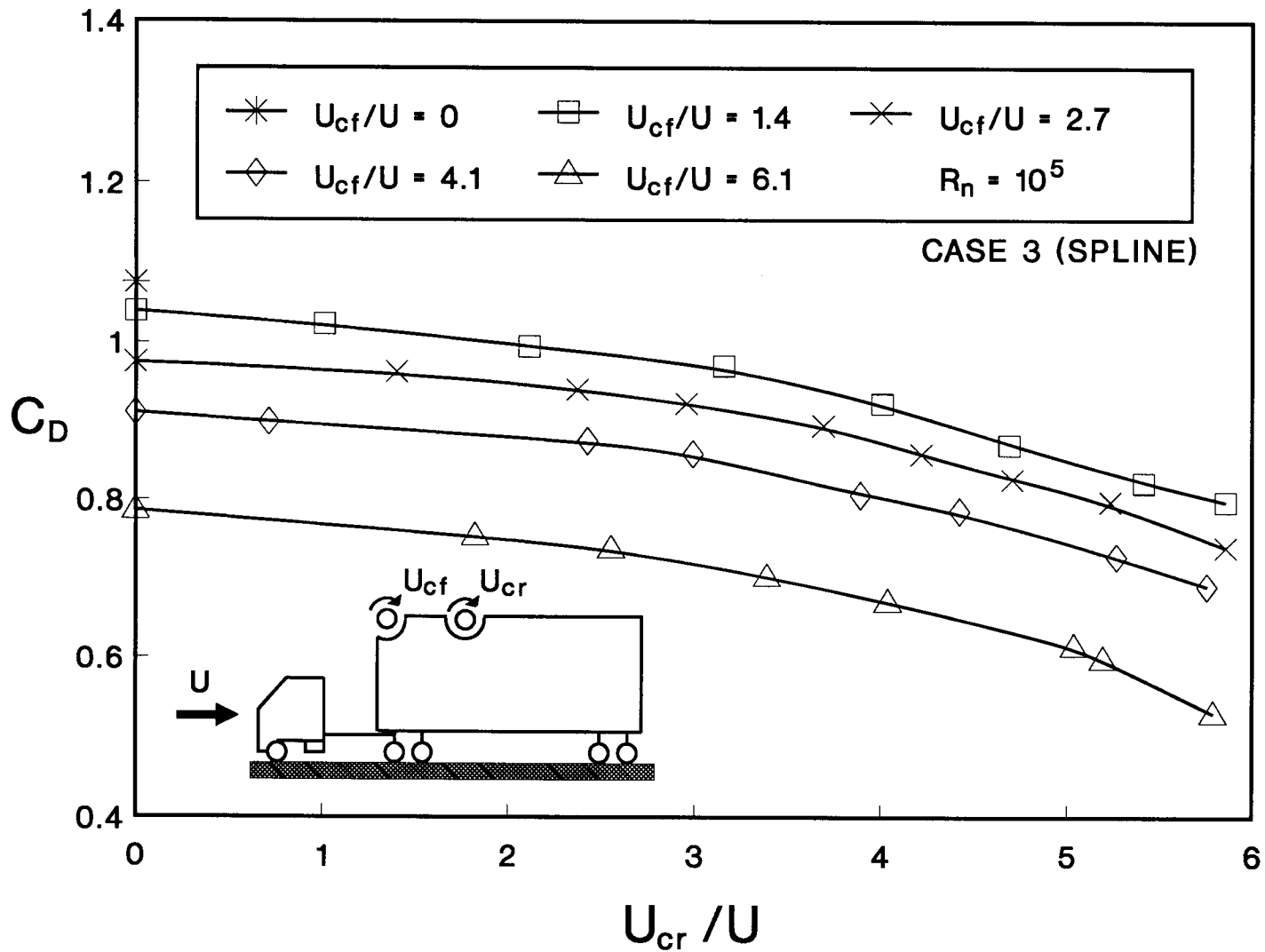


Figure 21. Variation of the drag coefficient C_D with the speed ratio for the twin spline cylinder configurations: (c) Case 3: front cylinder flush, rear cylinder raised 12.7 mm;

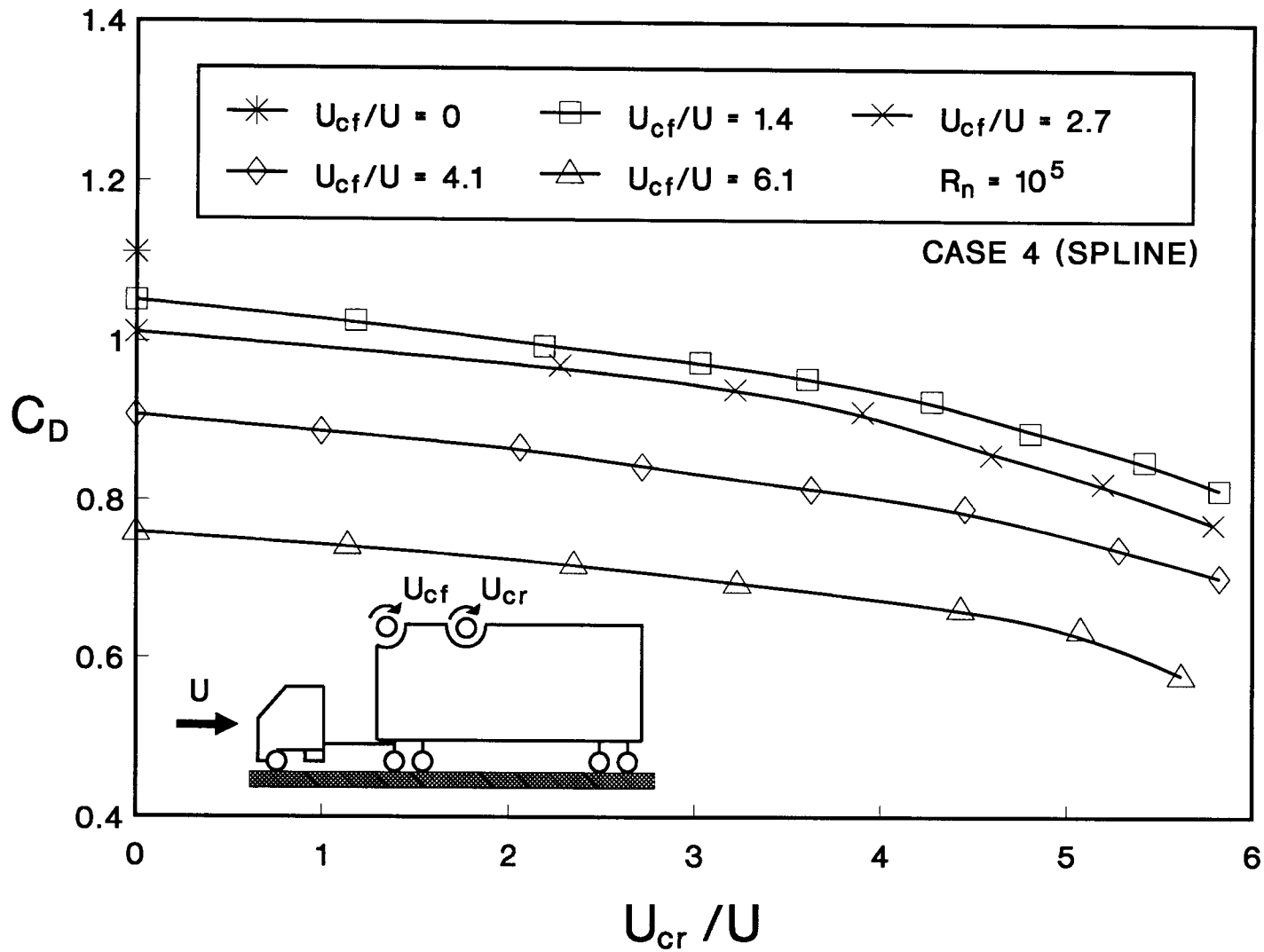


Figure 21. Variation of the drag coefficient C_D with the speed ratio for the twin spline cylinder configurations: (d) Case 4: front cylinder raised 6.35 mm, rear cylinder raised 12.7 mm;

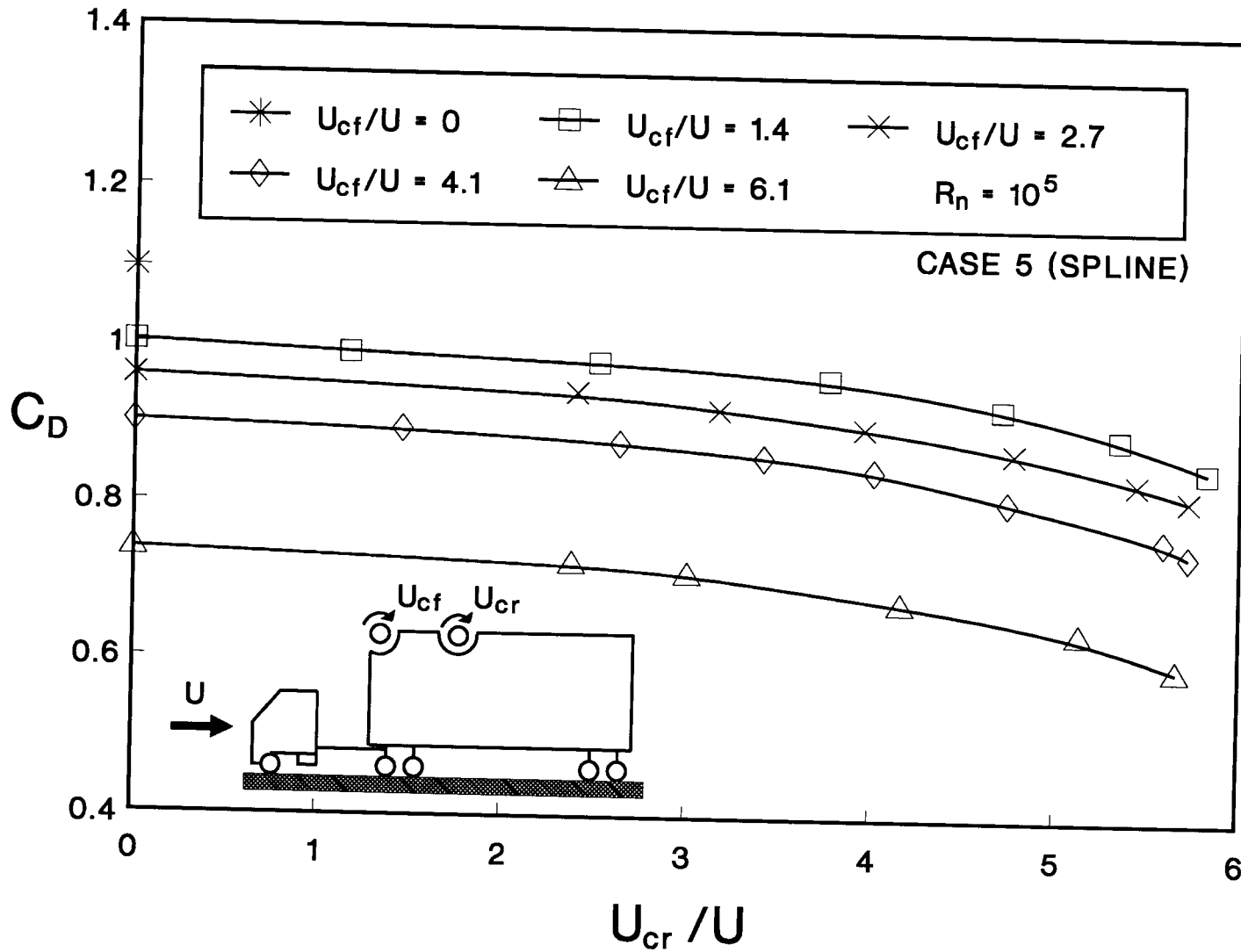


Figure 21. Variation of the drag coefficient C_D with the speed ratio for the twin spline cylinder configurations: (e) Case 5: front cylinder raised 6.35 mm, rear cylinder flush;

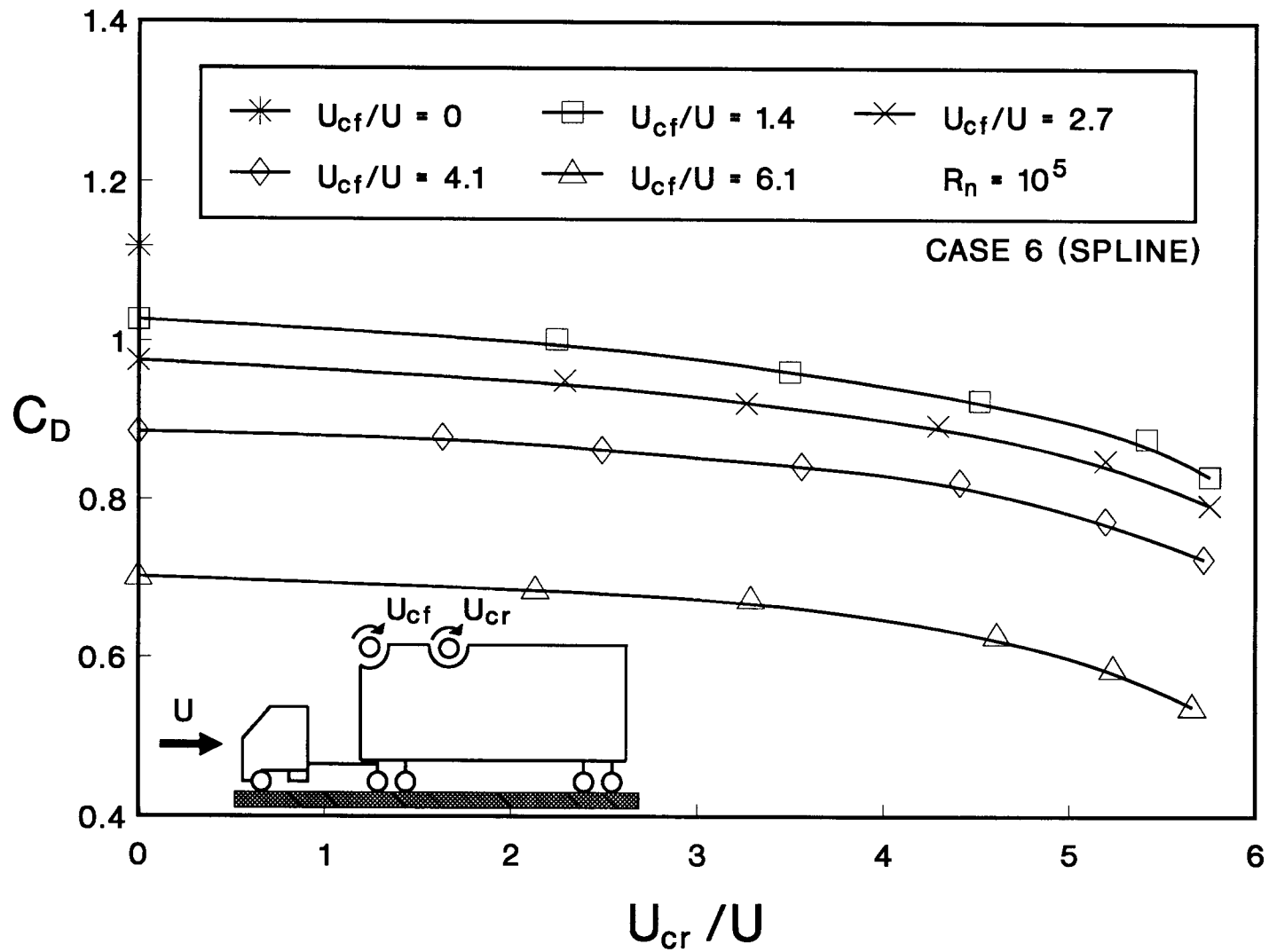


Figure 21. Variation of the drag coefficient C_D with the speed ratio for the twin spline cylinder configurations: (f) Case 6: front cylinder raised 12.7 mm, rear cylinder flush;

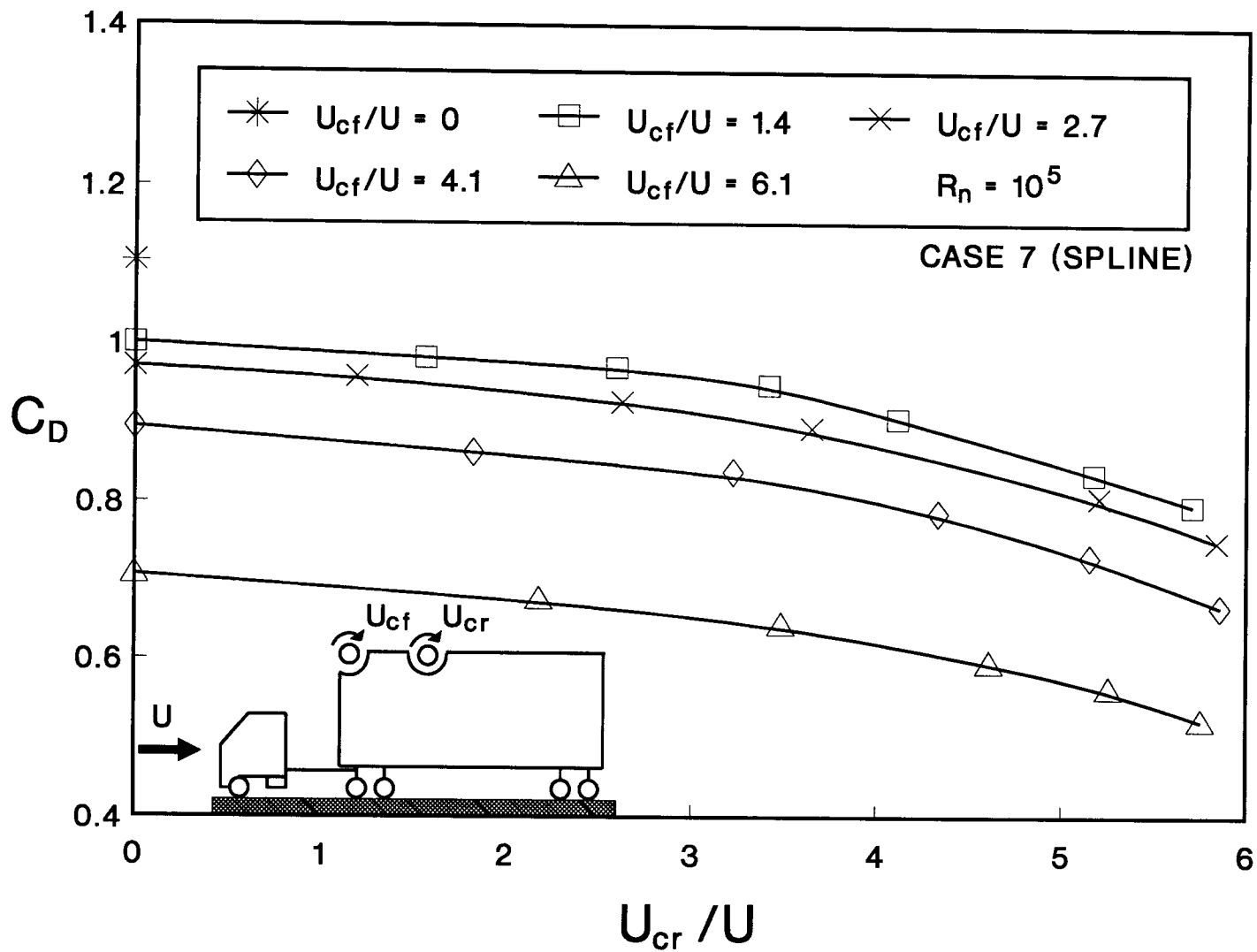


Figure 21. Variation of the drag coefficient C_D with the speed ratio for the twin spline cylinder configurations: (g) Case 7: front cylinder raised 12.7 mm, rear cylinder raised 6.35 mm;

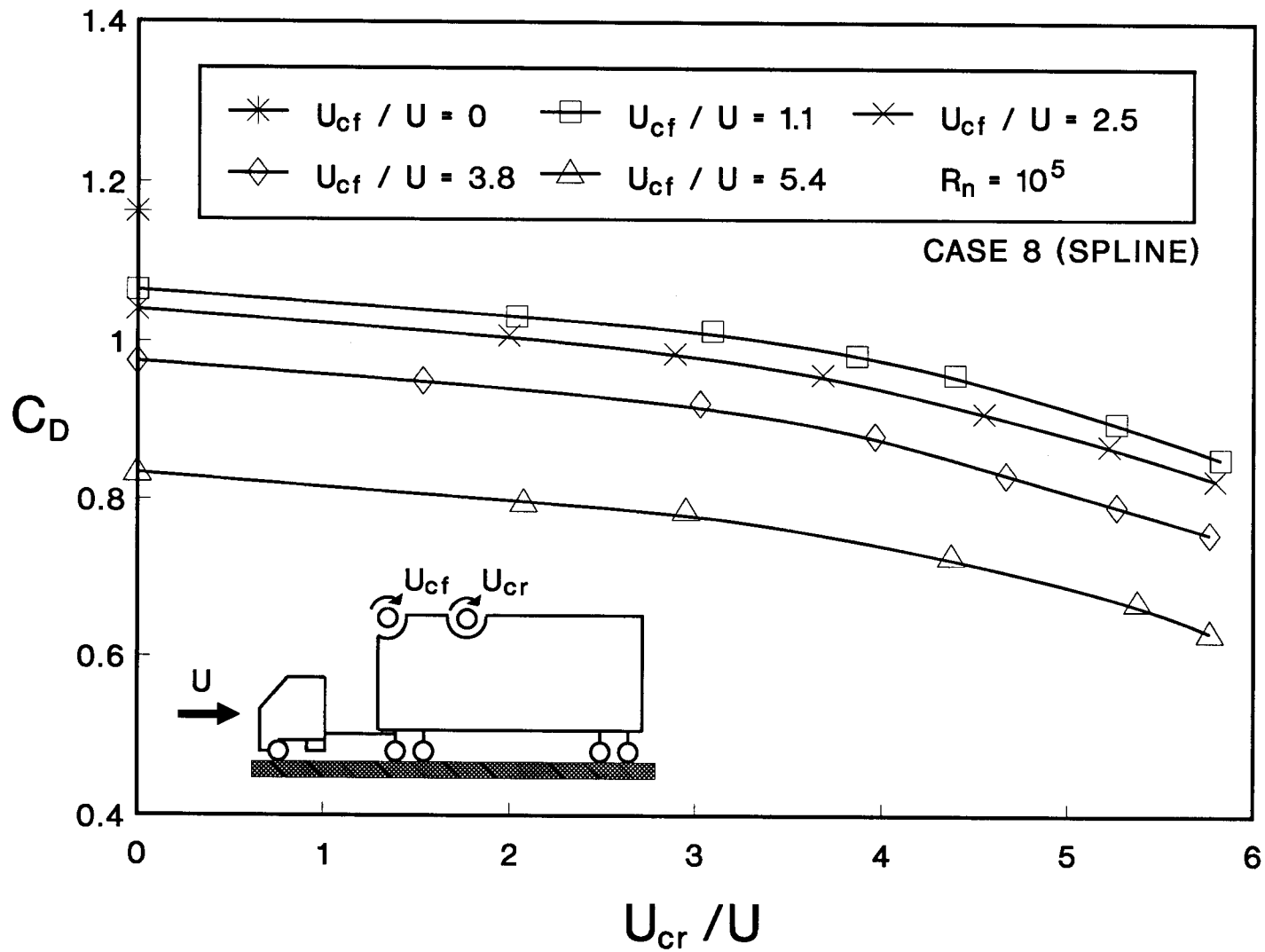


Figure 21. Variation of the drag coefficient C_D with the speed ratio for the twin spline cylinder configurations: (h) Case 8: front cylinder raised 12.7 mm, rear cylinder raised 12.7 mm;

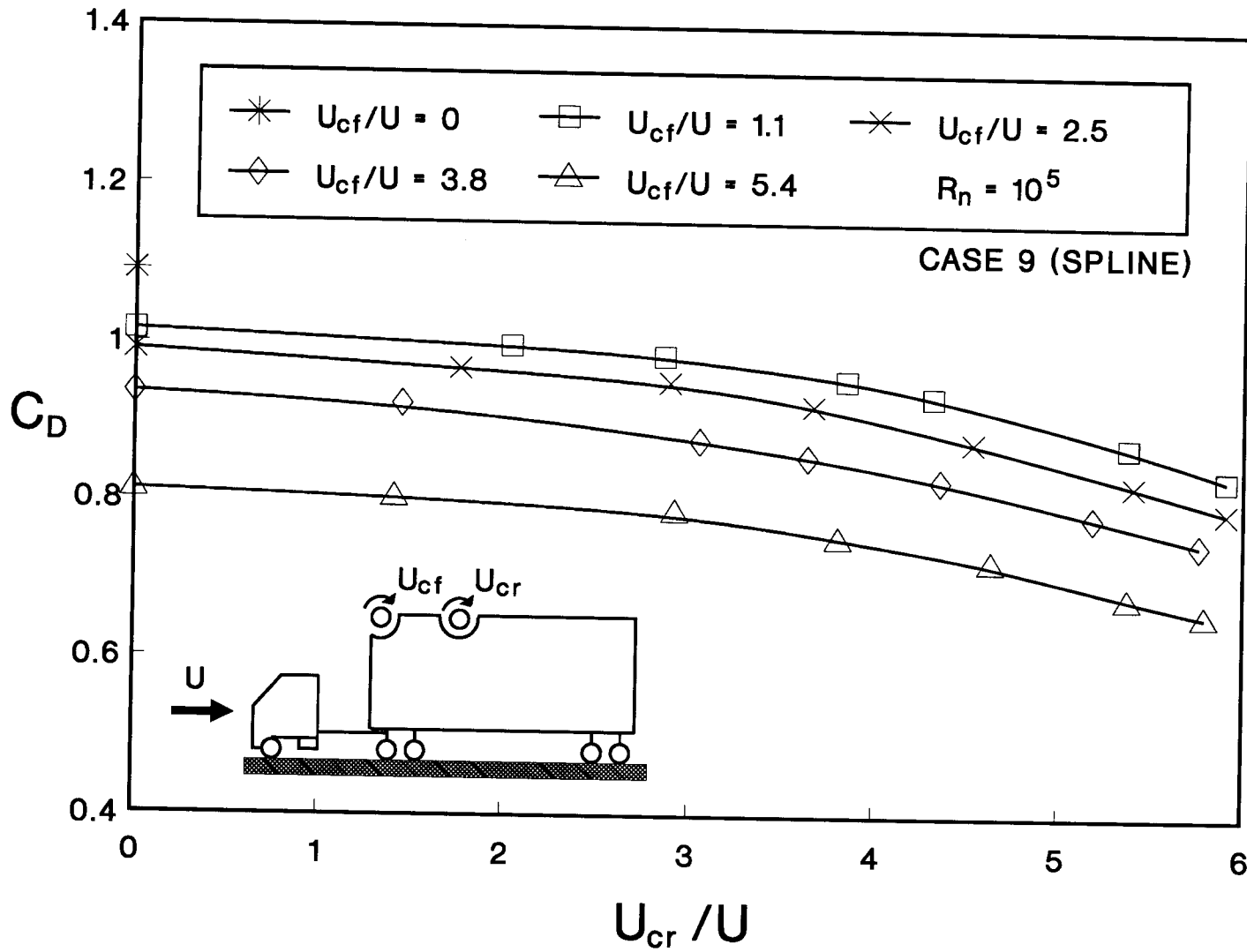


Figure 21. Variation of the drag coefficient C_D with the speed ratio for the twin spline cylinder configurations: (i) Case 9: front cylinder raised 6.35 mm, rear cylinder raised 6.35 mm.

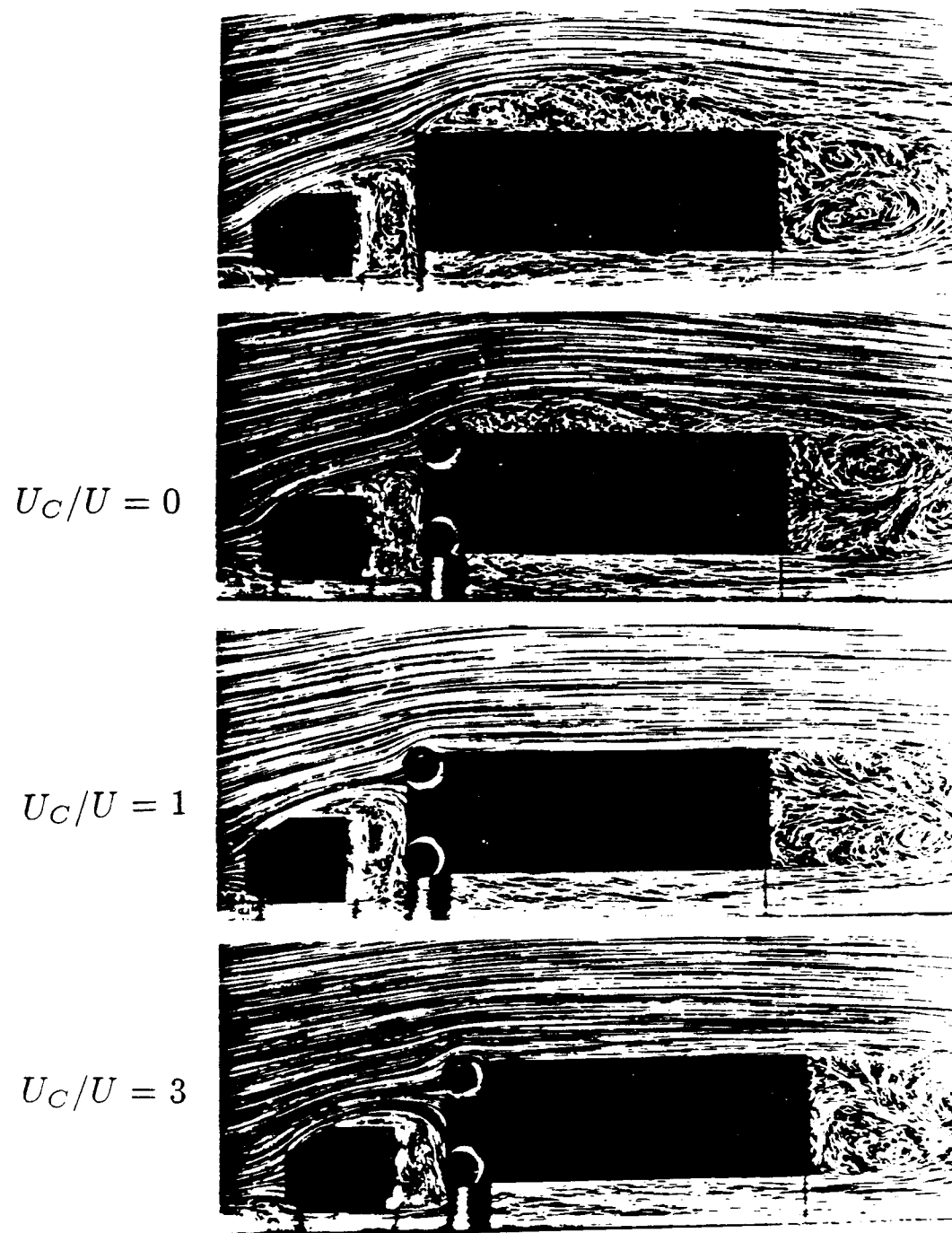
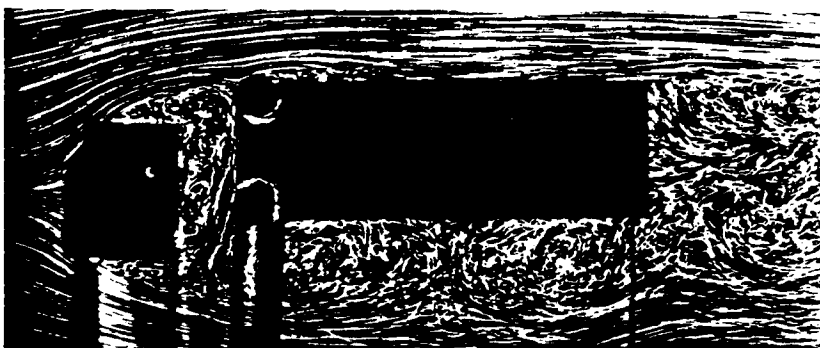
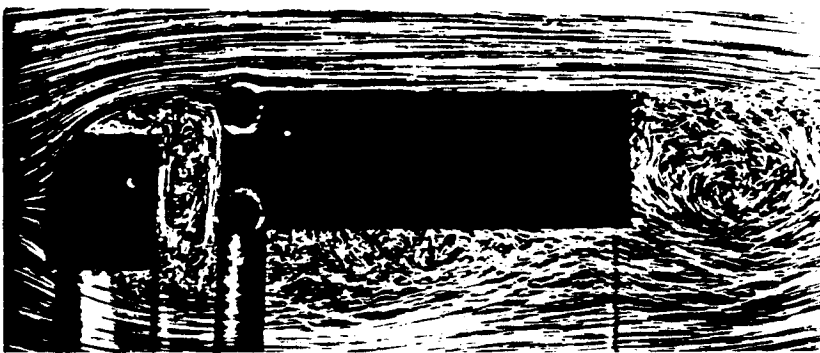


Figure 22. Effect of cylinder rotation on the flow past a tractor-trailer truck configuration.

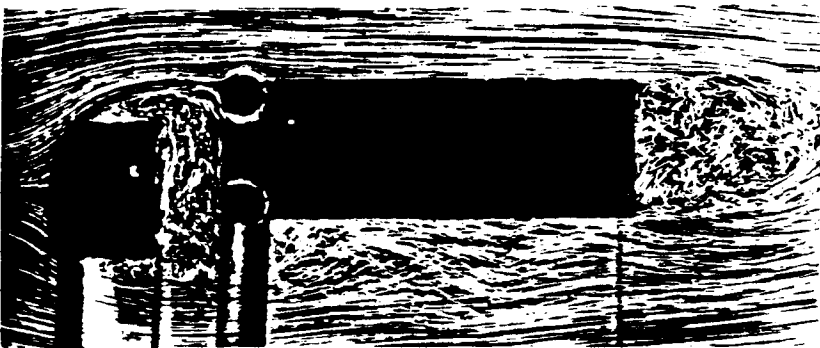
$$U_C/U = 0$$



$$U_C/U = 1$$



$$U_C/U = 2$$



$$U_C/U = 3$$



Figure 23. Effect of cylinder rotation on the flow past a tractor-trailer truck configuration. Note, the tractor geometry and spacing between the tractor and trailer are different here.

Figure 23 considers a truck configuration where trailer projects over the cab by a relatively small amount. Note, the character of the flow is significantly different compared to the previous case. The size of the separation bubble on the trailer's top face is rather small (with cylinder, i.e. smooth corners, but $U_c/U = 0$), however, there is a large turbulent field on the bottom face. This results in a rather wide wake. The cylinder rotation progressively improves the situation as U_c/U increases, and for $U_c/U = 3$ there is an essentially attached flow on top and bottom faces of trailer with a dramatic reduction in the wake-size.

3.3 Rectangular Prism with Fences

As against the momentum injection to delay boundary-layer separation, fences located on the front face of a bluff body tend to trip the boundary-layer thus creating a low pressure region by interrupting the pressure recovery. This, in turn, can reflect as a reduction in the drag of the body. To assess effectiveness of the fences as a drag reducing device a comprehensive wind tunnel test-program was undertaken.

As pointed out before, typical fence is a thin flat plate of width (b_f), height (h_f), and negligible thickness. The fences were mounted normal to the frontface. The fence dimensions are presented in a nondimensional form (d , hydraulic diameter of the projected area normal to the flow).

Figure 24 shows variation of C_D with the geometry of the fence for a three-dimensional rectangular prism ($H = 22.8$ cm, $B = 21.5$ cm, $L = 101.5$ cm, $d = 25.4$ cm). Four fences were mounted on the front face of the prism to form a square about its geometric center. Note, there appears to be an optimum height as well as width of the fences. The maximum reduction in C_D obtained was from 1.25 to 0.85 (31%) for $h_f/d = 0.13$ and $b_f/d = 0.5$.

3.4 Tractor-trailer Truck Model with Fences

With this encouraging trend, it was decided to explore application of the fences on the front exposed area the trailer (Figure 25). Of course, as part of the area is shielded by the cab, the available exposed space for mounting fences on the trailer is relatively small. The trailer dimensions in this case were $H = 25$ cm, $B = 22.6$ cm, and $L = 128.4$ cm with a hydraulic diameter of 31.14 cm.

Based on the earlier results on the fence height and width, h_f/d and b_f/d were fixed at as 0.087 and 0.683, respectively, and an optimum location of a horizontal fence (fence 1) in the vertical direction (i.e. along y_f) was searched (Figure 26). The critical position was given by $(y_{f1}/d)_{cr} \approx 0.36$ leading to a minimum $C_D = 1.048$. When fence 1 held at its critical location, similar procedure was applied to fence 2 to arrive at its optimum location (Figure 27). For the reference drag coefficient without fences, C_{D0} , at 1.124, the two horizontal fences in their optimum location resulted in a drag reduction of

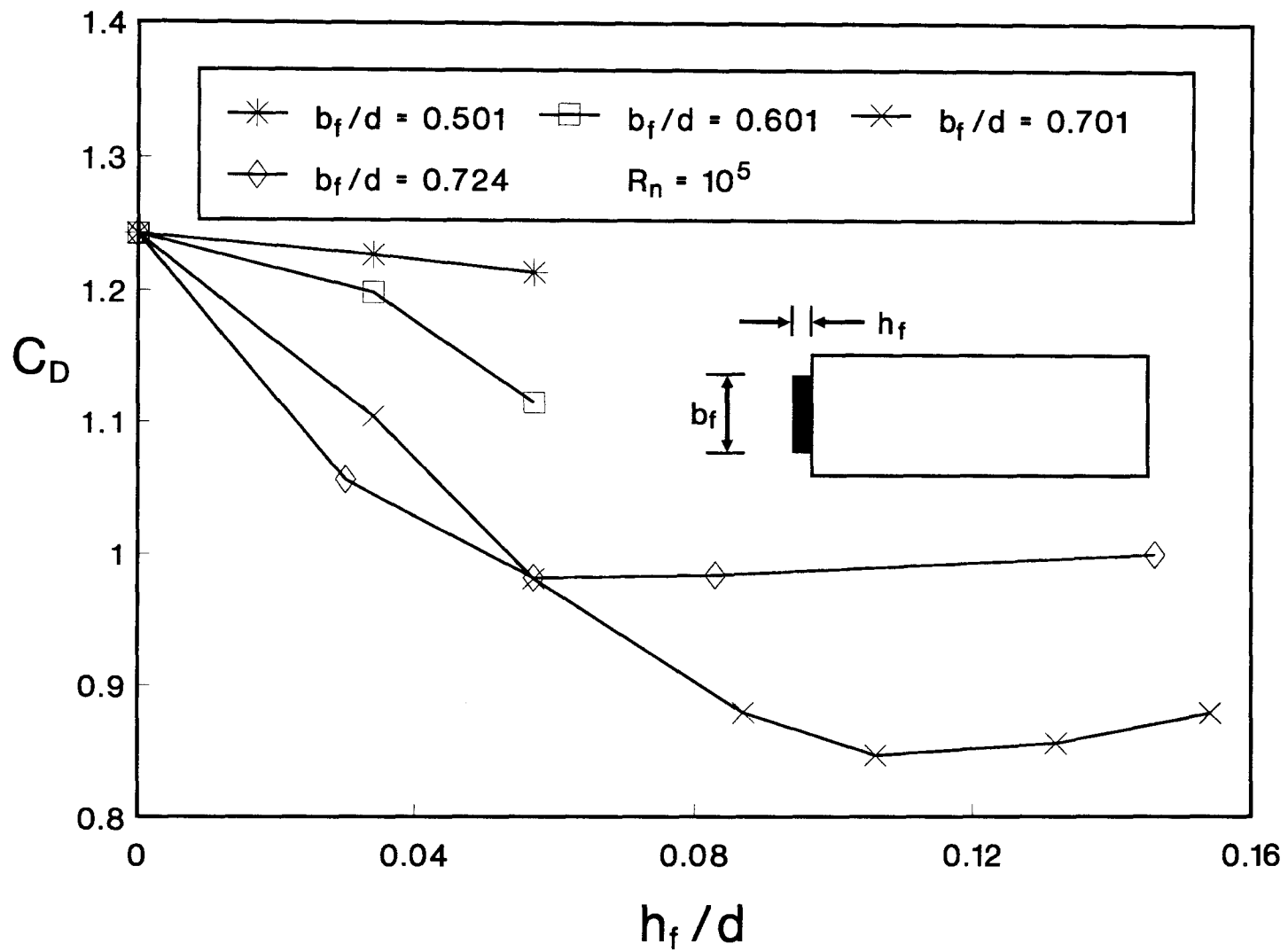


Figure 24. Effect of the fence width and height on the drag of a three-dimensional prism.

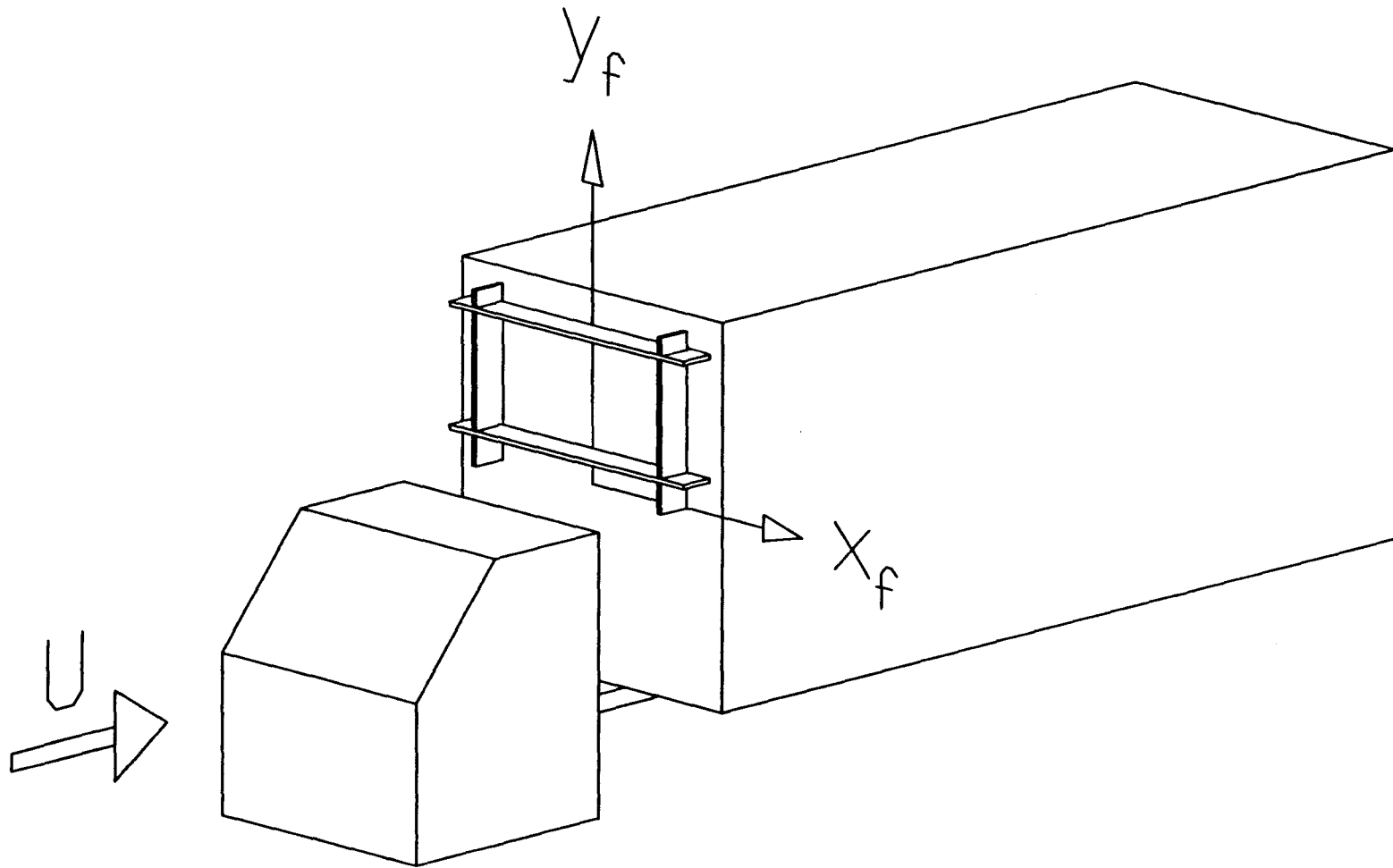


Figure 25. A schematic diagram showing application of the fences on the front, exposed face of the trailer of a truck.

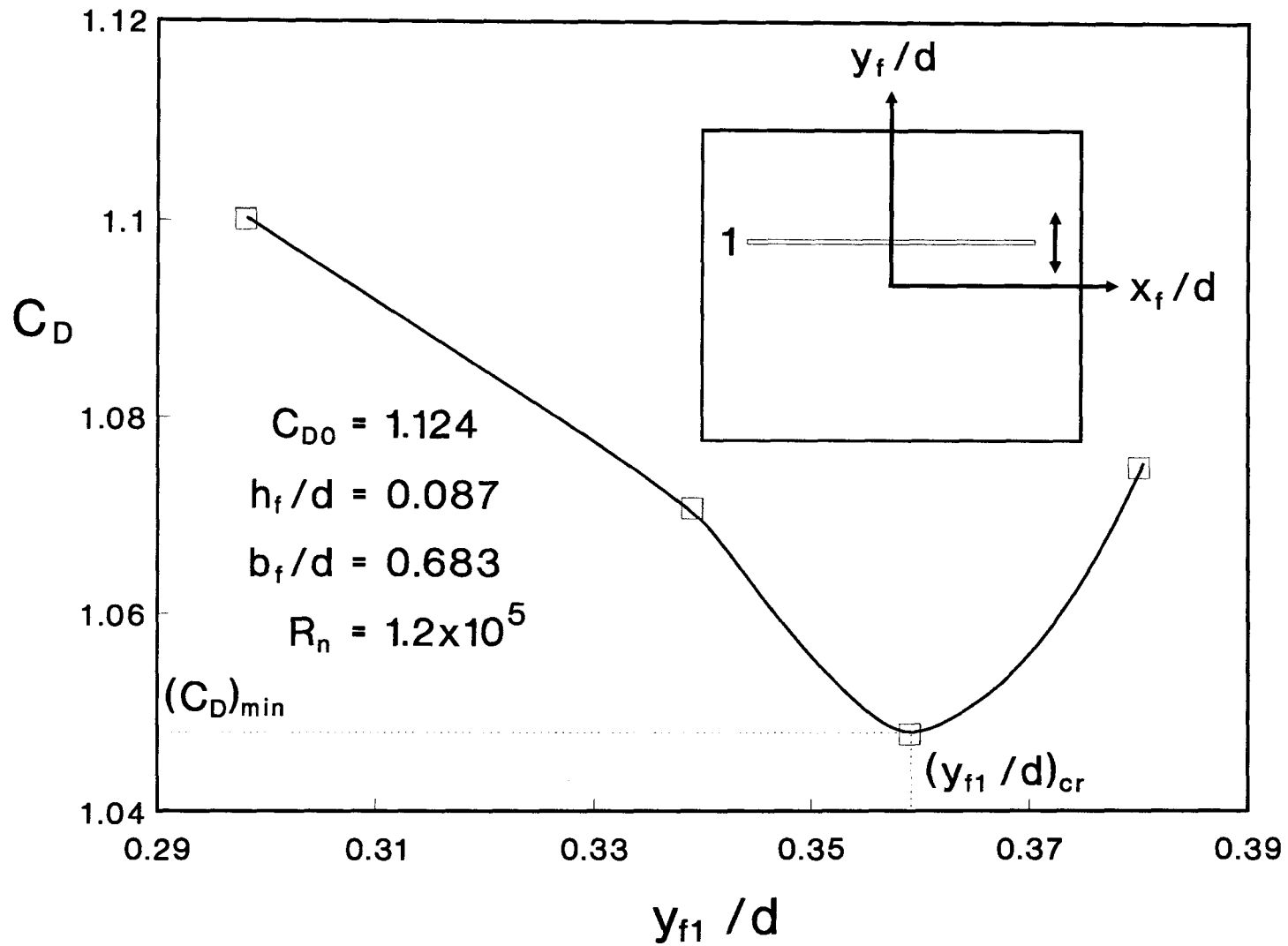


Figure 26. Variation of the drag coefficient with the position of horizontal fence 1.

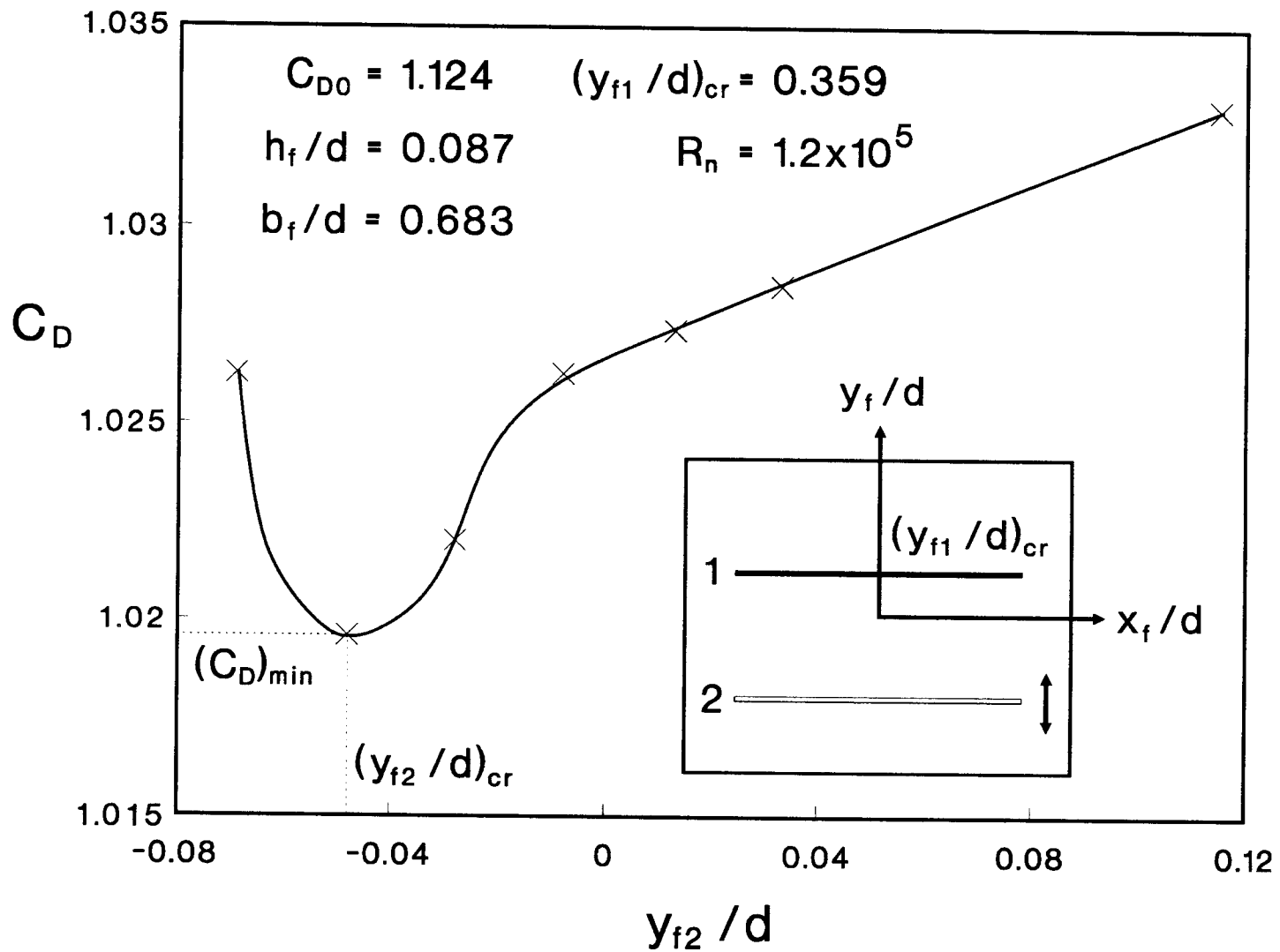


Figure 27. Variation of the drag coefficient with the position of horizontal fence 2 when fence 1 is fixed at its critical orientation.

around 10.6%. Introduction of vertical fences improved the situation further (Figure 28) giving, for optimum locations of the four fences, $C_D \approx 0.9$, a reduction of 20% !

It was felt that by fine-tuning of the fence dimensions further improvement in their performance can be achieved. The improved fence configuration and the associated drag coefficient are shown in Figure 29. Note, the horizontal fences are extended over the entire width of the trailer's front face. The vertical fences are also longer and reach to the top edge. The fence arrangement lowered C_D to around 0.85, a reduction from the reference value by 24.6% !

3.5 Tractor-trailer Truck Model with both Twin Cylinders and Fences

It was tempting to explore a hybrid combination of the momentum injection in presence of the fences to have some appreciation as to the possible favourable trends. To that end the previous tractor-trailer with twin rotating cylinders was used. The optimum configuration of the vertical fences and the cylinder orientations (spline cylinder, Case 6) were used in the study. The horizontal fences were avoided as they would create a turbulent flow field just in front of the leading edge cylinder. The results are presented in Figure 30. The cylinder rotation in presence of the vertical fences improves the performance only a little. For $U_{cf} \approx 4$ and $U_{cr} = 0$, the drag coefficient changes

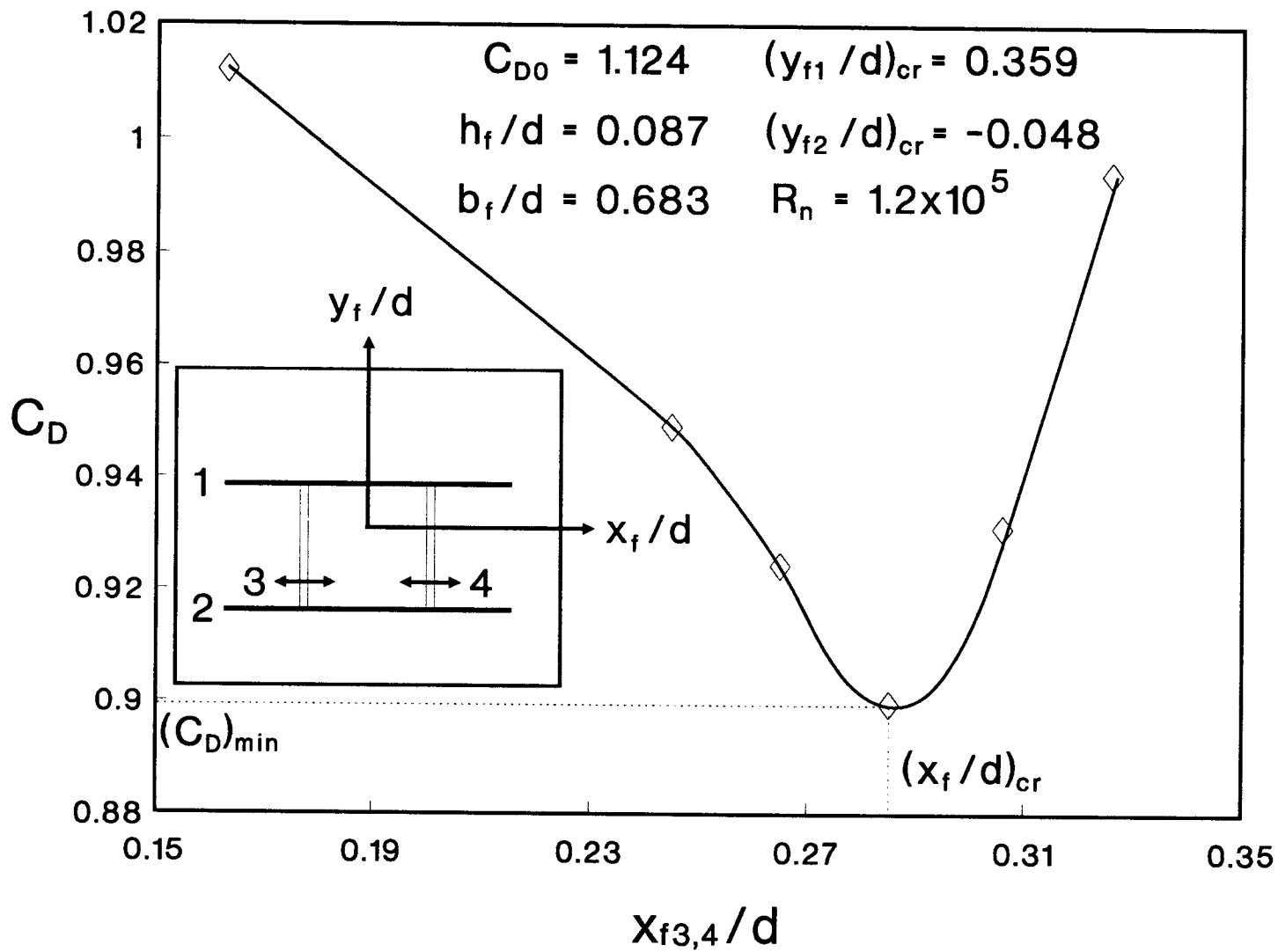


Figure 28. Variation of the drag coefficient with the position of twin vertical fences 3 and 4 when fences 1 and 2 are fixed at their critical orientations.

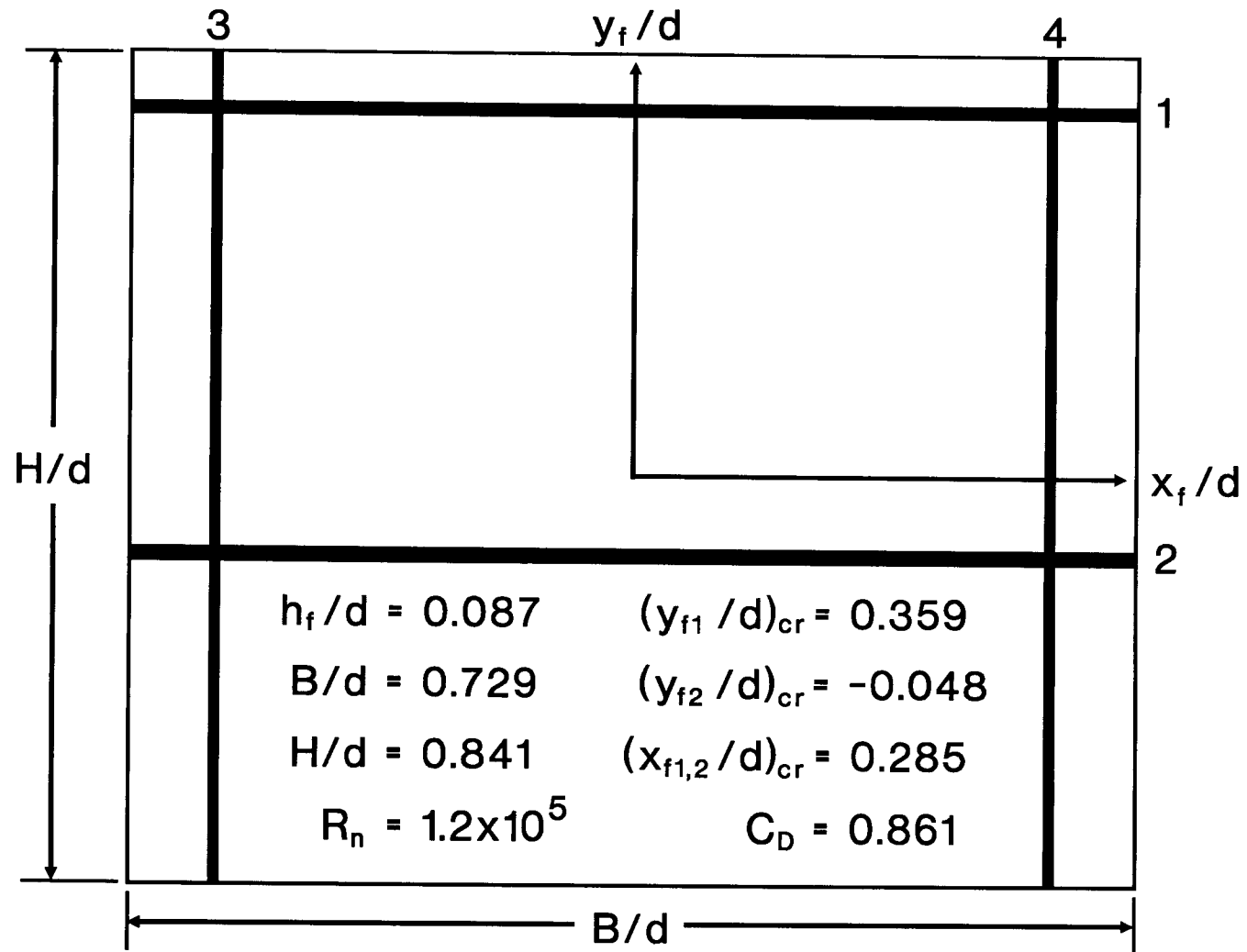


Figure 29. Stages in fine tuning of the fence dimensions and associated drag coefficient: (a) The fences were extended to the edges of the trailer front face in both horizontal and vertical directions.

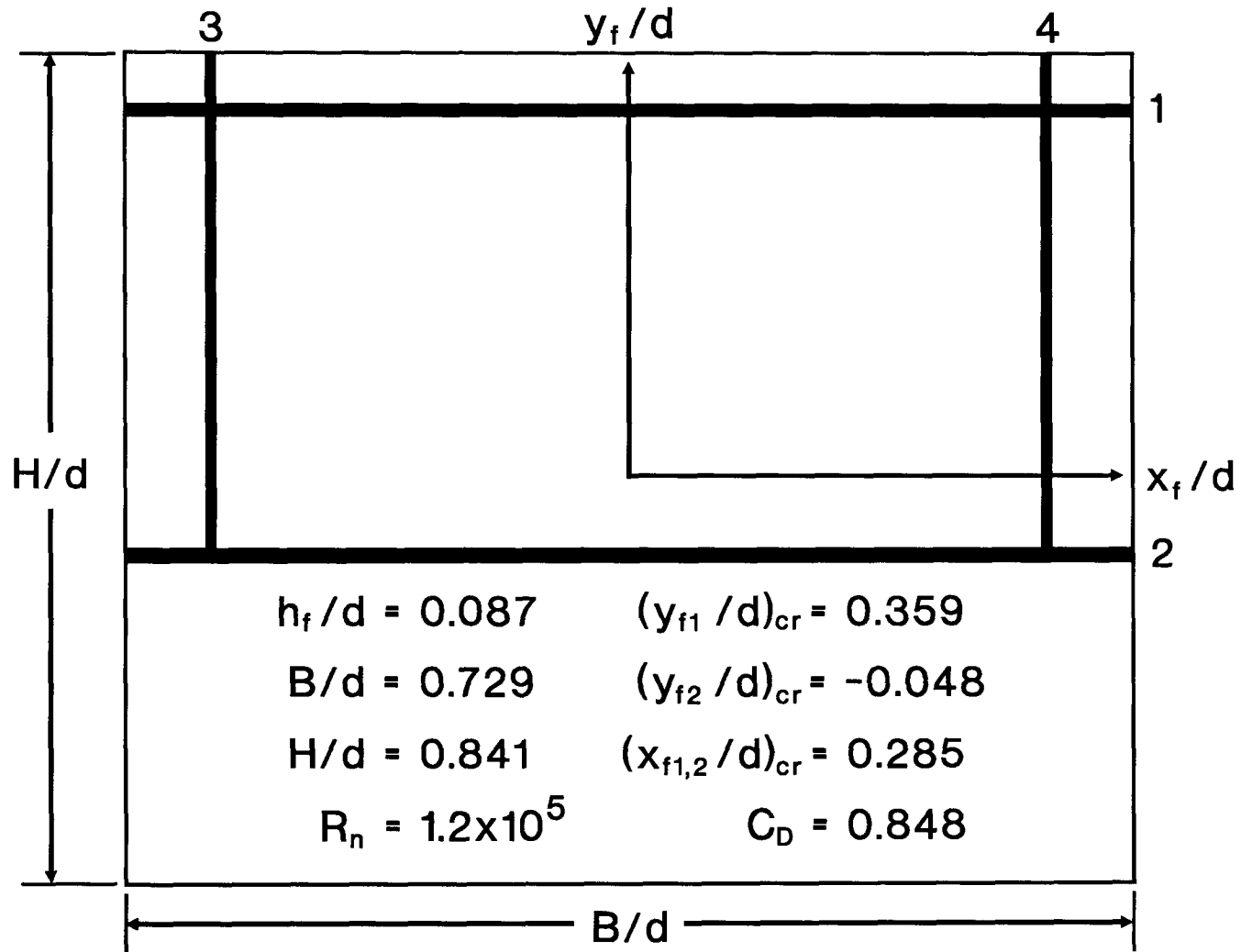


Figure 29. Stages in fine tuning of the fence dimensions and associated drag coefficient: (b) The twin vertical fences were truncated to horizontal 2 fence position from the bottom edge of the trailer front face.

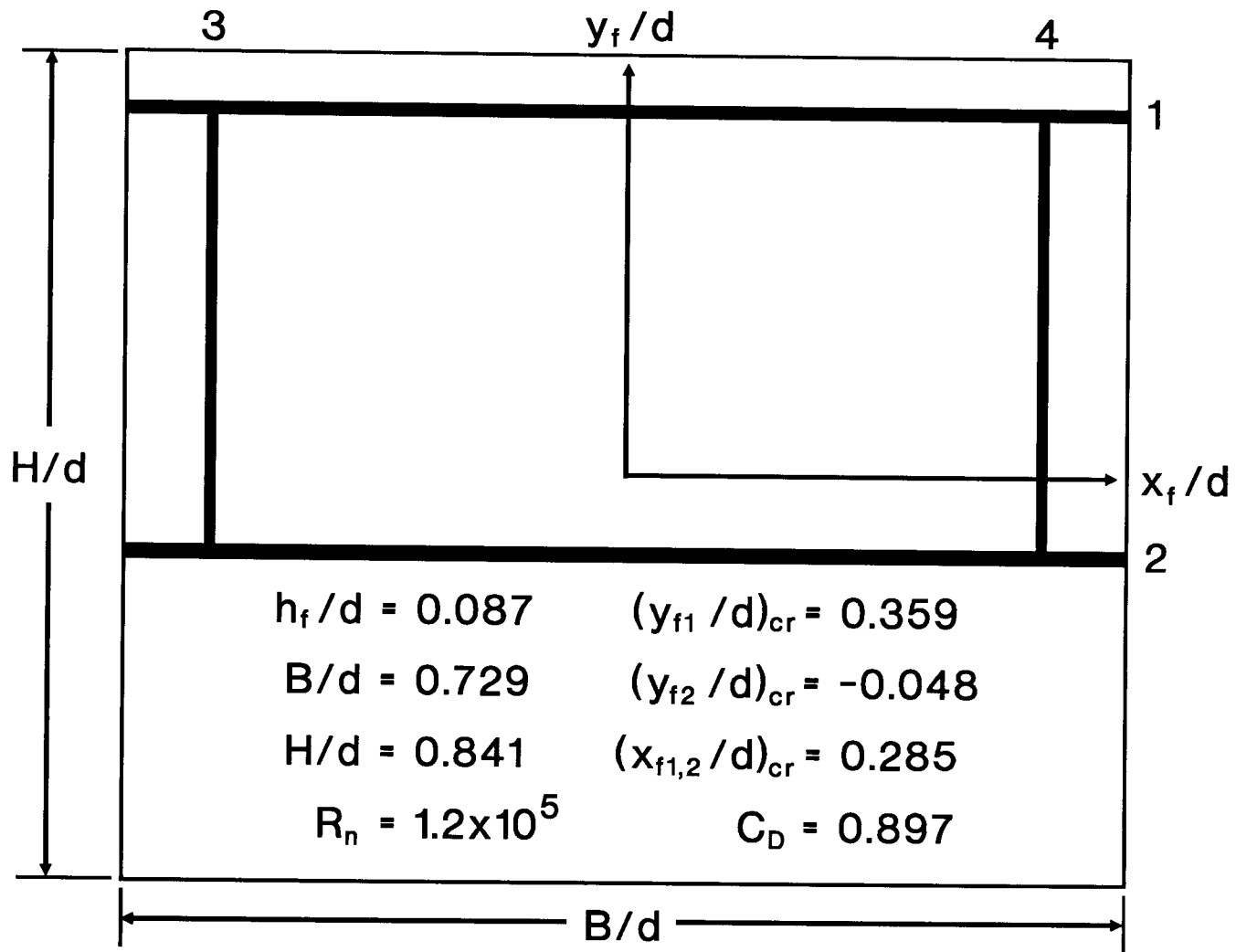


Figure 29. Stages in fine tuning of the fence dimensions and associated drag coefficient: (c) The twin vertical fences were truncated further to horizontal 1 fence position from the top edge of the trailer front face.

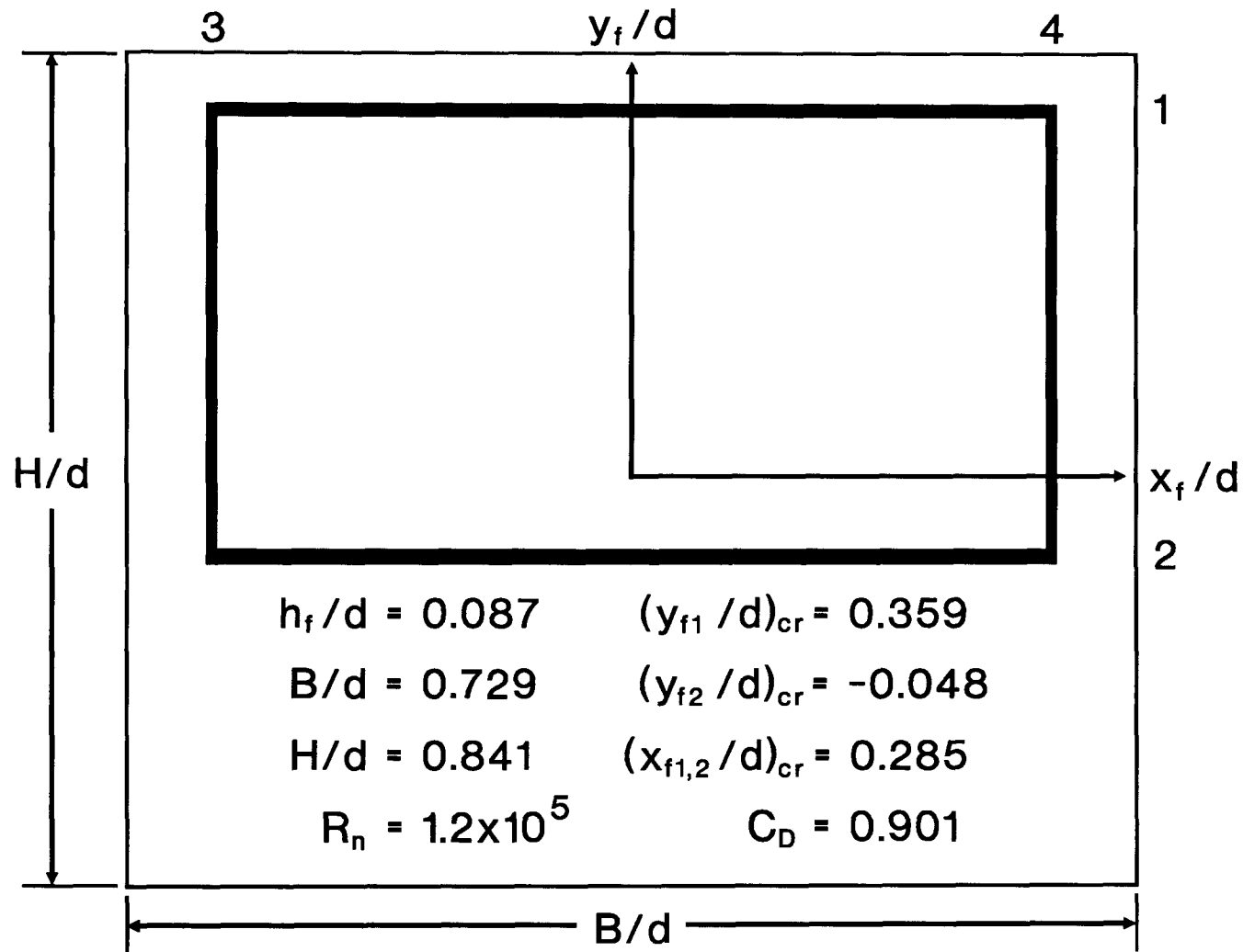


Figure 29. Stages in fine tuning of the fence dimensions and associated drag coefficient: (d) The twin horizontal fences had offset from both side edges of the trailer front face.

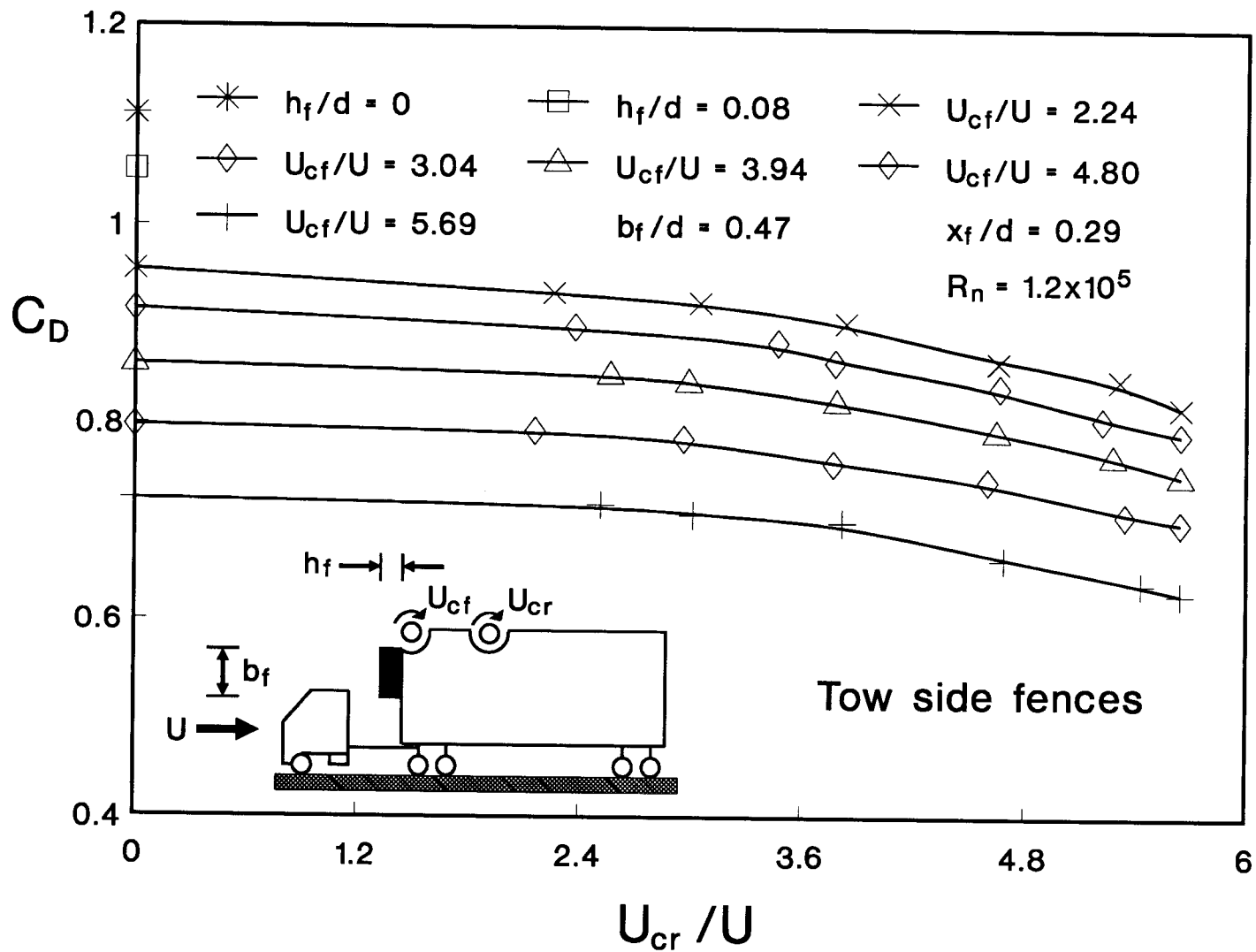


Figure 30. Variation in the drag coefficient with the cylinder speed ratio for a hybrid configuration involving two vertical fences and twin rotating cylinders in their optimum geometry.

from 1.12 to 0.86 (as against 0.885 for the no fence case). This corresponds to a reduction in the drag coefficient by 23%. Note, rotation of the rear cylinder improves the situation only marginally.

3.6 Tractor-trailer Truck Model with a Cylinder Kit

With effectiveness of the MSBC and boundary-layer trip devices established, the attention was directed towards their practical implementation. Of course, application of fences presents no problem. They are merely plate elements, judiciously oriented on the front exposed face of a trailer. Being entirely passive in character, no power input units are involved. They provide 18-24% reduction in the drag coefficient depending on the geometry of the fences and available frontal exposed area of the trailer. Obviously this is a rather attractive option for drag reduction of trucks.

On the other hand, the MSBC did provide a spectacular reduction in the pressure drag and one would like to exploit it in practice. Ideally, it should be integrated with the next generation of trailer designs. However, acceptance of any new idea usually takes time. Considering the history of the truck industry, in terms of its reluctance to change and passion for add-on devices (deflectors, shrouds, skirts, etc.), a simple approach to implementation of the MSBC concept on existing trucks will have to be explored. There is also the question of payload volume lost due to presence of the rotating element at the top front

edge of the trailer. Also, installation of the power unit and transmission system will have to be considered.

These consideration led to the development of the “cylinder-fence kit” idea. The kit, essentially an add-on device, consists of a housing containing a rotating cylinder with power (motor/electric or hydraulic) and transmission systems. The flat upstream surface of the housing permits attachment of fences thus resulting in a hybrid drag reducing device. The kit can be mounted readily on the front face of the existing trailer, without modifying the top leading edge or paying penalty in terms of the lost cargo space. It was obvious that, with the momentum injection unit no longer an integral part of the trailer, the boundary-layer control effectiveness will suffer to some extent. However, if the penalty is not severe, the kit idea may find wide acceptance with the existing trucks. It may also lead to a small kit manufacturing industry in Canada.

The idea evolved into the development of two slightly differing kit configurations (Figure 7) and assessment of their effectiveness through extensive wind tunnel tests. The main difference between the two kits is the extent to which the cylinder projects into the fluid stream. In the first case the cylinder immersion is to an extent of 12.7 mm, while in the second case the cylinder is immersed up to its center (i.e. radius, 1.25 in. = 31.8 mm). Only some typical results useful in establishing trends are recorded here.

3.6.1 Cylinder kit 1

The kit fits in the gap between the tractor and the trailer, and is adjustable in the vertical direction to arrive at an optimum position. Furthermore, it is provided with a removable cover in the front (upstream direction) where the fences, when used, are attached. The wind tunnel tests were aimed at assessing the effect of cover, vertical location of the kit as specified by H_k , fence geometry and the cylinder rotation. The results presented in Figure 31-33.

Effect of vertical orientation of the kit, in absence of fences and the cover, on the drag coefficient as affected by the MSBC is assessed in Figure 32a. Four different values of H_k/d (0.12, 0.08, 0.06 and 0.04) were used in the tests. Note, for $H_k/d = 0.12$ and the cylinder stationary, the drag coefficient is a minimum at ≈ 1.027 . This is because of the favourable alignment between the top of the cylinder and top leading edge of the trailer. However, with the momentum injection the pattern changes and $H_k/d = 0.08$ configuration appears to be more favourable. For $U_c/U = 4$, $C_D \approx 0.935$, which represents a reduction of 12.8% from the stationary value of 1.077. It is apparent that the efficiency of the momentum injection process has suffered primarily due to:

- (a) spacing between the cylinder and the trailer leading edge;
- (b) turbulent flow created due to absence of the cover, which exposes the motor and belt drive system to the fluid stream.

Figure 31b evaluates the kit performance with the cover in place. Note, the positive influence of the cover. Now the drag coefficient for $U_c/U = 4$ is \approx

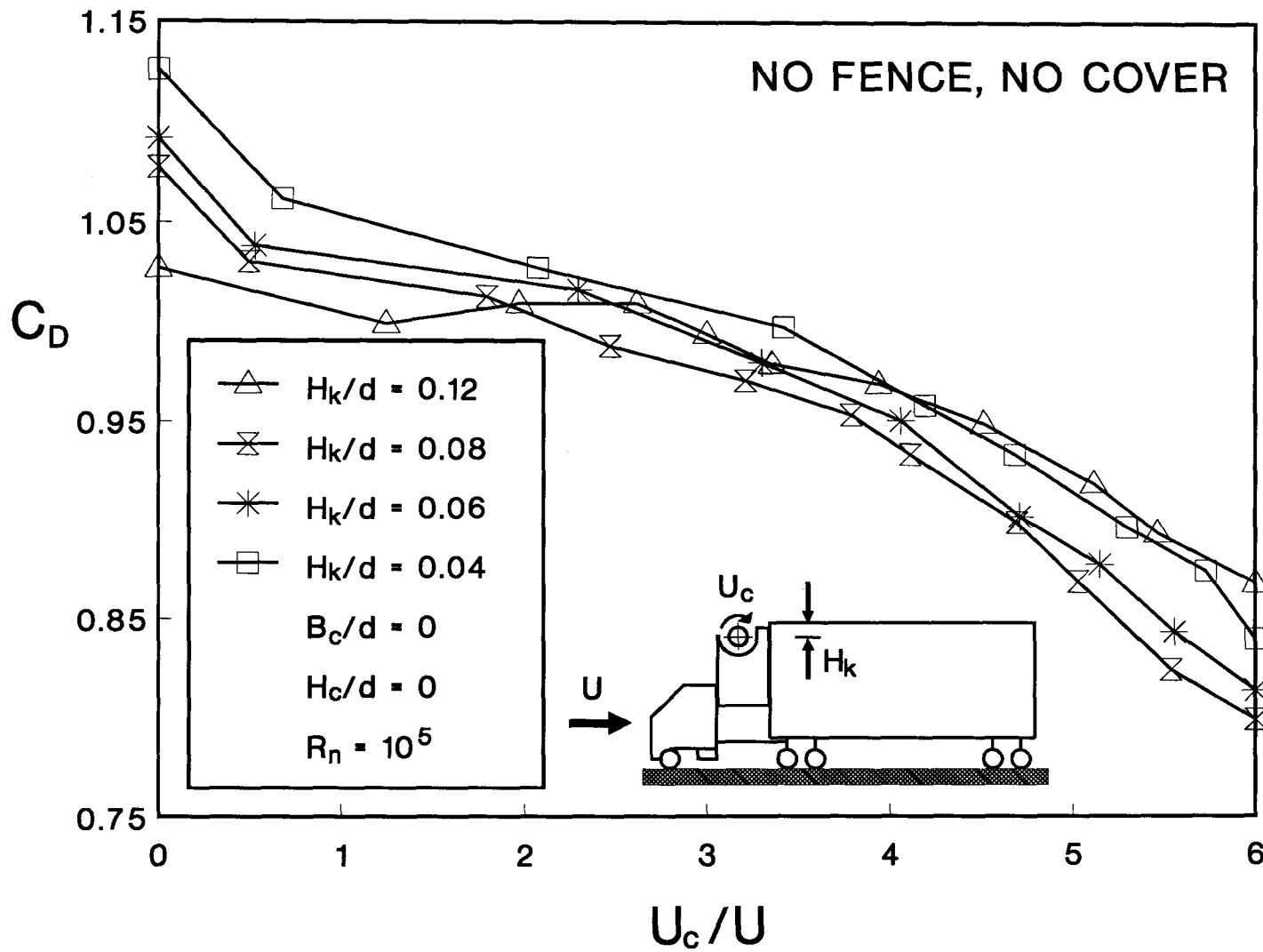


Figure 31. Variation in the drag coefficient with the cylinder speed ratio as affected by kit 1 vertical orientation: (a) absence of the front cover;

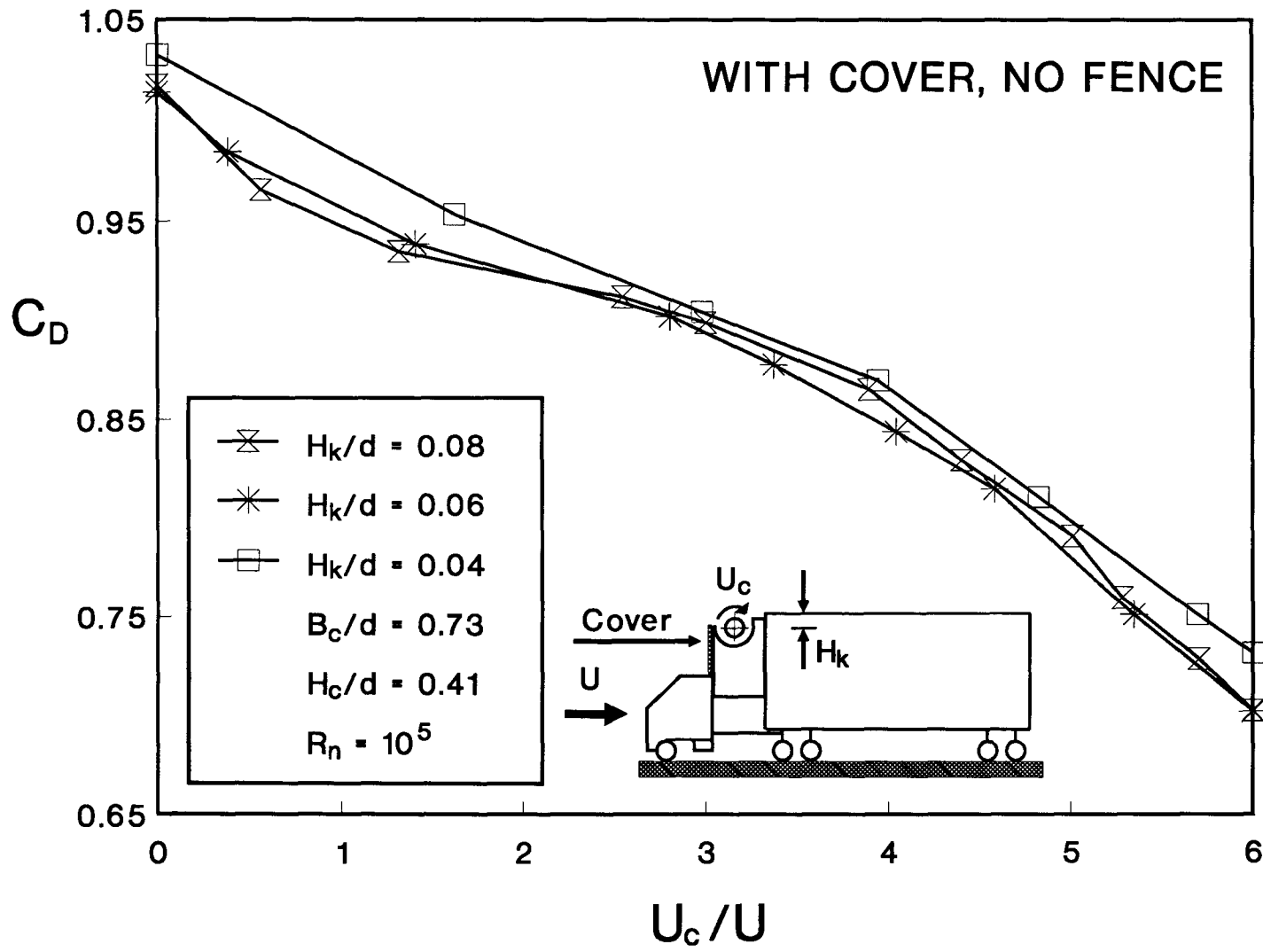


Figure 31. Variation in the drag coefficient with the cylinder speed ratio as affected by kit 1 vertical orientation: (b) with the front cover.

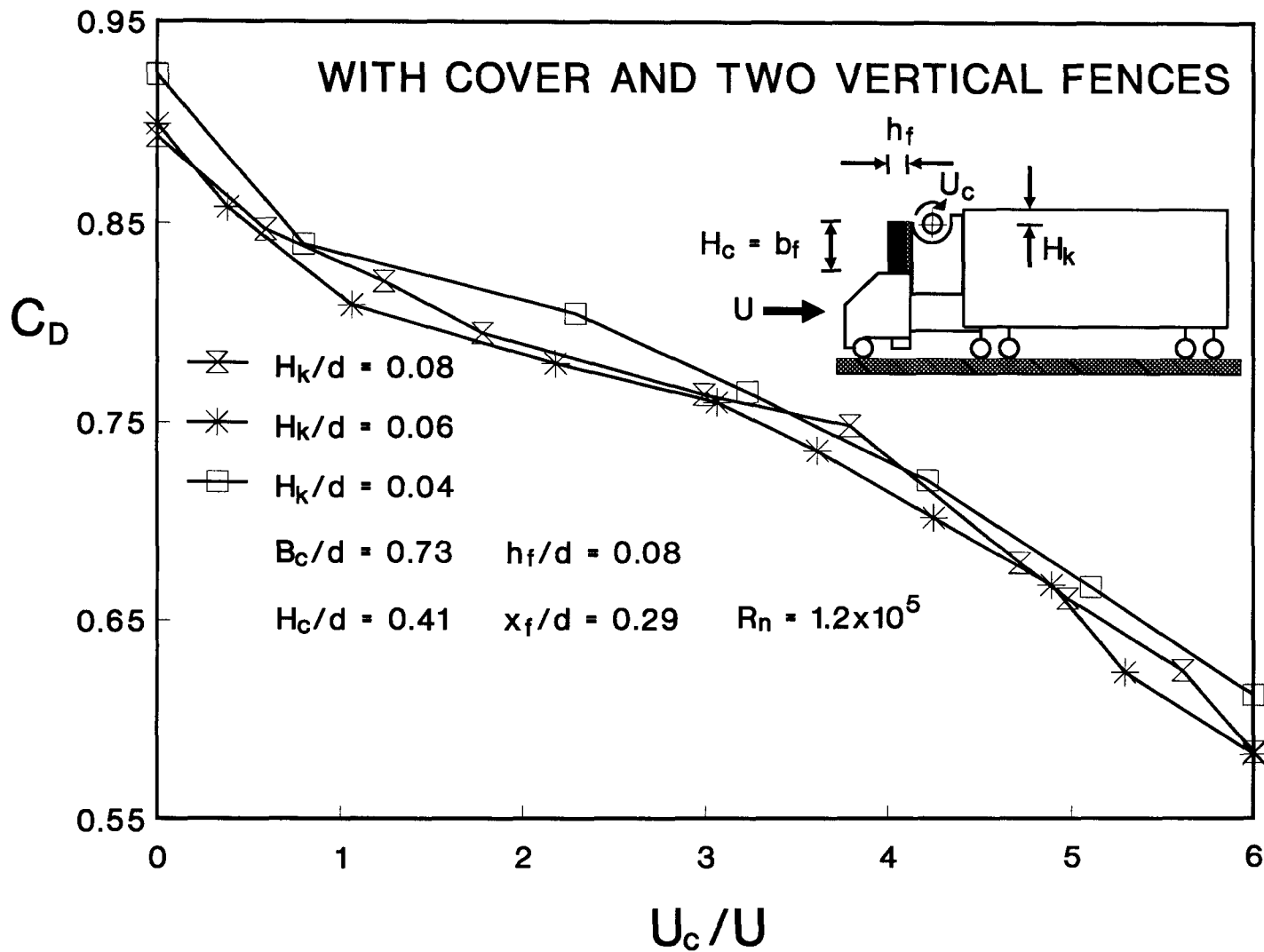


Figure 32. Variation in the drag coefficient with the cylinder speed ratio and kit 1 position with two vertical fences mounted optimally on the front face of the kit.

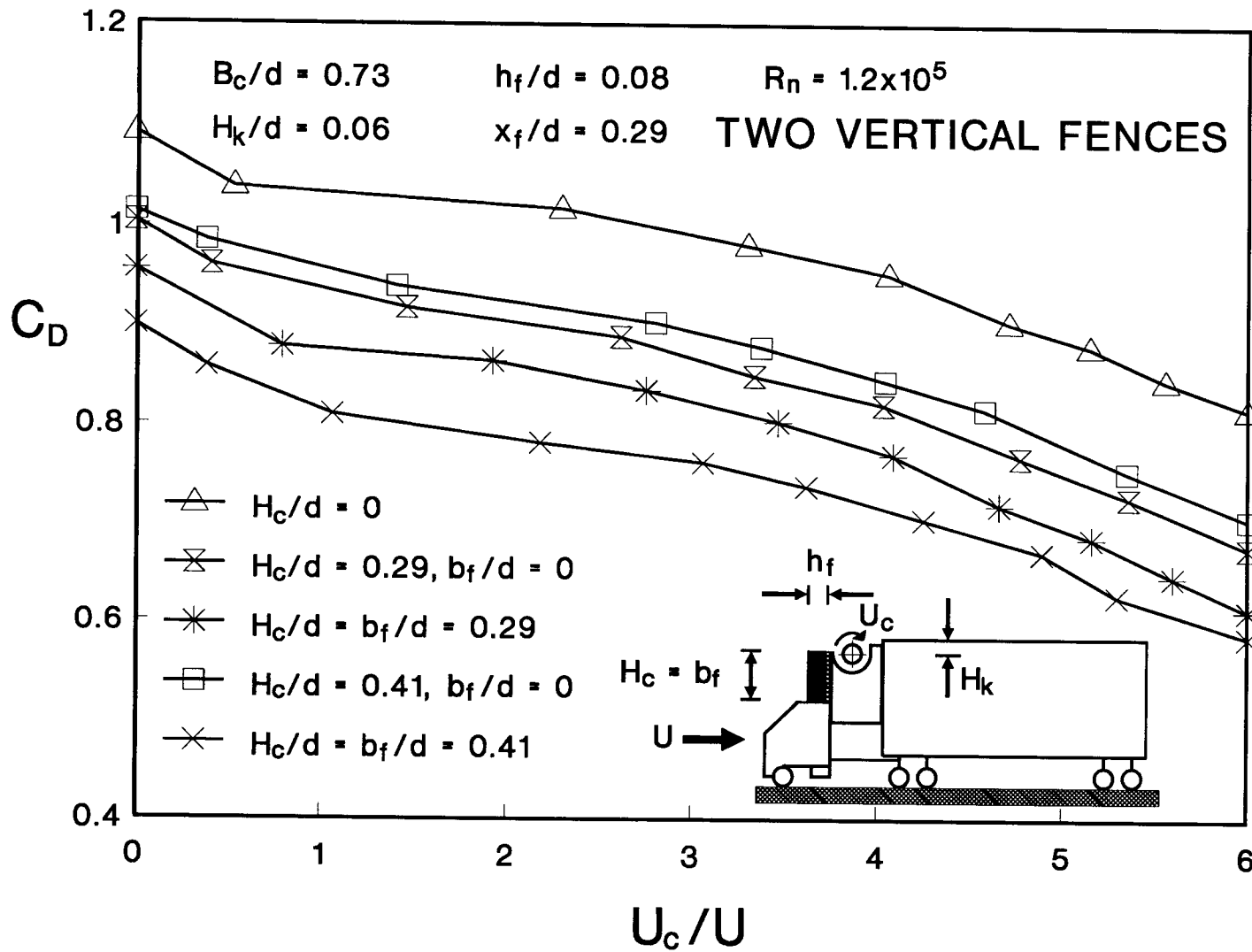


Figure 33. Variation in the drag coefficient with the cylinder speed ratio for kit 1 at the optimum vertical orientation. Note the influence of cover and fence geometry.

0.85 for $H_k/d = 0.06$, a reduction of 16.2%.

Effect of two vertical fences placed on the cover was evaluated next as shown in Figure 32. Note, even in the absence momentum injection ($U_c/U = 0$), the drag coefficient for $H_k/d = 0.06$ reduces from 1.014 (no fence case) to 0.9 (with two vertical fences), a drop of 11.2%. With cylinder rotation at $U_c/U = 4$, the $C_D = 0.72$ suggesting the reduction in aerodynamic resistance by 29% ! Note, the drag coefficient is relative insensitive to the kit positions tested. Thus such hybrid combination of the MSBC together with trip fences in a kit form appears quite promising for the prototype application.

It is apparent that larger the frontal area of the kit, more effective can be the fences. Of course, the fence geometry itself plays an important role in effective tripping of the boundary-layer and arresting the pressure recovery. Hence, it was decided to study influence of the exposed height (H_c) of the cover available for mounting fences and the fence height (b_f). The results are presented in Figure 33. There are five distinct cases considered. Note, for $U_c/U = 0$:

- (i) the highest drag coefficient $C_D \approx 1.092$ corresponds to the no cover case ($H_c/d = 0$);
- (ii) in absence of the fences, and the kit cover exposing 3/4 of the cylinder's frontal area, the drag coefficient drops to around 1.004 ($H_c/d = 0.29$, $b_f/d = 0$);
- (iii) introduction of twin vertical fences on the cover configuration

corresponding to (ii) leads to a drag coefficient of 0.96 ($H_c/d = b_f/d = 0.29$);

- (iv) with the cover extending to the center point of the cylinder (the cylinder half exposed to the free stream) and with no fences, the drag coefficient is ≈ 1.014 , higher than that in case (ii) or (iii);
- (v) with the twin vertical fences mounted on the cover described in case (iv), C_D reached the lowest value of 0.9 in this series of studies.

Thus, even in absence of rotation, judicious selection of the fence geometry and orientation can lead to a significant reduction in drag of a complex bluff body like a tractor-trailer truck. Recognizing that the reference drag coefficient (tractor-trailer without kit, cylinders or fences) is 1.124, a reduction in aerodynamic resistance by 19.92% through entirely passive means is indeed remarkable.

As can be expected, with momentum injection, the performance improves further with a reduction C_D by 30.6% at $U_c/U = 3$ ($U_c/U = b_f/d = 0.41$).

3.6.2 Cylinder kit 2

The cylinder-fence kit 2, being thinner, does not completely fill the gap between the tractor and the trailer. Of course, the gap can be covered by a plate if desired. As pointed out before, now the cylinder projects in the free

stream by an amount equal to its radius.

Figure 34 studies the effect of gap and the kit's vertical position on the drag coefficient without and with the cylinder rotation. Five different cases representing the gap condition (covered or uncovered) and the kit location (H_k/d) are considered. It is apparent that, irrespective of the cylinder rotation speed, covering the gap reduced the drag. Note, with the gap covered and the cylinder center aligned with the trailer's top face ($H_k/d = 0$), the drag is minimum over the entire range of U_c/U studied. However, the drag reduction obtained was significantly less than that obtained with kit 1 under corresponding condition (Figure 31b).

Figure 35 presents results for the kit performance as affected by two vertical plates in absence of cylinder rotation. Note, the gap condition and kit position correspond to the optimum found in the previous study (Figure 34, gap covered, $H_k/d = 0$). The critical position, $(x_f/d)_{cr}$, of the twin vertical fences was found to be 0.285 with $(C_D)_{min} \approx 0.983$, a reduction of around 8% (reference $C_D \approx 1.071$).

With the vertical fences at their critical positions, a horizontal fence was introduced and its optimum location established (Figure 36). It is apparent that a further reduction in the drag coefficient is relatively small. Now the minimum C_D attained is around 0.952 with $(y_f/d)_{cr} \approx 0.2$, with corresponds to a drag reduction of around 11.1%. Thus the horizontal fence by itself reduces the C_D by approximately 3%.

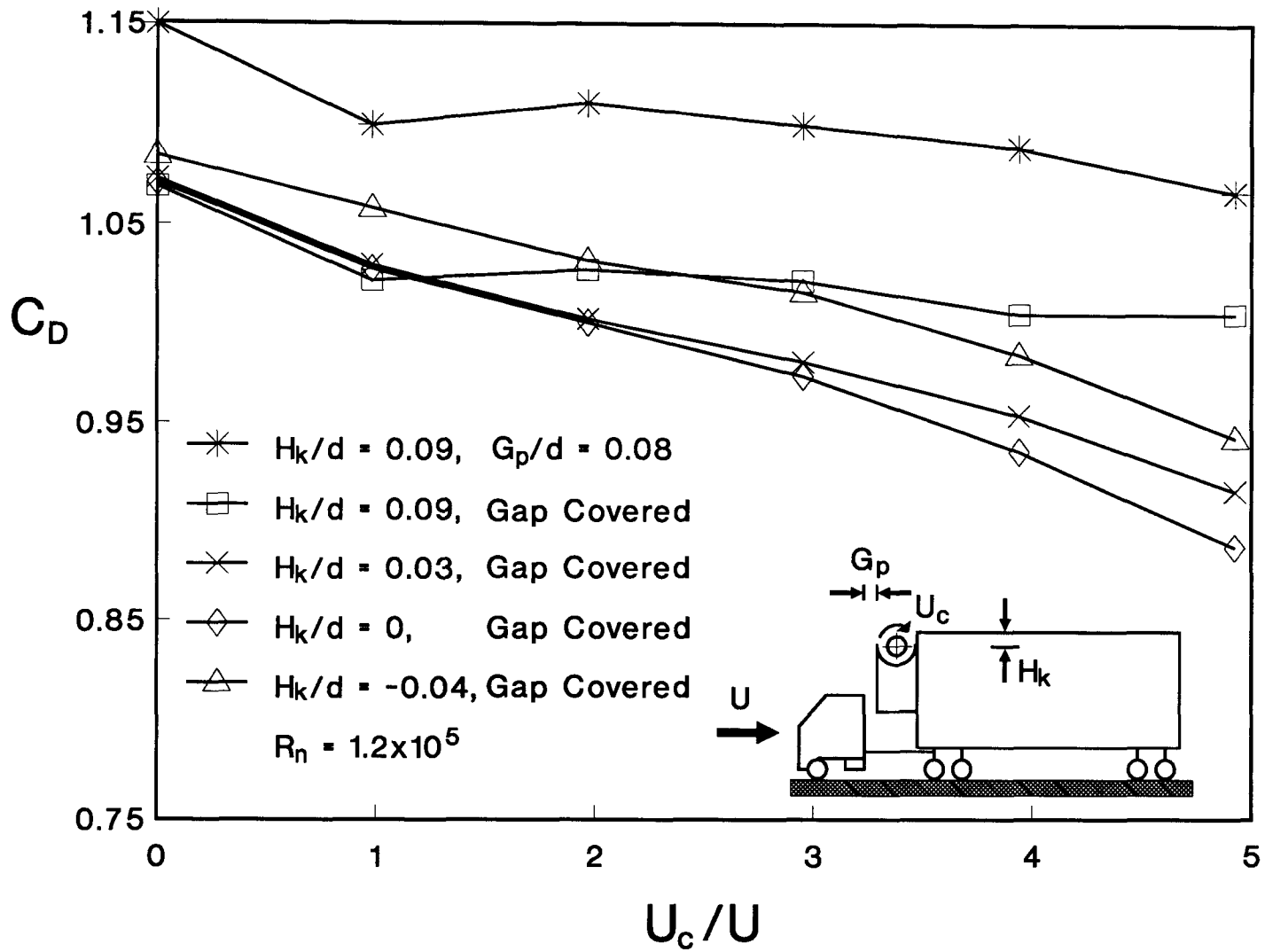


Figure 34. Variation in the drag coefficient with the cylinder speed ratio for kit 2 at different vertical position. Note the effect of gap.

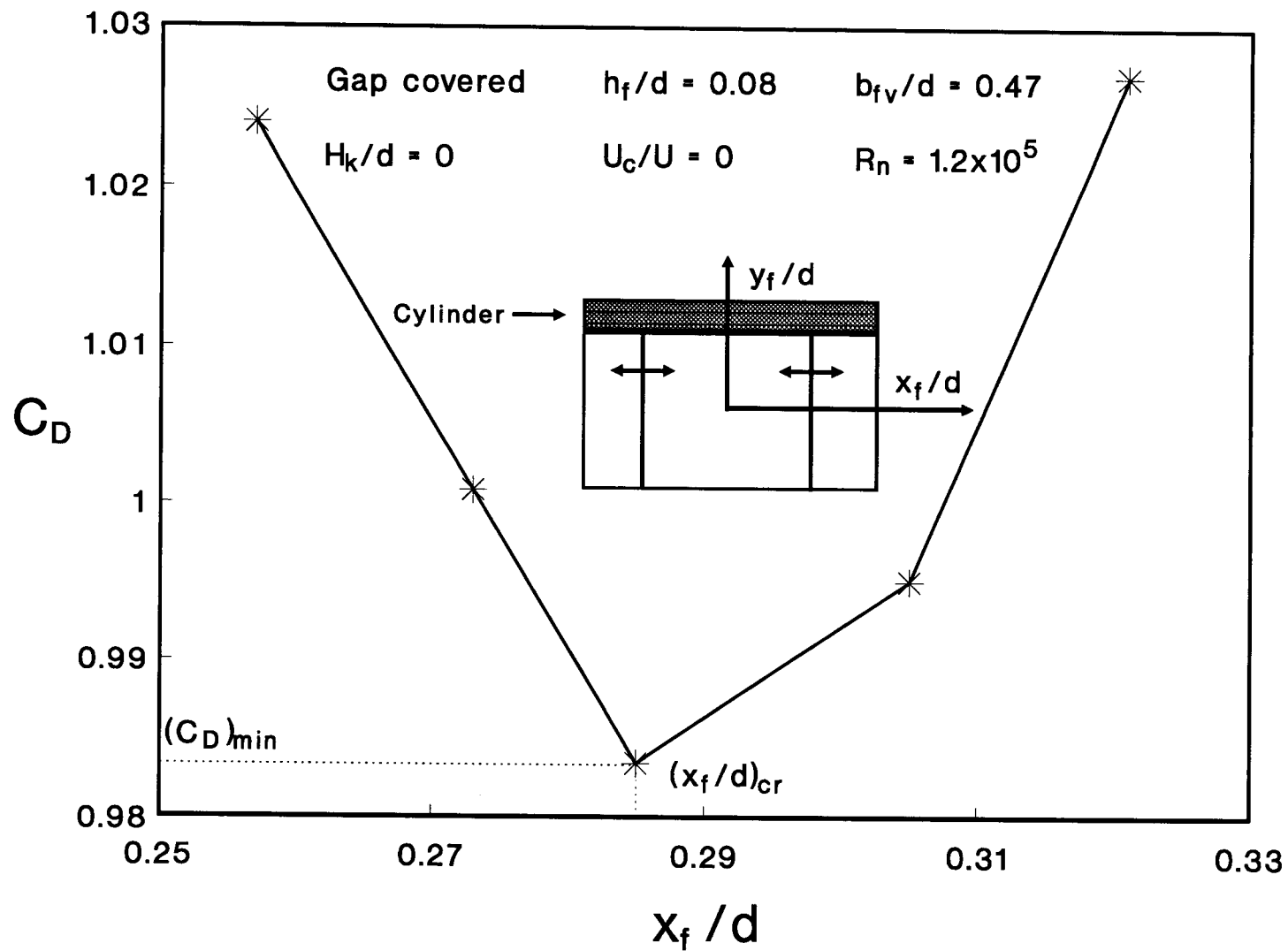


Figure 35. The drag coefficient as affected by position of the two vertical fences on the front face of kit 2, set at the optimum position, with the gap covered and stationary cylinder.

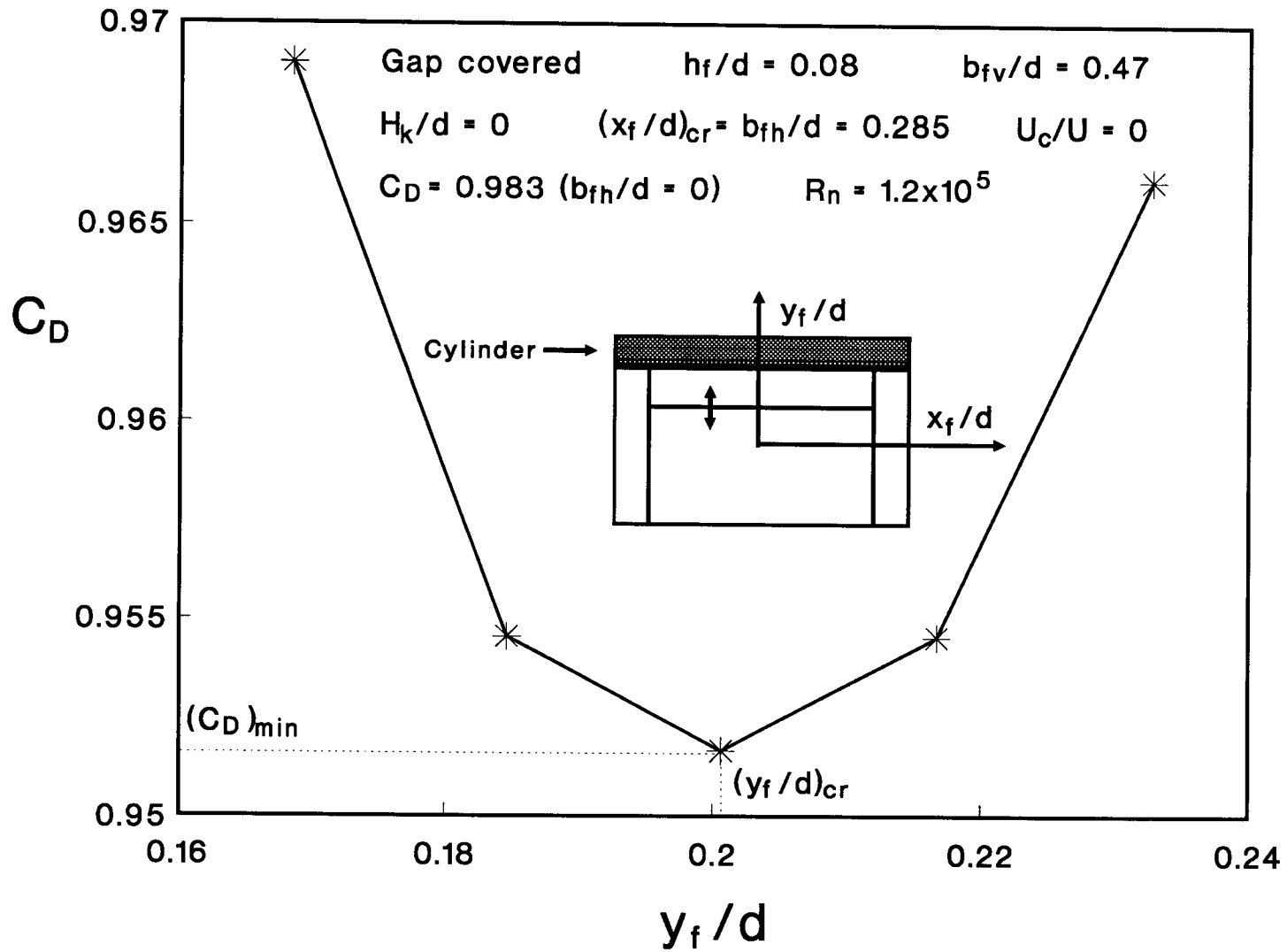


Figure 36. Variation in the drag coefficient as affected by the position of a horizontal fence with two critically-oriented vertical fences on the front face of kit 2. The gap was covered and the cylinder was held stationary.

The next logical step was to assess the effect of cylinder rotation without the fences as well as with their optimum orientation (Figure 37). As can be expected, the momentum injection improves the drag reduction, however, it is significantly less than that obtained with kit 1. For example, at $U_c/U = 3$, the minimum C_D corresponds to the twin vertical fence case and has a value of around 0.8. This represents a drag reduction of 22.5% compared to 30.6% given by kit 1.

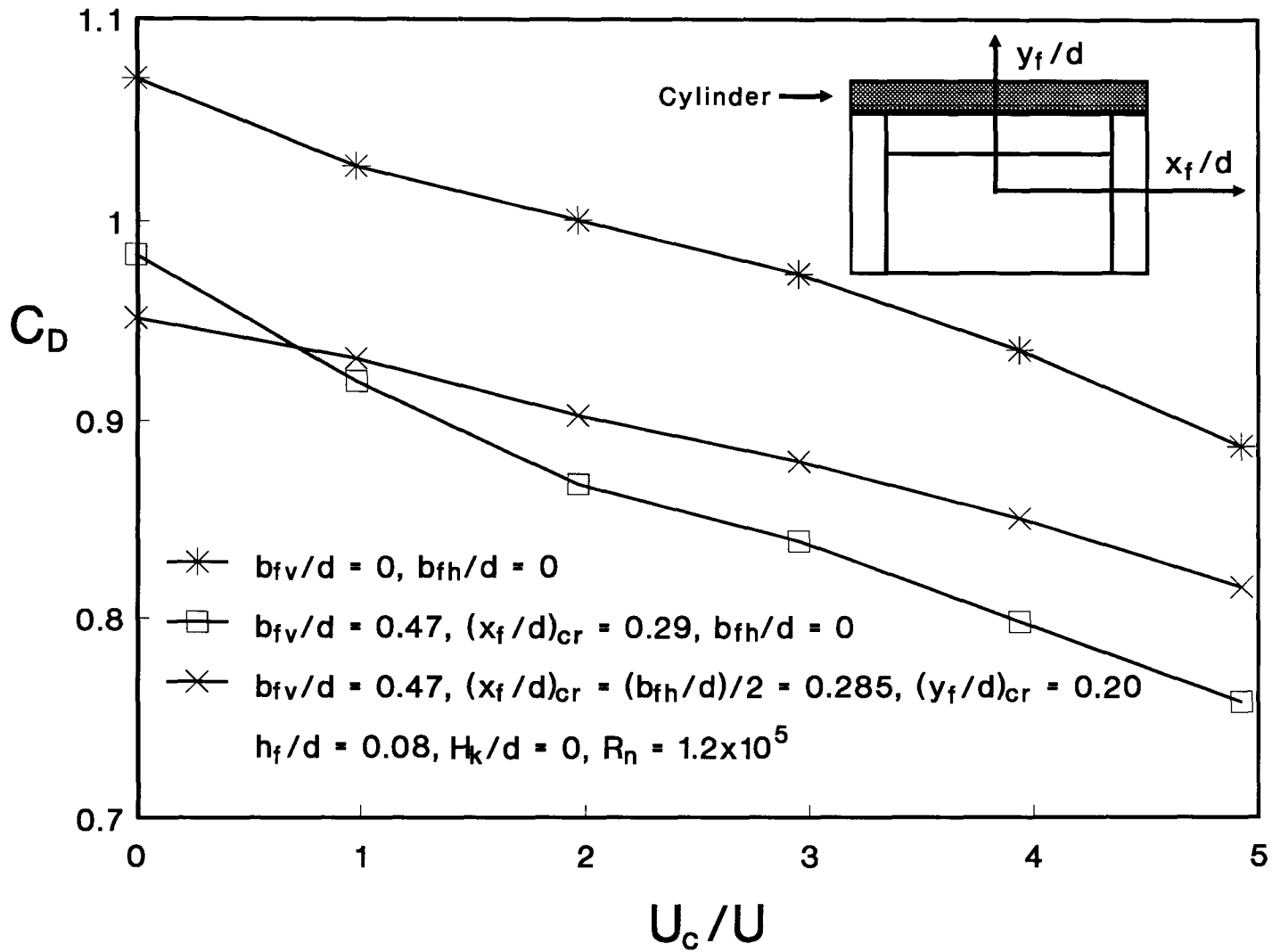


Figure 37. Variation in the drag coefficient with the cylinder speed ratio for kit 2 at its optimum vertical orientation, gap covered and fences in critical geometry.

4. CONCLUDING REMARKS

4.1 Summary of Results

4.1.1 Application of the MSBC to a 2-D wedge airfoil model

Based on a rather fundamental study of *Moving Surface Boundary-layer Control* (MSBC) with a two dimensional wedge airfoil model, conducted at a subcritical Reynolds number of 3×10^4 , following general conclusions can be made:

- (i) Rotation of the leading edge cylinder results in increased suction over the nose. It is the propagation of the lower pressure downstream that determines effectiveness of the rotation. This depends mainly on the speed of rotation, surface roughness and smoothness of transition from the cylinder to the airfoil surface. A large gap (> 3 mm) substantially decreases beneficial effect of the cylinder rotation.
- (ii) The increased momentum injection into the boundary-layer, with an increase in speed and appropriate surface roughness, delays separation of the flow from the upper surface resulting in higher lift and reduced drag. The existence of a critical speed is also evident beyond which the momentum injection through a moving surface appears to have relatively less effect.

- (iii) With the rotation of the cylinder the onset of flow separation occurs at higher angles of attack. The upper surface flow remains attached up to a distance downstream of the leading edge at which point it separates followed by, at times, reattachment downstream.
- (iv) Rotation of the smooth cylinder resulted in the increase of C_{Lmax} by 170%. The corresponding decrease in drag was about 36%.
- (v) Among the cylinder surfaces tested, the splined configuration proved to be the most successful in increasing lift as well as reducing drag. It raised the C_{Lmax} from 1.47 (reference case) to 4.3 (spline-2 case), an increase of around 193%! The reduction in drag was also quite impressive. In fact, the maximum C_L/C_D increased from 1.53 to 78.93. Although the splined cylinder proved to be the best, the results showed that an increase in roughness of the cylinder surface, in general, improves the boundary-layer control.
- (vi) The large C_L/C_D attained here through MSBC can be used to advantage in designing next generation of high performance airplanes.
- (vii) As the separation of shear layers is delayed, or even suppressed, the process of vorticity generation and its shedding in the wake will be affected. Hence the *moving surface boundary-layer control* may prove effective in suppressing vortex induced and galloping type of instabilities. Investigation in this area is in progress and

appears quite promising.

- (viii) The concept of MSBC is essentially semi-passive in character requiring negligible amount of power for its implementation. In the present set of model tests a 1/8 H.P. (≈ 90 W) motor was more than adequate to obtain $U_c/U = 4$.

4.1.2 Application of the MSBC and fences to a 3-D truck

This study is aimed at assessing the effect of momentum injection and tripping of the boundary-layer on drag reduction of three dimensional models of the rectangular prism and the tractor-trailer truck. Based on the wind tunnel data, following general conclusions can be made:

- (i) Both the concepts are quite promising in reducing the drag.
- (ii) Effectiveness of the momentum injection procedure diminishes when the rotating element is submerged in the wake.
- (iii) Helical surface roughness of the rotating element improves efficiency of the MSBC only by a small amount. The maximum drag reduction even with twin cylinders (Case 2, Figure 20) was found to be around 14.4%.
- (iv) A splined rotating cylinder injects momentum into the boundary-layer more directly presenting an exciting possibility of a further reduction in C_D . With the twin splined cylinders (Case 6, Figure

21), the drag reduction of 52% was realized ($U_{cf}/U = U_{cr}/U \approx 6$) ! Even with the speed ratio of 4, the C_D reduction was as large as 26%.

- (v) The *moving surface boundary-layer control* (MSBC) process is essentially semi-passive, i.e. it requires very little energy. For the model tests, 1/8 H.P. motors (≈ 95 W) were more than adequate to attain $U_c/U = 6$. For a prototype truck, a little over 1.5 H.P. would be required, which is negligible compared to 400-500 H.P. engine of a typical truck.
- (vi) The concept of fences to trip boundary-layer appears to be even more promising. For a three-dimensional prism, simulating a trailer, 31% reduction in the drag coefficient was observed. A reduction in C_D by around 24.6% for a truck configuration is indeed exciting. Note, the process is entirely passive requiring no additional energy.
- (vii) A hybrid combination of fences and the MSBC appears favourable. A cylinder-fence kit would make application of the concepts to existing trucks more attractive. Among the two kits tested, kit-1 proved more efficient promising the drag reduction of around 30% at $U_c/U = 3$.

4.2 Recommendation for Future Work

A comment concerning the future plan of study would be appropriate. Effectiveness of the MSBC and fence concepts having been established, several exciting possibilities present for further study and diverse application:

- (i) More precise wind tunnel tests using accurate models, simulation of relative road motion and the side wind induced yaw conditions in supercritical Reynolds number range represent obvious extension of the project.
- (ii) The road tests using prototype truck with MSBC and fences should provide valuable field data.
- (iii) Development a numerical code for multielement airfoil and bluff bodies with momentum injection represents the area that received virtually no attention. Of course, it is enormously challenging task but, if successful, should prove equally satisfying. Even a computational tool for a two-dimensional flat plate with MSBC would represent a major advance in the field.
Similar studies with fences also need attention.
- (iv) As the momentum injection affects the separating boundary-layer and the associated wake, it could be used to advantage in controlling vortex resonance and galloping type of wind induced instabilities often encountered in industrial aerodynamics problems.
- (v) Enormous opportunity exists for application of the MSBC to high

performance next generation of aircraft, both at the leading edge of the wing and the control surfaces. The same is true for underwake application with hydrofoils and rudders.

- (vi) The concept of MSBC can be applied at the end of three dimensional wings to counter tip vortices thus facilitating their dispersion, minimizing the downwash, and providing improved lift/drag characteristic. It was tried out by Prof. V.J. Modi in a preliminary fashion in 1986 and appeared promising. However, more precise study is necessary.
- (vii) The MSBC can be used to advantage in design of an efficient diffuser with large diverging angle as often encountered in chemical industry.
- (viii) The fence concept can also be applied quite effective in industrial aerodynamics problems mentioned in (iv). They can be used to reduce drag of a wide variety of bluff bodies including buses, railway carriages, marine vehicles and others.

REFERENCES

- [1] Simanaitis, D., "Reduced Resistance Equals Increased Miles per Gallon," *Road and Truck*, June 1980, pp. 88-90
- [2] McDonald, A. T., Palmer, G. M., et al., "Truck and Bus Aerodynamics Investigated," *Automotive Engineering*, Society of Automotive Engineers, Vol. 88, No. 11, November 1980, pp. 50-57.
- [3] Goldstein, S., *Modern Developments in Fluid Mechanics*, Vols. I and II, Oxford University Press, 1938.
- [4] Lachmann, G. V., *Boundary layer and Flow Control*, Vols. I and II, Pergamon Press, 1961.
- [5] Rosenhead, L., *Laminar Boundary Layers*, Oxford University Press, 1966.
- [6] Schlichting, H., *Boundary Layer Theory*, McGrawHill Book Company, 1968.
- [7] Chang, P. K., *Separation of Flow*, Pergamon Press, 1970.
- [8] Favre, A., "Contribution a l'Etude Experimentale des Mouvements Hydrodynamiques a Deux Dimensions," Thesis presented to the University of Paris, 1938.
- [9] Alvarez-Calderon, A., and Arnold, F. R., "A Study of the Aerodynamic Characteristics of a High Lift Device Based on Rotating Cylinder Flap," Stanford University Technical Report RCF-1, 1961.

- [10] Cichy, D. R., Harris, J. W., and MacKay, J. K., "Flight Tests of a Rotating Cylinder Flap on a North American Rockwell YOY-10A Aircraft," NASA CR-2135, November 1972.
- [11] Weiberg, J. A., Giulianetti, D., Gambucci, B., and Innis, R. C., "Takeoff and Landing Performance and Noise Characteristics of a Deflected STOL Airplane with Interconnected Propellers and Rotating Cylinder Flaps," NASA TM X-62, 320, December 1973.
- [12] Cook, W. L., Mickey, D. M., and Quigley, H. G., "Aerodynamics of Jet Flap and Rotating Cylinder Flap STOL Concepts," AGARD Fluid Dynamics Panel on V/STOL Aerodynamics, Delft, Netherlands, April 1974, Paper No. 10.
- [13] Johnson, W. S., Tennant, J. S., and Stamps, R. E., "Leading Edge Rotating Cylinder for Boundary-layer Control on Lifting Surfaces," *Journal of Hydrodynamics*, Vol. 9, No. 2, April 1975, pp. 76-78.
- [14] Modi, V. J., Sun, J. L. C., Akutsu, T., Lake, P., McMillian, K., Swinton, P. G., and Mullins, D., "Moving Surface Boundary-layer Control for Aircraft Operation at High Incidence," *Journal of Aircraft*, AIAA, Vol. 18, No. 11, November 1981, pp. 963-968.
- [15] Mokhtarian, F., and Modi, V. J., "Fluid Dynamics of Airfoil with Moving Surface Boundary-layer Control," *AIAA Atmospheric Flight Mechanics Conference*, August 1986, paper No. 86-2184-CP; also *Journal of Aircraft*, Vol. 25, No. 2, February 1988, pp. 163-169.

- [16] Mokhtarian, F., Modi, V. J., and Yokomizo, T., "Rotating Air Scoop as Airfoil Boundary-layer Control," *Journal of Aircraft*, AIAA, Vol. 25, No. 10, October 1988, pp. 973-975.
- [17] Mokhtarian, F., Modi, V. J., and Yokomizo, T., "Effect of Moving Surfaces on the Airfoil Boundary-layer Control," *AIAA Atmospheric Flight Mechanics Conference*, Minneapolis, Minnesota, August 1988, Paper No. AIAA-88-4303CP; also *Proceedings of the Conference*, Editors: R. Holdway and B. Kaufman, AIAA Publisher, pp. 660-668; also *Journal of Aircraft*, AIAA, Vol. 27, No. 1, January 1990, pp. 44-50.
- [18] Sovaran, G., Morel, T., and Mason, T. W. Jr., "Aerodynamic Drag Mechanisms of Bluff Bodies and Road Vehicles," *Proceedings of the Symposium held at the General Motors Research Laboratories*, Plenum press, New York, 1978.
- [19] Koernig-Facsenfeld, F. R., *Aerodynamik des kraftfahrzeugs: Verlay der Motor-Rundschau*, Umshau Verlag, Frankfurt, West Germany, First Edition 1951, Reprinted 1980.
- [20] Kramer, C., and Gerhardt, H. J., "Road Vehicle Aerodynamics," *Proceedings of the 4th Colloquium on Industrial Aerodynamics*, Aachen, June 1980.
- [21] Kurtz, D. W., "Aerodynamic Design of Electric and Hybrid Vehicles: A Guidebook," *U. S. Department of Energy*, Report No. 5030-471, September 1980.

- [22] Bearman, P. W., "Review of Bluff Body Flows Applicable to Vehicle Aerodynamics," *Transactions of ASME, Journal of Fluids Engineering*, Vol. 102, Sept. 1980, pp. 265-274.
- [23] Wacker, T., "A Preliminary Study of Configuration Effects on the Drag of a Tractor-trailer Combination," *M.A.Sc. Thesis*, University of British Columbia, Vancouver, Oct. 1985.
- [24] Kataoka, T., China, H., Nakagawa, K., Yanagimoto, K., and Yoshida, M., "Numerical Simulation of Road Vehicle Aerodynamics and Effect of Aerodynamic Devices," *SAE International Congress and Exposition*, Detroit, Michigan, U.S.A., 1991, Paper No. 91-0597.
- [25] Larsson, L., Broberg, L., and Janson, C., "A Zonal Method for Predicting External Automobile Aerodynamics," *SAE International Congress and Exposition*, Detroit, Michigan, U.S.A., 1991, Paper No. 91-0595.
- [26] Modi, V. J., Shih, E., Ying, B., and Yokomizo, T., "On the Drag Reduction of Bluff Bodies through Momentum Injection," *AIAA 8th Applied Aerodynamics Conference*, Portland, Oregon, Paper No. 90-3076; also *Journal of Aircraft*, AIAA, in press.
- [27] Mason, W. T., Jr. and Beebe, P. S., "The Drag Related Flow Field Characteristics of Trucks and Buses," *Proceedings of the Symposium on Aerodynamic Drag Mechanisms of Bluff Bodies and Road Vehicles*, Ed. G. Sovran, T. Morel and W. T. Mason, Jr., Plenum Press, New York, 1978, pp. 77-78.